Blank Page

AN ABSTRACT OF THE THESIS OF

Paul D. Barker for the degree of Master of Science in Civil Engineering presented on March 12, 2012.

Title: Effects of Soil Slope on the Lateral Capacity of Piles in Cohesionless Soils.

Abstract approved:

Scott A. Ashford

Deep foundations, including driven piles, are used to support vertical loads of structures and applied lateral forces. Many pile supported structures, including bridges, are subjected to large lateral loads in the form of wind, wave, seismic, and traffic impact loads. In many practical situations, structures subjected to lateral loading are located near or in excavated and fill slopes or embankments. Full-scale research to examine the effects of soil slope on lateral pile capacity is limited. The purpose of this study is to examine the effects on lateral capacity of piles located in or near cohesionless soil slopes.

A full-scale lateral load testing program was undertaken on pipe piles in a cohesionless soil at Oregon State University. Five piles were tested near a 2H:1V test slope and located between 0D to 8D behind the slope crest, where D is the pile diameter. Two vertical baseline piles and three battered piles were also tested

in level ground conditions. The cohesionless backfill soil was a well-graded material with a fines content of less than 10% and a relative compaction of 95%, meeting the Caltrans specification for structural backfill.

Data collected from the instrumented piles was used to back calculate p-y curves, load-displacement curves, reduction factors, and load resistance ratios for each pile. The effects of slope on lateral pile capacity are insignificant at displacements of less than 2.0 inches for piles located 2D and further from the crest. For pile located at 4D or greater from the slope crest, the effect of slope is insignificant on p-y curves. A simplified p-multiplier design procedure derived from back-calculated p-y curves is proposed to account for the effects of soil slope.

Comparisons of the full-scale results were made using proposed recommendations from the available literature. Lateral resistance ratios obtained by computer, centrifuge, and small scale-models tend to be conservative and overestimate the effects of slope on lateral capacities. Standard cohesionless p-y curve methods slightly over predict the soil resistance at very low displacements but significantly under predict the ultimate soil resistance. Available reduction factors from the literature, or p-multipliers, are slightly conservative and compare well with the back-calculated p-y curves from this study.

Effects of Soil Slope on the Lateral Capacity of Piles in Cohesionless Soils

by

Paul D. Barker

A THESIS

submitted to

Oregon State University

in partial fulfillment of
the requirements for the
degree of

Master of Science

Presented March 12, 2012
Commencement June 2012

Master of Science thesis of Paul D. Barker presented on March 12, 2012.

APPROVED:

Major Professor, representing Civil Engineering

Head of the School of Civil and Construction Engineering

Dean of the Graduate School

I understand that my thesis will become part of the permanent collection of Oregon State University libraries. My signature below authorizes release of my thesis to any reader upon request.

Paul D. Barker, Author

ACKNOWLEDGEMENTS

The author expresses sincere appreciation to all of those who provided assistance with this research project. He would like to acknowledge the support, guidance, and the exceptional opportunity provided by his graduate advisor, Professor Scott A. Ashford.

The author is very grateful for the support and comments provided by the graduate thesis committee: Professor Armin Stuedlein, Professor Ben Mason, and Professor John Simonsen.

Successful testing would not have been possible without the knowledge and support of Mr. James Batti and Mr. Michael Dyson. The author greatly appreciates the help of Dr. Nontapat Nimityongskul for his guidance in project background and setup and also Mr. Deepak Rayamajhi with his assistance in data analysis. The sponsorship from the California Department of Transpiration under Facilities Contract No. 59A0645 should be acknowledged and is greatly appreciated by the author.

Lastly, the author expresses sincere appreciate for the love, support, and understanding from his wife and parents throughout this project as this could not have been possible without them.

TABLE OF CONTENTS

TABLE OF CONTENTS (Continued)

TABLE OF CONTENTS (Continued)

TABLE OF CONTENTS (Continued)

TABLE OF CONTENTS (Continued)

LIST OF FIGURES

LIST OF FIGURES (Continued)

LIST OF FIGURES (Continued)

LIST OF FIGURES (Continued)

LIST OF FIGURES (Continued)

LIST OF FIGURES (Continued)

LIST OF FIGURES (Continued)

LIST OF FIGURES (Continued)

LIST OF TABLES

LIST OF TABLES (Continued)

1. INTRODUCTION

Deep foundations, including driven piles, are used to support vertical loads of structures and applied lateral forces. Typical structures subjected to lateral loads include bridge abutments, transmission towers, offshore platforms, and traffic sign foundations (Caduto, 2001). Traffic, wind, wave, and seismic forces are common types of lateral loads subjected to pile foundations. In many practical situations, structures subject to lateral loading are located near excavated slopes or embankments. Piles are frequently driven at a batter to increase foundation stiffness.

Bridge abutments, in most circumstances, are constructed on or near a slope crest, as presented in **Figure 1-1**, to accommodate grade separations or geographical feature. Lateral loads applied to deep foundations are transferred into the surrounding soil. The interaction between the soil-pile systems resists lateral movement of the foundation. The horizontal deflection of a pile is inter-related to the soil resistance, thus, both the pile and soil must be analyzed together (Reese et al., 2006).

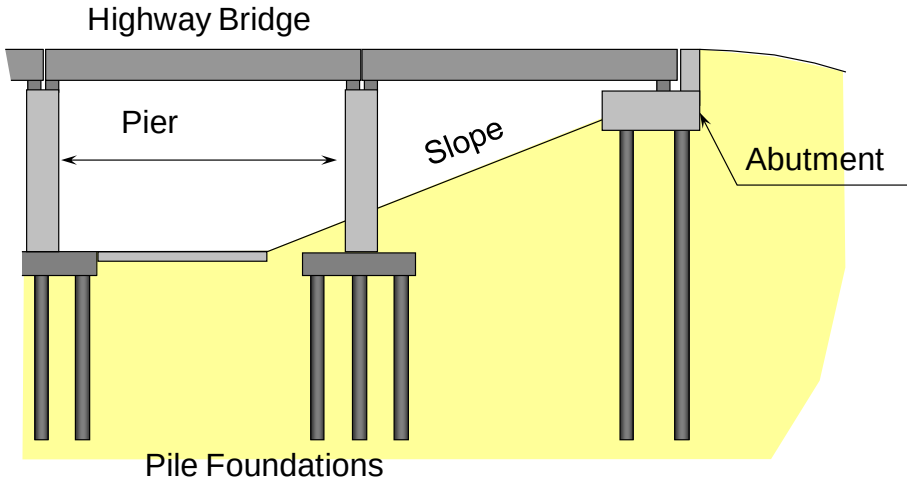

Figure 1-1. Typical bridge foundation (after Nimityongskul, 2010)

Many design methods have been developed to account for lateral loads on pile foundations in a horizontal soil profile. The most common of these methods is the use of p-y curves, where p is the unit soil resistance and y is the pile displacement, obtained from the Winkler Spring Method (Reese et al. 1974). This method models the soil resistance as a set of independent nonlinear springs along the length of a pile. To resist lateral loads, piles mobilize passive resistence as they move laterally in the surrounding soil. The reaction in the soil-pile system to resist movement depends on the stiffness of the pile, the stiffness of the soil, and whether the pile tip is fixed in the soil (Das, 2007).

The presence of a slope on deep foundations loaded in a downslope direction can decrease the overall lateral capacity of the system. Ignoring the effects a slope may result in an over prediction of lateral resistance by as much as

50% (Gabr and Borden, 1990). The majority of research conducted to examine the effects of soil slope on lateral capacities of piles and nonlinear p-y curves has been done using scaled model tests and finite element analyses. These models have provided reduction factors, or p-multipliers, for piles located in level ground conditions. There is a lack of full-scale test results to verify these model predictions (Mirzoyan, 2007). Some existing methods (Reese et al., 2004) to analyze lateral loads on battered piles is to model them as vertical piles located on a slope with a batter angle equivalent to the slope angle. High costs are the main disadvantage of full-scale tests and is the likely reason for the absence of testing results.

1.1 **Project Scope**

There have been very few full-scale tests conducted to examine the effects of a cohesionless soil slope on the lateral capacity of piles. During the summer of 2001, a full-scale lateral loading testing program was conducted to examine the effects of a slope and batter angle on the lateral capacity of piles. All lateral load tests were conducted on a cohesionless embankment at the Geotechnical Engineering Field Research Site (GEFRS) at Oregon State University.

A total of ten steel pipe piles were driven into the cohesionless embankment. Five piles were tested in proximity to a 2 horizontal to 1 vertical (2H:1V) test slope. These piles were located either on the slope, on the crest, or

certain distances behind the crest. Two baseline tests were conducted in free-field, or horizontal ground conditions, to compare with the near slope test results. Three battered piles, two with positive batter and one with negative batter, were also tested. The cohesionless embankment was constructed with less than 10% fines and placed in 8 inch lifts at 95% relative compaction with respect to Caltrans Soil Test 216. The soil gradation and compaction specifications are similar to those used for bridge abutments and meet the structural backfill requirements in the Caltrans Bridge Design Specifications (Caltrans, 2006).

Along the length of each pile, strain gauges and tiltmeters were installed to measure strain and rotation during lateral loading. This data was used to back-calculate curvature, rotation, moment, shear, deflection, and soil reaction profiles for each vertical test pile. **Figure 1-2** presents an example of these profiles for a fixed end pile. This information was used to produce p-y curves and load-displacement curves to examine the effects of a slope. The main objectives of this research include:

1. Review existing p-y curves and methods used to account for soil slope in cohesionless soils.
2. Evaluate existing methods to account for slopes with back-calculated full-scale testing results.

3. Propose generalized p-multipliers for near slope piles based on distance from the crest slope and depth.

4. Recommend simplified lateral resistance design procedures to account for a cohesionless slope.

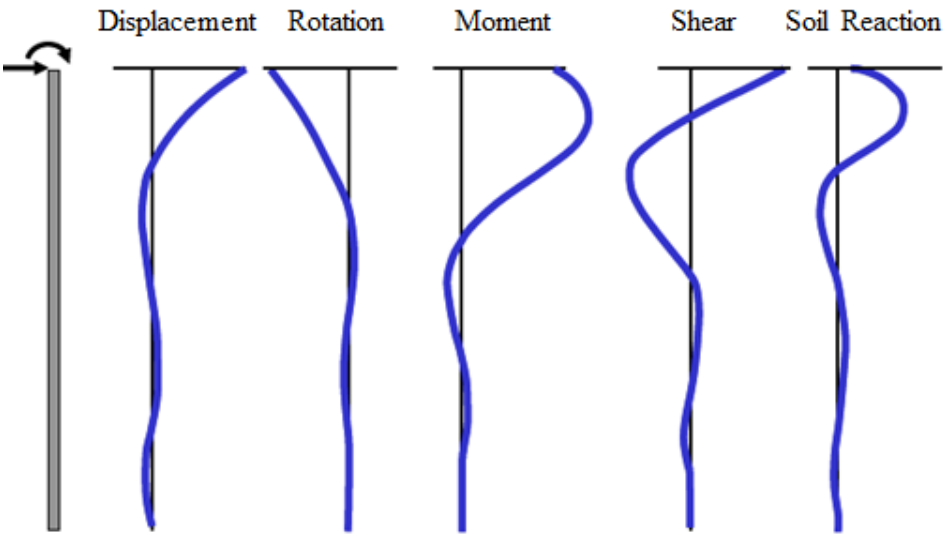

Figure 1-2. Example of fixed end pile profiles in free head conditions (from Reese et al., 2004)

2. LITERATURE REVIEW

2.1 Introduction

Driven pile foundations are used to support a wide variety of structures. In many cases, lateral loads are often the critical factors considered in the design of foundations. To resist lateral loads piles can be driven at an angle from vertical (battered) to resist lateral movement with axial pile loading. Vertical piles can also be designed to resist lateral movement by analyzing the effects of soil-pile interaction.

Engineers typically did not evaluate lateral loads on deep foundations until the early 1950s and designed foundation only to resist axial loads (Coduto, 2001). Commonly, these engineers would design foundations to resist lateral loads with a battered pile. These engineers would consider only the axial loading in the battered piles to resist lateral movement and not interaction between the sides of the pile with the soil. As the oil industry in the mid-twentieth century grew, the need to analyze significant lateral loads from wind and ocean currents applied to large offshore structures was essential. Driving battered piled of the required size and at the necessary angle was becoming unpractical to support the lateral loads. Thus, in the early 1950's the oil industry conducted some of the initial research on lateral capacity of deep foundations (Reese et al., 2006).

Over the past several decades, the lateral capacities of piles have been the focus of many types of research. Multiple methods have been developed to model

the soil-pile response when subjected to lateral forces. These methods have been developed from analytical solutions, laboratory models, and full scale tests. When evaluating and designing piles for lateral load capacity the following should be considered (Coduto, 2001):

(1) Determine the depth of embedment required to transfer lateral loads to the surrounding soil.

2) Given the design loads, the lateral movement of the foundation must comply with the service limits of the supported superstructure.

(3) The shear and moment in the pile resulting from lateral forces must be under the capacity of the pile to prevent structural failure and buckling of the pile.

This literature review presents research conducted on lateral load testing and the effects of slope on lateral capacity on piles in cohesionless soils. An overview of the different methods and theories used in the analysis of the lateral capacity of piles in level (horizontal) ground is briefly presented. A more in depth review of laterally loaded piles near sloping ground in cohesionless soils is then covered, as this is the main focus of this research. Nimityongskul (2010) conducts a thorough review of research for laterally loaded piles near a slope in cohesive soil conditions.

2.2 Background on Models

The analysis of piles subjected to lateral loading requires considerations of both the foundation and surrounding soil properties. Soil resistance is dependent on pile deflection, and pile deflection is dependent on the pile rigidity and soil resistance (Reese et al. 2006). This inter-relationship between the pile and the soil necessitates a soil-structure interaction analysis where each is examined relative to the other. There have been multiple theories and analytical methods proposed to account for this interaction. None of the models can account for all factors impacting the relation between soil and pile during lateral loading, but many can predict, with some degree of confidence, lateral capacities and deflections in piles (Juirnarongrit, 2002).

An early method, as presented by Hetenyi (1946), depicts a laterally loaded pile as a long elastic beam resting on independent linear-elastic springs. This series of linear springs on a beam is commonly known as the Winkler Spring Method (Winkler, 1867) or the subgrade reaction method. Hetenyi modeled the soil subgrade modulus on the pile as a set of Winkler springs. Due to the simplicity of this model it has been employed and improved upon by many researchers conducting investigations on lateral pile capacities (e.g. Barber 1953; Reese and Matlock, 1956; and Davisson and Gill, 1963). These researchers improved the existing model by concluding that the modulus of subgrade reaction was interrelated to depth and only considered a single soil layer.

Differing from assumptions used in early models, soil does not react as an elastic material and responds nonlinearly. For a better representation of soil behavior during lateral loading, a technique deploying a series of nonlinear springs was developed known as the p-y curve method (McClelland and Focht, 1958; Matlock, 1970; Reese et al., 1974; Reese and Welch, 1975). This method is one of the most widely accepted models currently used to determine soil-pile interaction subjected lateral forces. Further explanation of common p-y curves are presented in the following sections.

The elastic continuum theory is an alternative analysis method to estimate lateral deflection of piles (Spillers and Stoll,1964; Banerjee and Davies, 1978; and Poulos and Davies, 1980). This method models the soil reaction of a point within a soil mass as a result of an applied load at a nearby point within the soil mass. This is determined from the assumptions that the soil around a pile is modeled as a homogeneous, semi-infinite, and isotropic material. This model is hindered because the modulus of elasticity and Poisson's ratio of soil are consistent throughout. Researchers have improved the theory by implementing procedures to account for increasing soil modulus with depth to account for layered soil conditions (Banerjee and Davies, 1978). The elastic continuum model is reasonable for determining pile response at small displacements, but it is considered to be flawed at larger displacements based on the assumption that the soil mass is a linear elastic material.

Many researchers have built upon ideas from the elastic continuum theory and now predict the effects of lateral loads using finite element (FE) analysis. In the finite element method (FEM) the soil mass is typically modeled as elasto-plastic. This allows for soil yielding to take place within the soil profile, which is a more realistic approach to analyze soil reaction for larger pile deflections. FEM are generated to model desired soil conditions and p-y curves from other studies can be built into these models (Reese and Van Impe, 2001). These models have the capability to predict soil-pile reaction to lateral loading with relative accuracy but are highly dependent on the input soil parameters and constitutive soil models (Juirnarongrit, 2002). FEM require intensive computer applications and generally require a considerable amount of time to construct accurate models.

These models (p-y curves, elastic continuum, and FEM) are commonly developed to evaluate the effects lateral loading on a pile foundation with the most widely used being the p-y curve method (Juirnarongrit, 2002).

2.2.1 **Winkler Spring Method Overview**

The Winkler Spring method, also referred to as the subgrade reaction method, was introduced by Winkler (1867) to model a beam on an elastic foundation, where the soil is modeled using independently acting linear-elastic springs (Caduto, 2001). This method was adopted by Hetenyi (1946) and Reese

and Matlock (1956) to design laterally loaded pile foundations. **Figure 2-1** presents this model.

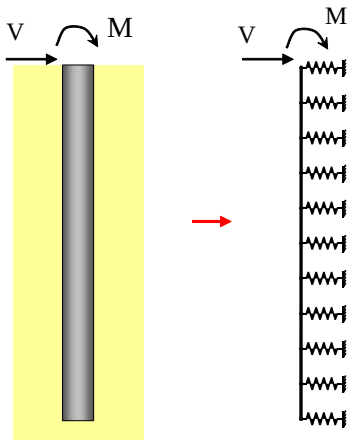

Figure 2-1. Implementation of Winkler Spring concept for laterally loaded piles (from Juirnarongrit, 2002)

The "soil" springs represent the modulus of subgrade reaction, *K*, which is a function of the soil reaction per unit length of pile, *p*, and displacement, *y*, as shown in equation (2.1).

$$K = \frac{p}{y} \tag{2.1}$$

The modulus of subgrade reaction has dimensions of (force/length^2). The soil reaction, p, and displacement, y, have units of (F/L) and (L), respectively.

Using the modulus of subgrade reaction, a fourth order differential equation can be solved to obtain the pile response under lateral loading. This equation is a function of the modulus of elasticity of the pile, E_p, the moment of

inertia of the pile, I_p, the modulus of subgrade reaction, K, and the depth, z, as shown in in equation (2.2).

$$E_p I_p \frac{d^4 y}{dz^4} + Ky = 0 \tag{2.2}$$

Solutions to equation (2.2) have been obtained both numerically and analytically. Hetenyi (1946) provided closed-form analytical solutions to this equation for a selection of subgrade reactions. For each analytical solution, the modulus of subgrade was held constant. Barber (1953) provided solutions to find pile head rotations and deflections at the ground surface as well as solutions with linearly increasing modulus of subgrade reaction with depth.

The Winkler spring method is capable of accounting for multiple soil layers and requires less calculation time than finite element and elastic continuum methods. The major disadvantages include the lack of continuity and the assumptions of a linear-elastic soil response. Methods to estimate the modulus of subgrade reaction for the Winkler spring method have been discussed by Terzaghi (1955) and Vesic (1961).

2.2.2 **Formation of *p-y* Curves**

The solutions to the Winkler spring method or subgrade reaction model is only accurate when the soil reacts to loading in a linear behavior. In actuality, soil reaction is nonlinear and it is dependent on the magnitude of loading and soil stiffness. Modifications of the subgrade reaction model were presented by McClelland and Focht (1958) and account for the nonlinearity of a soil mass and apply independently acting nonlinear soil springs to the previous models. This is commonly known as the p-y curve method, where, p, is the soil pressure per unit length and, y, is the pile deflection.

p-y curves are the most common method to model pile-soil interaction subjected to lateral loading due to the relative ease of modeling multiple soil layers independently with nonlinear soil properties. The stress distribution around a vertically driven pile is assumed to be equal around the circumference when no lateral load is present (Reese et al., 1974). The stress distribution on the face of the pile changes with the application of a lateral load. The soil stresses increase on the pile face in the direction of movement and a decrease on the opposite face as shown in **Figure 2-2**. The decrease in soil pressure behind the pile is typically considered to be in an active state (Gabr and Borden, 1990). The active pressure behind the pile is reduced to zero if a gap forms behind the pile and will affect the predicted displacements and result in a lower actual displacement. Many of the commonly used p-y curves have been developed on the basis of back calculated

results of full-scale lateral load tests conducted on pile foundations (Nimityongskul, 2010).

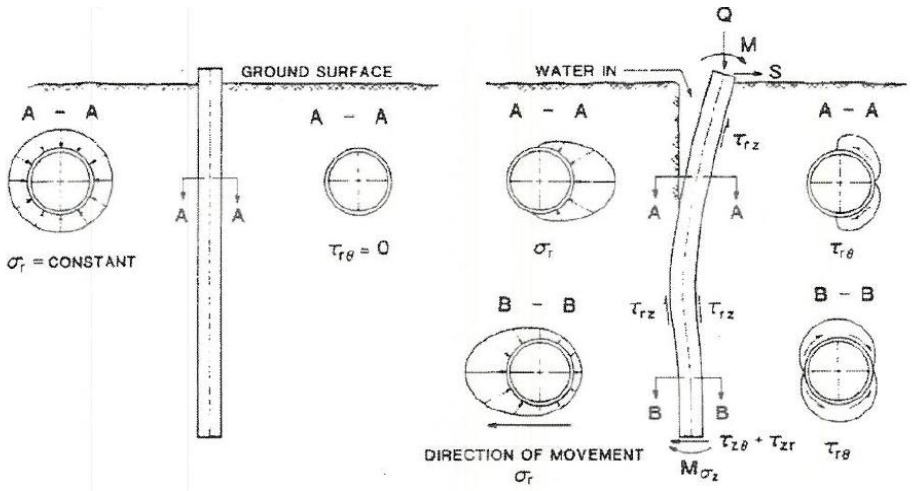

Figure 2-2. a) Soil pressure on a pile at rest b) Soil pressure after lateral load application (from Dunnavant, 1986)

The stress change in the soil from a pile deflection at a given depth is called the soil reaction, p, for that displacement. A p-y curve depicts the nonlinear change in soil reaction as a function of different pile displacement at a defined depth. A set of p-y curves is typically used when analyzing lateral capacities. With increasing depth and changes in soil layers the soil reaction can vary greatly. Sets of p-y curves with differing soil reactions with displacements are modeled along the length of the pile to predict the resulting behavior. This is demonstrated in **Figure 2-3**. Once a set of p-y curves is determined, Equation (2.2) can be solved to produce the deflection, pile rotation, moment, shear, and soil reaction profiles for the length of the pile for a given lateral load (Reese et al., 1974).

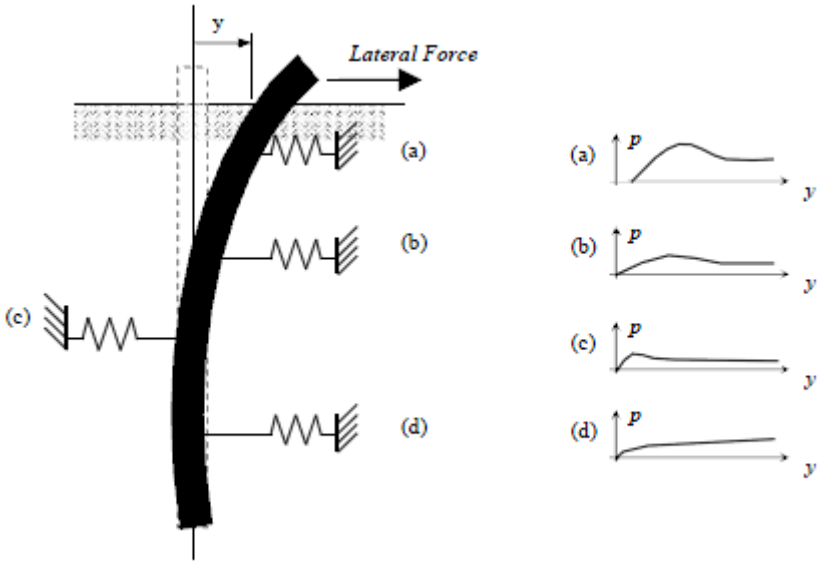

Figure 2-3. Typical set of p-y curves modeled for a pile (from Mirzoyan, 2007)

Research has been conducted to predict p-y curves for a wide range of soil conditions and pile types (e.g. Matlock 1970, Reese et al. 1974, API 1987). Many of these models were developed from full-scale or model tests for piles located in horizontal ground. The following sections will focus on past research conducted on p-y curves development in cohesionless soils accounting for the effects of natural and cut slopes.

2.3 Common p-y Curve Models for Level Ground Conditions in Cohesionless Soils

Several procedures have been suggested by researchers (Brinch 1961; Reese et al. 1974; Poulos and Davis 1980; API 1987) to determine p-y curves and ultimate lateral resistances for piles in cohesionless soils. Common factors influencing these models include estimation of the modulus of subgrade reaction, K, confining pressure, and friction angle. Widely used methods to predict ultimate resistance and p-y curves in cohesionless materials are summarized in the following section.

2.3.1 Reese et al. 1974

Reese et al. (1974) conducted full scale tests on 24 inch diameter piles in clean fine to silty sands with a friction angle, ϕ, of 39°. The water table was above the ground surface during these tests. Static and cyclic lateral load tests were carried out on the test piles. A set of p-y curves and equations were developed based on the experimental results.

Figure 2-4 shows a typical p-y curve for the model presented by Reese et al. (1974). The initial subgrade modulus, E_{si}, considers the soil behavior to be linear elastic at low displacements and is expressed by equation (2.3):

$$E_{si} = kx \tag{2.3}$$

where k is the coefficient of subgrade reaction constant in lb/in^3 and x is the depth below ground surface in inches. The values determined for k from these tests were 2.5 times higher than the values recommended by Terzaghi. **Table 2-1** presents values from Terzaghi (1955) and Reese et al. (1974).

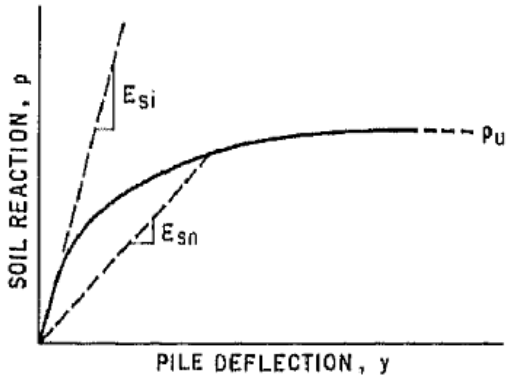

Figure 2-4. Typical p-y curve for the model presented by Reese et al. (1974)

Table 2-1. Recommendations for coefficient of subgrade reaction constant for laterally loaded piles in dry and submerged sand by Terzaghi (1955) and Reese et al. (1974)

	Relative Density of Sand →	**Loose**	**Medium**	**Dense**
Terzaghi (1955)	Dry or moist sand, *k* (lb/in^3)	3.5-10.4	13-40	51-102
Terzaghi (1955)	Submerged sand, *k* (lb/in^3)	2.6-7.7	7.7-26	26-51
Reese et al. (1974)	Submerged sand, *k* (lb/in^3)	20	60	125
Reese et al. (1974)	Dry or moist sand, *k* (lb/in^3)	25	90	225

Figure 2-5 shows the method used by Reese et al. (1974) to compute the ultimate lateral resistance. An assumed passive wedge failure is the source of resistance near the ground surface, acting in front of the pile and active pressures acting behind the pile during lateral movement. The resistance at certain at a critical depth below the ground surface is assumed to be from lateral flow around the pile.

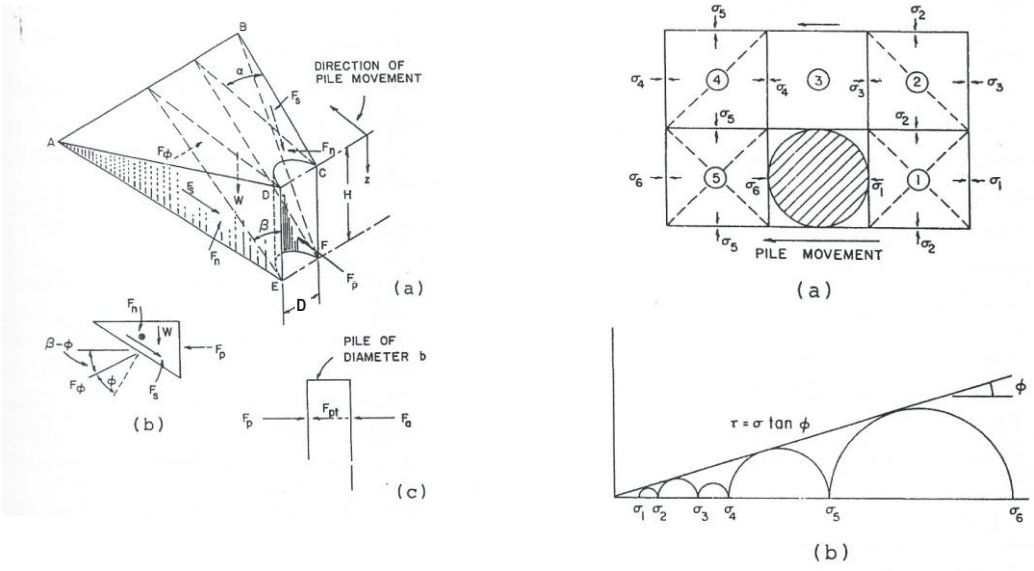

a) assumed passive wedge failure b) assumed lateral flow failure

Figure 2-5. Cohesionless soil failure modes in laterally loaded pile problem. a) assumed passive wedge failure; b) lateral flow failure (after Reese *et al*. 1974)

Based on the results from the full-scale lateral load tests and the presented soil failure modes, Reese et al. (1974) proposed a method to compute p-y curves for cohesionless soils. A typical set of p-y curves is shown in **Figure 2-6** with the procedure and equations summarized in **Table 2-2**. An empirical adjustment factor was used in this method to adjust calculated resistances (from the wedge and soil flow models) to more closely replicated results obtained from the full scale tests.

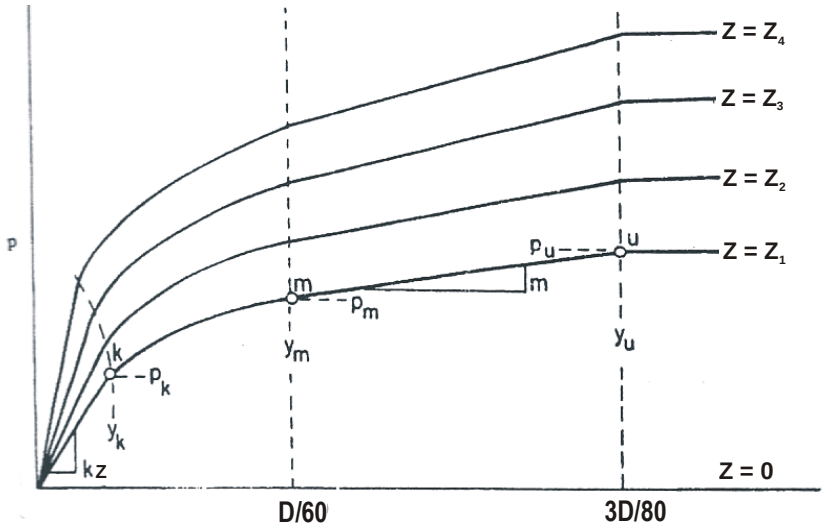

Figure 2-6. Characteristic shapes of p-y curves for sand (Reese *et al*. 1974)

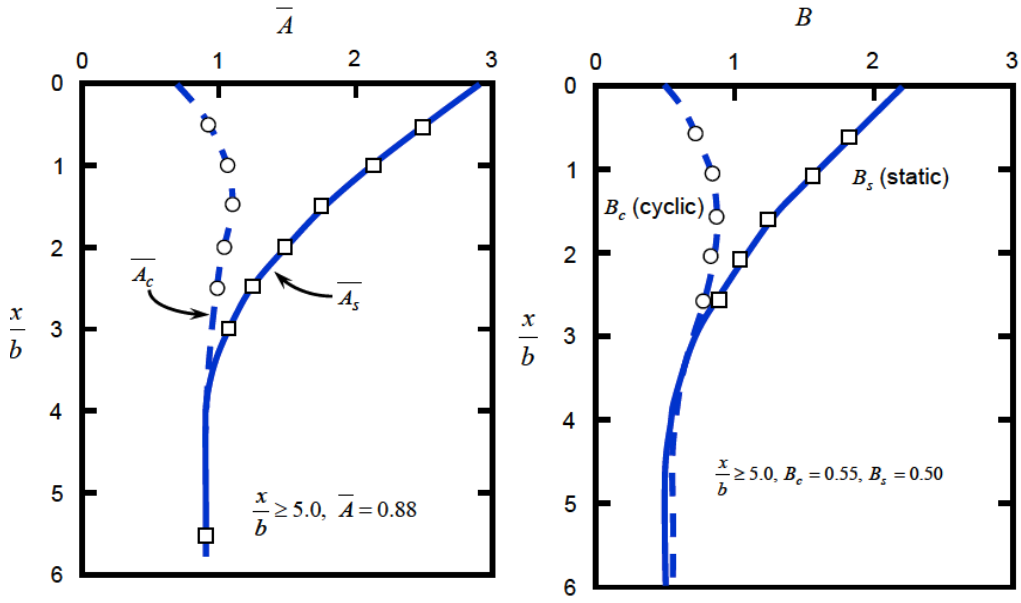

a) Coefficient A b) Coefficient B

Figure 2-7. Values of coefficients used for developing p-y curves for sand; a) Coefficient A ; b) Coefficient B (from Reese *et al*. 1974)

Table 2-2. Summary of procedure in developing Reese et al. 1974 sand p-y curves (table after Nimityongskul, 2010)

Steps	Formula	Eqn.
1. Preliminary Computation	$\alpha = \frac{\phi}{2},\ \beta = 45 + \frac{\phi}{2},\ K_0 = 0.4,\ K_a = \tan^2\left(45 - \frac{\phi}{2}\right)$	(2.4)
2. Compute Ultimate Soil Resistance from Wedge Failure, p_{st}	$p_{st} = \gamma' z \left[\frac{K_0 z \tan\phi \sin\beta}{\tan(\beta-\phi)\cos\alpha} + \frac{\tan\beta}{\tan(\beta-\phi)}(D + z\tan\beta\tan\alpha) + K_0 z \tan\beta(\tan\phi\sin\beta - \tan\alpha) - K_a D \right]$	(2.5)
3. Compute Ultimate Soil Flow Resistance, p_{sd}	$p_{sd} = K_a D\gamma' z(\tan^8\beta - 1) + K_0 D\gamma' z \tan\phi \tan^4\beta$	(2.6)
4. Select Governing Ultimate Soil Resistance, p_s	p_s = the smaller of the values copmuted from Eqn. (2.5) and Eqn. (2.6)	-
5. Ultimate Soil Resistance, p_u	$p_u = \overline{A}_s p_s$ for static loading	(2.7)
6. Soil Pressure at D/60 , p_m	$p_m = B_s p_s$ for static loading	(2.8)
7. Initial Straight Line Curve	$p = (k_{py} z) y$	(2.9)
8. Establish Parabolic Section of *p-y* Curves	$p = \overline{C} y^{1/n},\ m = \frac{p_u - p_m}{y_u - y_m},\ n = \frac{p_m}{m y_m},\ \overline{C} = \frac{p_m}{y_m^{1/n}},$ $y_k = \left(\frac{\overline{C}}{k_{py} z}\right)^{n/(n-1)}$	(2.10)

Variables are defined below:

$\bar{A}_s$	=	Adjustment Coefficient for Static p-y Curves from **Figure 2-7a**
B_s	=	Non dimensional Coefficient for Static p-y Curves from **Figure 2-7b**
D	=	Pile Diameter
k_{py}	=	Coefficient of modulus of subgrade reaction
p_{sd}	=	Theoretical ultimate soil resistance due to flow failure
p_{st}	=	Theoretical ultimate soil resistance due to wedge failure
p_s	=	Govern ultimate soil resistance
p_u	=	Ultimate soil resistance
z	=	Depth
ϕ	=	Friction angle
γ'	=	Effective soil unit weight for soil under water
y_k	=	Transition point between linear and hyperbolic curves
K_0	=	Coefficient of at-rest earth pressure
K_a	=	Coefficient of active earth pressure

2.3.2 **American Petroleum Institute**

The American Petroleum Institute (API) suggested a model to develop p-y curves in cohesionless soils (API, 1987) based on the methods presented by Reese et al. (1974). The API model provides simplified calculation procedures and results in an ultimate lateral resistance of similar magnitude to Reese el. Al (174). The main modification compared to Reese et al. (1974) of the API model is the shape of the p-y curve before the ultimate resistance is reached, thus a change in the initial subgrade reaction**.** **Figure 2-8a** presents a chart to determine this initial subgrade reaction based on a hyperbolic function.

Table 2-3 presents the API method to calculate lateral soil resistance. Similar to the empirical adjustment factor used by Reese et al (1974), API applies

three coefficients to the model as shown in **Figure 2-8b**, which are functions of friction angle.

Table 2-3. Summary of procedure in developing API sand *p-y* curves (table after Nimityongskul, 2010)

Steps	Formula	Eqn.
1. Compute Resistance from Wedge Failure, p_{st}	$p_{st} = (C_1 z + C_2 D)\gamma' z$	(2.11)
2. Compute Soil Resistance from Flow Failure, p_{sd}	$p_{sd} = C_3 D \gamma' z$	(2.12)
3. Select Ultimate Soil Resistance, p_s	p_s = smaller of the values of step 2 and 3	(2.13)
4. Adjustment Coefficient for Static Loading	$\overline{A}_s = \left(3.0 - 0.8\frac{z}{D}\right) \geq 0.9$ for static loading	(2.14)
5. Develop Characteristic Shape of p-y Curves	$p = \overline{A} p_s \tanh\left(\frac{kz}{\overline{A} p_u} y\right)$	(2.15)

where: $\overline{A}_s, \overline{A}_c$ = Adjustment Coefficient for Static and Cyclic p-y Curves
C_1, C_2, C_3 = Coefficients from **Figure 2-8b**
D = Pile Diameter
k = Coefficient Modulus of Subgrade Reaction in **Figure 2-8a**
p_{sd} = Theoretical Ultimate Soil Resistance due to Flow Failure
p_{st} = Theoretical Ultimate Soil Resistance due to Wedge Failure
p_s = Govern Ultimate Soil Resistance
p_u = Ultimate Soil Resistance
z = Depth
ϕ = Friction Angle
γ' = Effective Soil Unit Weight for Soil under Water

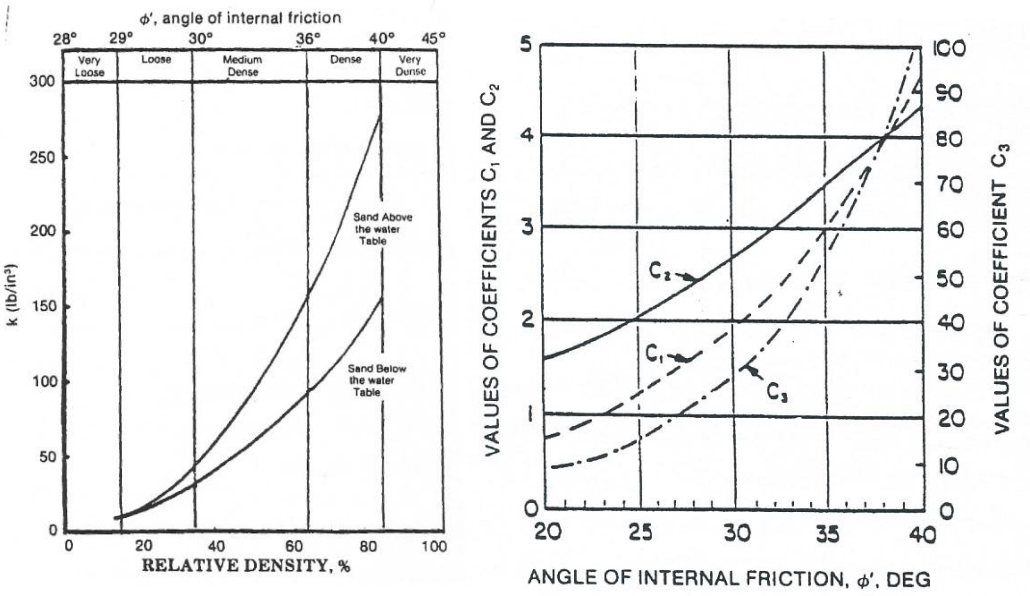

(a) (b)

Figure 2-8. Charts for developing sand *p-y* curves (API 1987); a) coefficients as function of ϕ ; b) coefficient of modulus of subgrade reaction

2.4 **Lateral Load Tests in Cohesionless Soils near Slopes**

In many of the studies conducted to examine slope effects on lateral capacities, near slope load-displacement curves are commonly normalized with baseline test results. This is typically known as the ultimate lateral resistance ratio or load ratio, Ψ. This ratio is calculated from the ultimate resistance:

$$\psi = \frac{p_{u\,slope}}{P_{u\,level}} \tag{2.16}$$

where $p_{u\,slope}$ is the ultimate lateral resistance for a near slope pile and $P_{u\,level}$ is ultimate lateral resistance for a pile located in level ground.

2.4.1 **Gabr and Borden (1990)**

Gabr and Borden (1990) examined lateral capacities of piers constructed in and near sloping ground. A model to estimate the ultimate soil resistance, Pu, is expressed by conducting a three-dimensional wedge equilibrium analysis. This model is then used to construct p-y curves for pier located in sloping ground and is based on the passive strain wedge model presented by Reese (1962).

Figure 2-9 shows the wedge model constructed by Gabr and Borden (1990) resisting lateral movement. An assumption of this wedge model is that the pier is a rigid cylinder moving laterally in the soil. The pier is compressed laterally until a passive state is reach in the soil in front of the pier. The soil behind the pier is in an active condition. The pier is assumed to be frictionless and vertical displacements are neglected. The ultimate soil resistance is calculated by summation of the resisting forces along the side and bottom plains of the assumed failure wedge in a lateral direction.

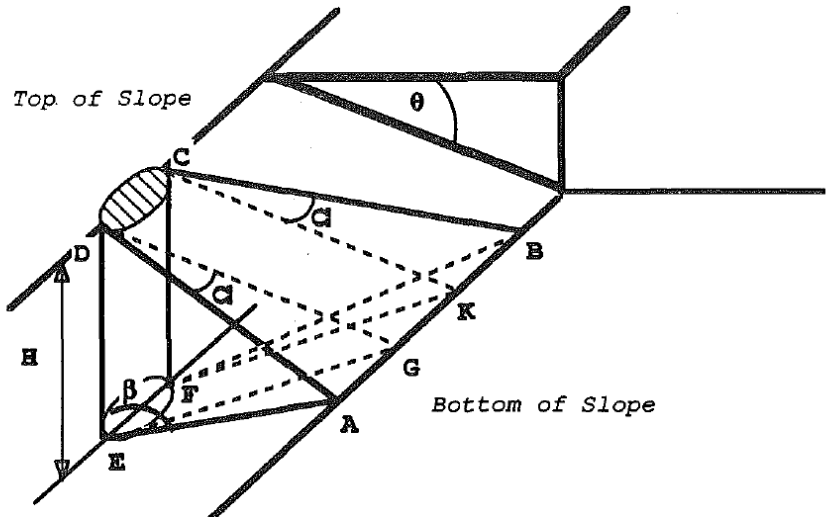

Figure 2-9. Assumed passive failure wedge (from Gabr and Borden, 1990)

The Gabr and Borden (1990) model relies on key soil parameters including friction angle and cohesion of the soil, slope angle, effective unit weight, and the modulus of subgrade reaction. These parameters are important in determining the angle that defines the displaced wedge size, Ω, and the angle of the failure wedge, β as shown **Figure 2-9**. According to Reese (1974) and API (1987), a common value for the angle, Ω, is ϕ/2 for horizontal soil profiles, where ϕ is the friction angle of the soil. Bowman (1958) recommends ϕ/3 to ϕ/2 for loose sands and ϕ for dense sands based on experimental results. Gabr and Borden (1990) assumed ϕ/2 for the developed strain wedge model. Equation (2.17) through Equation (2.23) is presented in this study to determine the ultimate lateral resistance, P_u.

$$P_u = \gamma H[H(S_{1\phi} + 3K_0 S_{3\phi}) + bS_{2\phi} - K_a b] + c[H(S_{1c} + S_{3c}) + bS_{2c} - 2bK_a{}^{0.5}] \quad (2.17)$$

Where:

$$S_{1\phi} = \frac{\lambda_2 \tan\Omega \tan\beta}{(\tan\theta\tan\beta + 1)^2}[(\tan\theta\tan\beta + 1)(3 + 4\tan\phi\tan\beta) - (2\tan\phi\tan\beta) \quad (2.18)$$

$$S_{2\phi} = \frac{2\lambda_2}{\tan\theta\tan\beta + 1}(1 + \tan^2\phi) \quad (2.19)$$

$$S_{1c} = \frac{2\tan\Omega\tan\beta}{(\tan\theta\tan\beta + 1)^2}[\lambda_1(1 + 2\tan\theta\tan^2\beta + \tan\beta) + 2\tan\beta(\tan\theta\tan\beta + 1) - \tan\beta)] \quad (2.20)$$

$$S_{2c} = \lambda_1 + \frac{1 + \lambda_1\tan\phi}{\tan\theta\tan\beta + 1} \quad (2.21)$$

$$S_{3\phi} = (\tan\phi - \tan\Omega)\left[\tan\beta - \frac{\tan^4\beta\tan^3\theta + \tan^3\beta\tan^2\theta}{(\tan\beta\tan\theta + 1)^3}\right] \quad (2.22)$$

$$S_{3c} = \tan\beta - \frac{\tan^3\beta\tan^2\theta + \tan^2\beta\tan\theta}{(\tan\beta\tan\theta + 1)^2} \quad (2.23)$$

P_u = total lateral resistance

K_a = coefficient of active earth pressure

K_0 = coefficient of at rest earth pressure

b = pile diameter

H, Ω, β, θ are defined in **Figure 2-9**

Gabr and Borden (1990) conducted a parametric analysis on the presented wedge model. **Figure 2-10** presents the lateral resistance ratio,Ψ, for a pile located on the crest of a slope with different friction angles and slope angles. To verify the assumed failure wedge model, Gabr and Borden (1990) conducted five full scale load tests. The lateral load test on the piles was carried out on a 3.5H:1V slope with the piles on the slope crest.

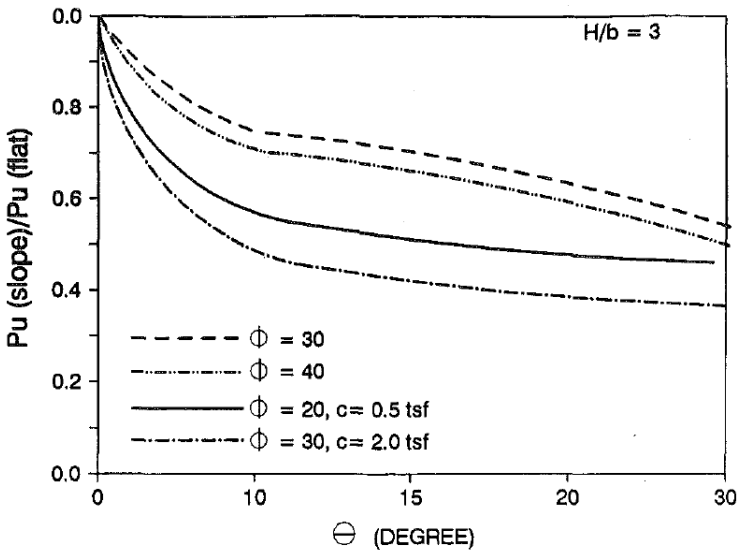

Figure 2-10. Ultimate lateral resistance ratio as a function of slope angle, θ, and friction angle, ϕ. (after Gabr and Borden, 1990)

Gabr and Borden (1990) concluded that this model tended to under predict the measured capacities in the field test at higher displacements. During field testing, a gap was observed behind the cohesionless test pile. This implies that the recommendation to account for active earth pressure behind the test pile is, at

least in part, leading to this underestimation. Accounting for the active force can account for a 5-10% decrease in estimated lateral resistance. A model including active pressure was considered to be conservative.

Ultimately, the slope model presented by Gabr and Borden (1990) was within 15%-25% of the measure response from field tests. Ignoring the presence of the slope may result in an overestimation of the lateral capacity of a pier or pile by up to 50%. The assumed failure wedge model reasonably predicted the failure mechanisms in cohesionless soils and the assumed value of $\phi/2$ for Ω is acceptable and considered conservative. The proximity of a slope and therefore the reduction in lateral capacity is dependent on the soil strength parameters and the slope angle, θ.

2.4.2 **Mezazigh and Levacher (1998)**

Mezazigh and Levacher (1998) conducted a program investigating slope effects on p-y curves. Centrifuge tests were carried out on scaled-piles driven into dry, fine sand. Each test pile was spun to 40 g in a test centrifuge. Multiple tests were performed in level ground conditions, and near two slopes with dimensions of 2H:1V and 3H:2V. Piles were tested at distances between 0 and 12 *D* from the test slope where D represents pile diameter. Relative densities, D_r of 51% and 81% were used during this experiment to examine the effects of density in relation to slope and lateral capacities.

The results from Mezazigh and Levacher (1998) tests demonstrated that for a given load, displacements are 1.6 times greater for a pile tested on the 2H: 1V slope when compared to the reference pile as shown in **Figure 2-11**. This factor increased to 2.4 times for a 3H:2V slope. The effects of the 2H: 1V slope are negligible for piles located at D = 8 or greater and for the 3H:2V slope at D = 12 or greater.

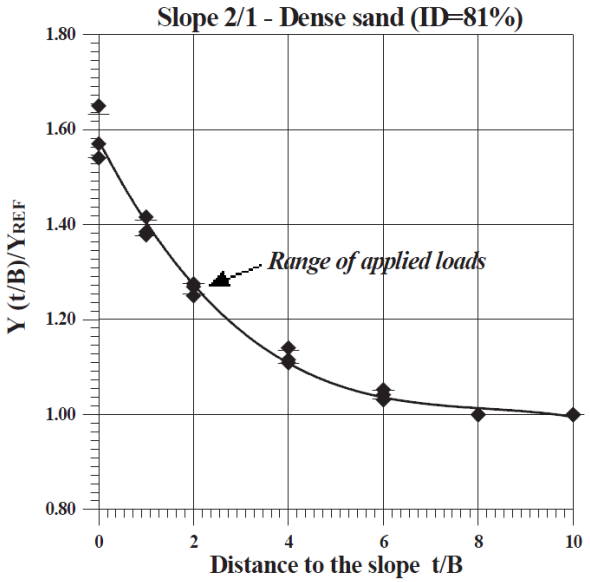

Figure 2-11. Displacement ratios for pile located near at 2H:1V slope, note: t/b is distance in pile diameters (after Mezazigh and Levacher, 1998)

Mezazigh and Levacher (1998) found that point of maximum moment developed at deeper locations as the pile approached the slope crest. This location varied from 0.2L to 0.3L, where L is the embedded pile length. The maximum moment for the pile on the slope crest (D = 0) was 25% greater at the slope crest than the reference pile, and it is even greater for the steeper slope. P-y curves

were back-calculated by double differentiation and double integration of the bending moment curves. Analysis of the p-y curves demonstrates a non-linear parabolic shape for soil-pile p. **Figure 2-12** presents resulting p-y curves for piles at different distances from the 2H:1V slope at a constant depth of 1.67m. This indicates that at a given depth, the influence of a slope is greater as the pile is located closer to the crest. The crest not only affects the capacity of the soil-pile system, but also the initial soil modulus. The 3H:2V slope had an ultimate resistance of 35% less than the 2H:1V slope.

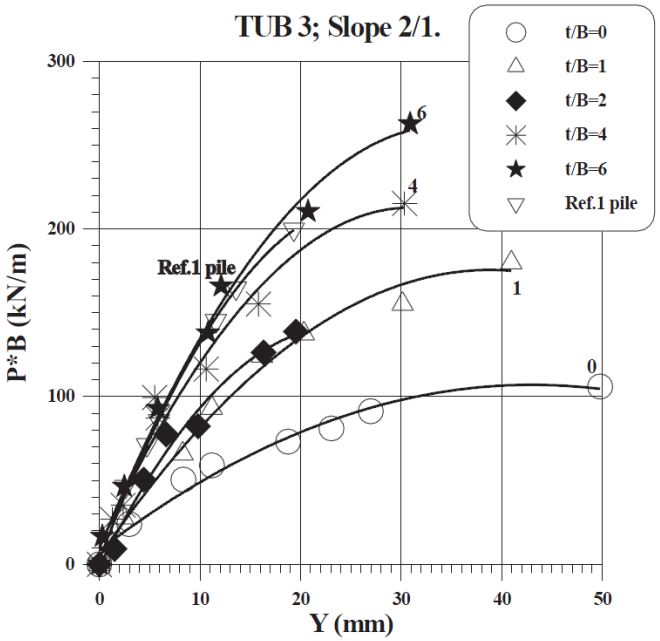

Figure 2-12. *p-y* curves at different distances from the crest at a depth of 1.67 pile diameters (after Mezazigh and Levacher, 1998)

From the results obtained from centrifuge tests in sands, Mezazigh and Levacher (1998) presented reduction coefficients, $r_{(D)}$ that can be applied to p-y curves for piles in level ground. The results recommend multiplying the resistance pressure, p, by a reduction coefficient, r, as shown in Equation (2.24) through Equation (2.26):

$$P_{(D)} = r_{(D)} P_{level} \tag{2.24}$$

$$\begin{cases} r_D = \dfrac{17 - 15\tan\beta}{100} \cdot \dfrac{t}{D} + \dfrac{1 - \tan\beta}{2} & \text{if} \quad t \le t_{\lim} \\ r_D = 1 & \quad\quad\; t > t_{\lim} \end{cases} \tag{2.25}$$

$$t_{lim} = 4D(6\tan\beta - 1) \tag{2.26}$$

where t is the distance from the slope crest to the center of the pile, D is the pile diameter, β is the slope angle, and t_{lim} is the distance of no slope effect. Mezazigh and Levacher (1998) compared these reduction coefficients with the curves obtained by the computer program PILATE (Frank et al. 1990, 1994). The centrifuge tests determined that the relative density of the sand had negligible effects on the corresponding reduction coefficients. A graphical interpretation of the determined reduction coefficients are shown in **Figure 2-13** for a 2H:1V slope and a 3H:2V slope.

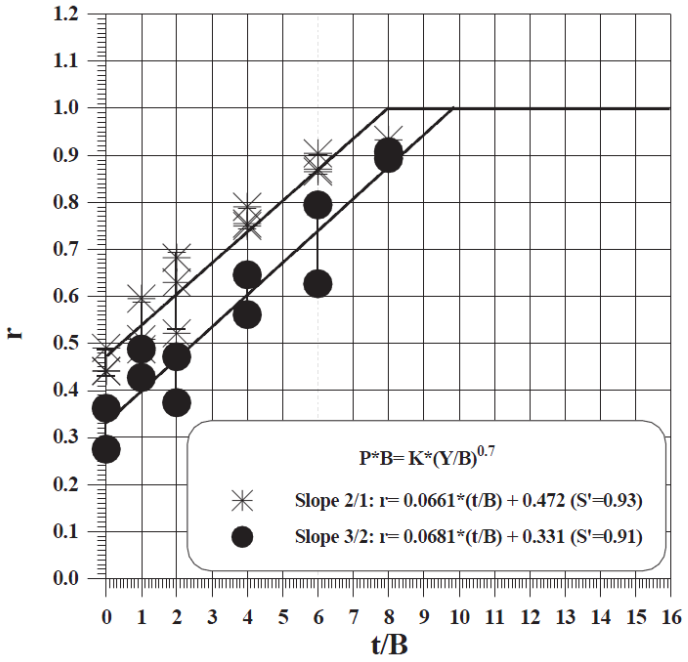

Figure 2-13. Values of the reduction coefficient proposed by Mezazigh and Levacher (1998); Note: t/B is distance in pile diameters

2.4.3 **Chen and Martin (2001)**

Chen and Martin (2001) examined the effects of an embankment slope on lateral pile response in c-ϕ soil conditions by conducting finite difference analyses. Using the computer modeling program FLAC, a wide-ranging parametric study was completed to determine the important parameters affecting p-y curves and lateral resistance. An investigation on the strain wedge model and passive wedge failure (Reese et al., 1974) was examined.

Chen and Martin (2001) verified the accuracy of the finite difference analyses by comparing results with two published full-scale load tests. This

verification was performed for a soft saturated clay soil and a dense clean to silty sand, from the Sabine River Test (Matlock, 1970), and the Mustang Island Test (Reese et al., 1974), respectively. **Figure 2-14** shows the effects of varying slope angles on the lateral resistance ratio as a function of distance of pile diameters to the crest. These ratios ranged from 0.73 to 0.11 for the c-ϕ soil analyzed in the finite difference model. For single piles placed at a distance of 6 pile diameters or greater from the slope crest, the effect on the ultimate soil resistance is less than 10% for slopes with angles less than 45° and the presence of the slope can be neglected.

For all tests conducted in the finite difference model, in level ground and near a slope, a clearly defined failure wedge was observed. In the level ground c-Φ soils analyses the failure wedge was semi-elliptical in shape. Chen and Martin (2001) suggest that the presence of a slope cause the soil wedge to form deeper, mobilize in a more horizontal angle, and have a larger wedge fan angle.

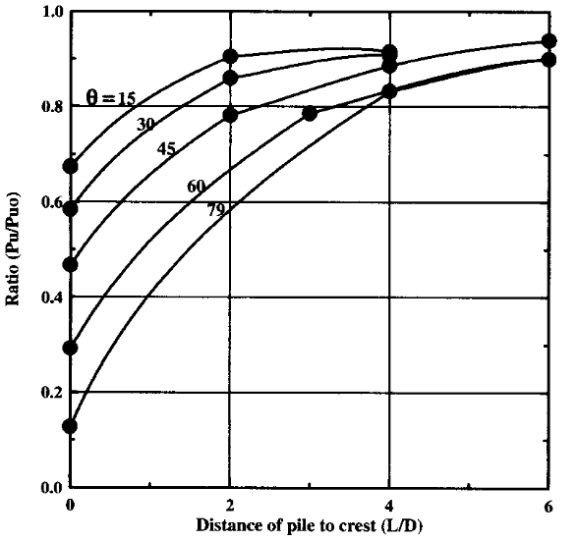

Figure 2-14. Effects of varying slope angles on the soil resistance ratio as a function of distance of pile diameters to slope crest (after Chen and Martin, 2001); Note: L/D is Distance in pile diameters

2.4.4 **Chae et al. (2004)**

Chae et al. (2004) conducted several studies investigating the lateral resistance of piles located near slopes. Three dimensional finite-element analyses along with scaled-model tests were conducted on laterally loaded short piles or pier foundations situated in proximity to slopes consisting of dense sand.

The scaled-model test was conducted for short piles near a 30° test slope and in horizontal ground conditions for use as a reference. A clean sand with a relative density Dr of 90% and a corresponding friction angle of 47.5° were used in this experiment. The scaled-model lateral testing was conducted at 0D, 2D, and 4D where D is the pile diameters from the crest.

Chae et al. (2004) considered the elastic-perfectly plastic behavior model as the most appropriate model to describe the soil in the three dimensional finite-element model analyses. In reality soil behaves in a nonlinear behavior. To represent the pile, a linear elastic model was employed. This FEM series was calibrated to represent similar soil conditions and friction angle of the scaled model.

Figure 2-15 shows load displacement curves from the FEM analyses and scaled-tests for piles located near a slope crest. The FEM analysis underestimates the lateral load for piles located in horizontal ground and 4 diameters behind the crest. The other results, piles closer to a slope crest, agree reasonably well between the FEM and scaled-model tests. As found in previous studies, the lateral load was adversely affected as the distance from a slope crest decreased.

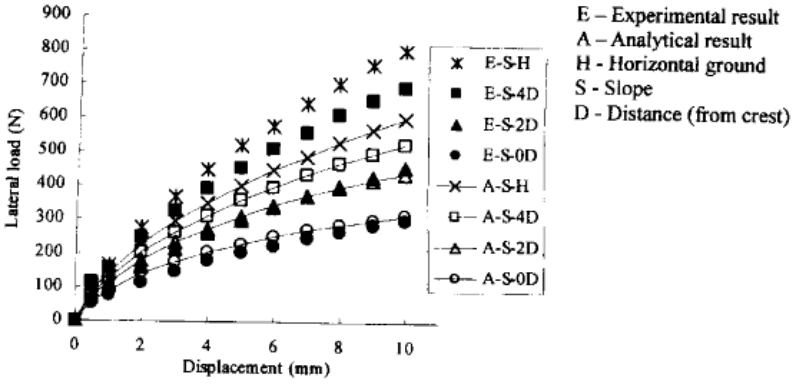

Figure 2-15. Loading curves for experimental and analytical results (after Chae et al., 2004)

Figure 2-16 shows the normalized load ratio with displacement for the experimental and analytical tests. The scaled-model test had an ultimate lateral resistance ratio of about 0.4, 0.6, and 0.85 for load tests located at 0, 2, and 4 diameters behind the slope crest, respectively. The results from the FEM analytical predicted ratios of 0.6, 0.8, and 0.9 for equivalent pile locations. Both models predict a slight decrease in load ratio with increased lateral load displacement. Chae et al. (2004) conclude that the lateral resistance from proximity of a soil slope is noticeable at small displacements and the change is relatively constant as pile head displacements increase.

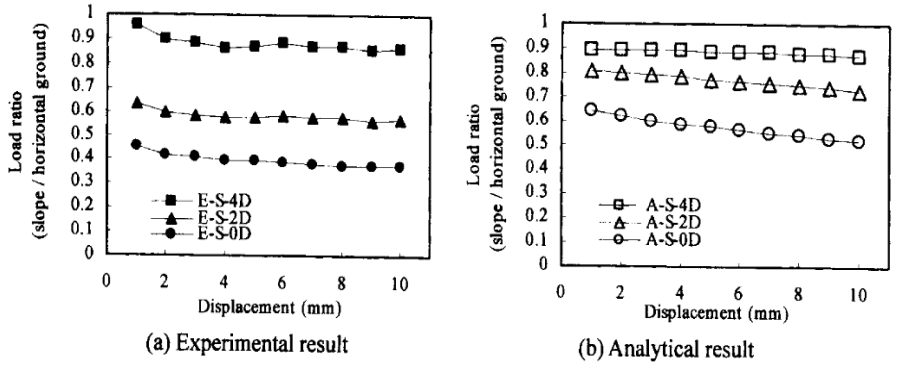

Figure 2-16. Normalized loading curves a) experimental results b) analytical results (after Chae et al., 2004)

To check the validity of the FEM Analyses, Chae et al. (2004) examined the results from full-scale field tests by Takeuchi and Okada (1986) on pier foundations. The FE results tended to slightly over predict the subgrade reaction with depth but held the same general shape. Overall, Chae et al. (2004) observed

that the 3D elasto-plastic FEM is an effective tool in the evaluation of short pile and pier foundations located near a soil slope.

2.4.5 **Reese et al. (2006)**

Reese et al. (2006) present a modified method of Reese et al. (1974) to determine the ultimate lateral resistance of a single pile located on a slope loaded in the downslope direction. This method, as shown in Equation (2.27), is valid for slopes less steep than the friction angle of the cohesionless materials. The modifications in this equation assumed that only the passive wedge failure needed modification and the flow-around failure is not affect by a slope (Reese et al., 2004).

$$(p_u)_{sa} = \gamma H \left[\begin{array}{l} \dfrac{K_0 z \tan\phi \sin\beta}{\tan(\beta-\phi)\cos\alpha}(4D_1^3 - 3D_1^2 + 1) + \dfrac{\tan\beta}{\tan(\beta-\phi)}(bD_2 + z\tan\beta\tan\alpha D_2^2) \\ +K_0 z \tan\phi \sin\beta - \tan\alpha)(4D_1^3 + 3D_1^2 + 1) - K_a b \end{array} \right] \quad (2.27)$$

Where:

$$\beta = 45° + \frac{\phi}{2} \quad (2.28)$$

$$D_1 = \frac{\tan\beta\tan\theta}{\tan\beta\tan\theta + 1} \quad (2.29)$$

$$D_2 = 1 - D_1 \quad (2.30)$$

$$K_a = \cos\theta \frac{\cos\theta - \sqrt{(\cos^2\theta - \cos^2\phi}}{\cos\theta + \sqrt{(\cos^2\theta - \cos^2\phi}} \quad (2.31)$$

b = Pile diamter

K_0 = Coefficient of at rest earth pressure

$\alpha = \phi$ for dense sand

$\alpha = \frac{\phi}{2}$ for loose sand

θ = Slope Angle

2.4.6 **Mirzoyan (2007)**

Mirzoyan (2007) carried out a near slope full-scale lateral load test in a cohesionless soil. The testing consisted of three lateral load tests on 12in diameter steel pipe piles located on the crest (0D) slope and three pile diameters (3D) behind the crest. A baseline tests was also conducted to in horizontal ground for comparison of results. Each pile was laterally loaded in partially saturated dense sand with a relative compaction of 95% and a friction angle of 39°. The 0D and 3D piles tests near a 30° slope as shown in **Table 2-4**.

Table 2-4. Mirzoyan (2007) near slope test variables

Pile Location, X/b:	0	3
Diameter, b (in.):	12.75	12.75
H/b ratio:	9.5	9.5
Angle β (deg.):	65	65
Angle Ω (deg.):	32	22.5
Slope angle, θ (deg.):	30	30
Soil unit weight, γ (pcf):	115	115
Internal friction, ϕ (deg.):	40	40

Figure 2-17 shows the resistance ratios between the baseline test and the near slope tests. The ultimate resistance was reduced by 23% and 7% for piles located at 0D and 3D respectively. The resistance ratio decreased from the beginning of the test to a displacement of 0.5 inches and remained relatively constant for larger pile head displacements. The presence of the slope increased the maximum bending moment by up to 30-40% depending on the pile location. The maximum bending moment ratio increased with increasing pile displacement.

Mirzoyan (2007) found that the computer program LPILE could only predict the results when greatly increasing the friction angle for the pile tested in level ground. LPILE greatly overestimated the reduction in lateral resistance from the presence of the 30° slope, by up to 20%. During full-scale testing a gap was formed behind each pile and it was suggested that no active force was applied behind the pile.

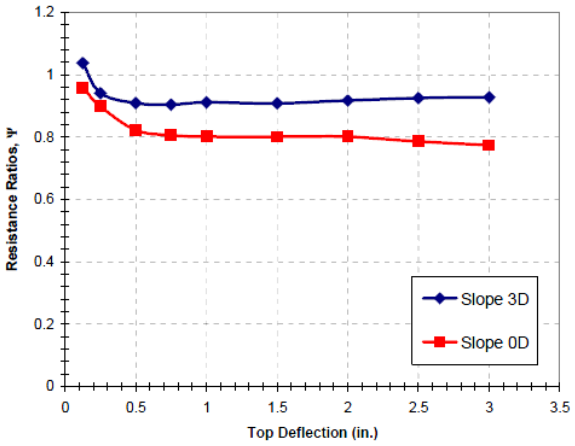

Figure 2-17. Resistance ratios at target deflections (after Mirzoyan, 2007)

2.4.7 **Muthukkumaran et al. (2008)**

Muthukkumaran et al. (2008) conducted extensive centrifuge model tests to examine the effects of slope on p-y curves in dry sand. Multiple tests were conducted in slopes of 1V:1.5H, 1V:1.75H, and 1V:2H. All lateral load tests conducted in the centrifuge model were conducted on the slope crest in relative densities ranging from Horizontal ground tests were also conducted for comparison of results.

Figure 2-18 presents the dimensionless p-y curves for the test pile located on the crest of 1V:1.5H slope with baseline results. This figure shows as depth increases the ultimate soil resistance increases. Muthukkumaran et al. (2008) suggestest that this is a result of an increase in passive resistance resulting from an increase in overburden pressure as the depth increases. **Figure 2-19** shows effects of slope angle on dimensionless p-y curves.

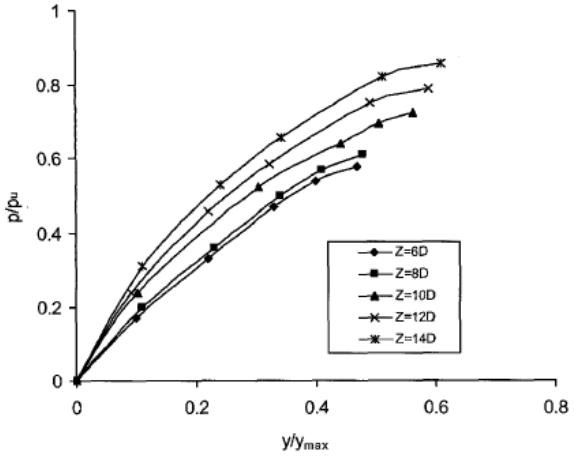

Figure 2-18. Non-dimensional p-y curves at various depths for a 1v: 1.5h slope (after Muthukkumaran et al., 2008)

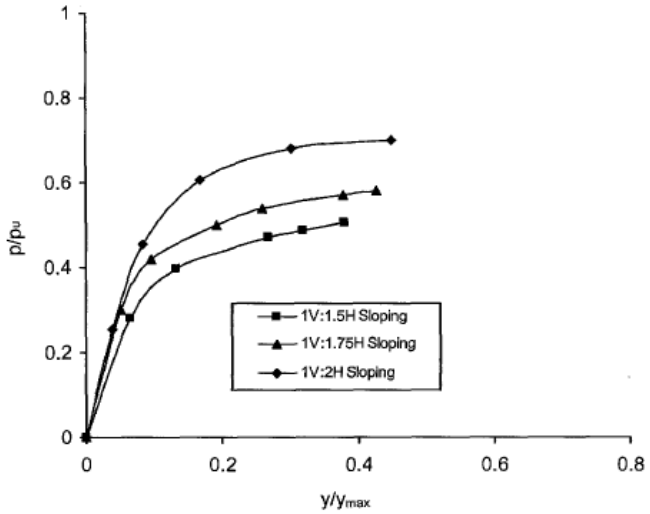

Figure 2-19. Effect of slope angle p-y curves (after Muthukkumaran et al., 2008)

Muthukkumaran et al. (2008) conducted a multiple regression analysis on the normalized p-y. A reduction factor, R, was developed to account for variable slope angles and depth (Z/D) as independent variables. This reduction factor was

applied to the resistance, p, for a given displacement, y, in the API (1987) method. The modified API RP 2A method (1987) is presented in Equation (2.32):

$$p = A \cdot R \cdot p_u \cdot \tanh\left[\frac{k \cdot z}{A \cdot R \cdot p_u} y\right] \tag{2.32}$$

Where:

$$A = \left(3.0 - 0.8\frac{z}{D}\right) \geq 0.9 \text{ for static loading} \tag{2.33}$$

R = Factor to account for sloping ground

p_u = Ultimate bearing capacity at depth,

k = Initial modulus of subgrade reaction

z = Depth

y = Lateral deflection

The reduction factor to account for a soil slope in cohesionless material, as proposed by Muthukkumaran et al. (2008), can be calculated by using Equation (2.34):

$$R = 0.74 + 0.0378\left[\frac{z}{D}\right] - 0.6315(S) \tag{2.34}$$

where R is less than one and S is the slope angle in radians (between 0.50 to 0.66 radians). **Figure 2-20** graphically depicts the reduction factor, R, presented in Equation (2.34), for slopes of 1V :1.5H, 1V :1.75H, and 1V :2H. Other findings

of this study include that an increase in slope increases the bending moment and an increase in relative density decreases the maximum bending moment.

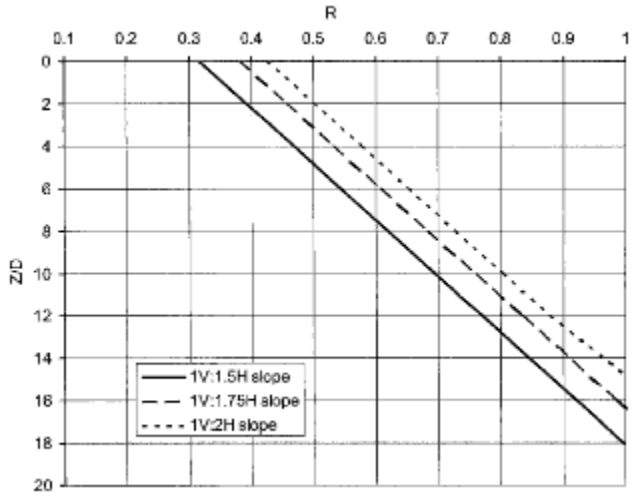

Figure 2-20. Proposed reduction factors to account for effects of slope angle as a function of depth (after Muthukkumaran et al., 2008)

2.5 **Other Considerations**

Other factors effecting lateral loading include pile diameter, loading rate, and pile group effects. Juirnarongrit and Ashford (2003) examined the effects of pile diameter during lateral loading by examining the initial modulus of subgrade reaction. Reese et al. (2006) discusses the effects of different loading types on p-y curves including short term static, long term static, repeated cyclic, and dynamic loading types. Many researchers have summarized the effects of pile groups in level ground including Bogard and Matlock, (1983); Brown et al., (1987); Rollins et al., (2003); Rollins et al., (2005); and Walsh, (2005). For a more in depth

review of lateral load methods in level ground or slope effects in cohesive soils, please see Juirnarongrit (2002) and Nimityongskul (2010), respectively.

2.6 **Summary**

The majority of the research examining the effects of a cohesionless slope on lateral pile capacity has been conducted using analytical, scaled, or computer models. Very few full-scale studies have been conducted near slopes, and it is important to determine if these models and procedures can accurately predict full-scale effects. Most researchers present either load resistance ratios or p-multipliers (reduction factors) to quantify to effects of the slope. These values vary, significantly in some cases, between studies. **Figure 2-21** presents a summary of load resistance ratios from different researchers. The variation in this figure can be attributed to the parameters used in each study including slope angle, density, friction angle, and modeling method (analytical, FEM, model, centrifuge, full-scale, etc.). The key conclusions from studies conducted for near slope piles include:

1. The effect of slope on the lateral resistance and p-y curves is decreases soil resistance and stiffness with increasing distance from the slope crest.
2. Slope effects are negligible at a distance somewhere between 5 to 18 pile diameters.
3. Slope angle, θ, has a significant impact on lateral resistance.

4. The subgrade reaction modulus is dependent on confining pressure.
5. The magnitude and depth of the maximum moment increase with the presence of a slope.

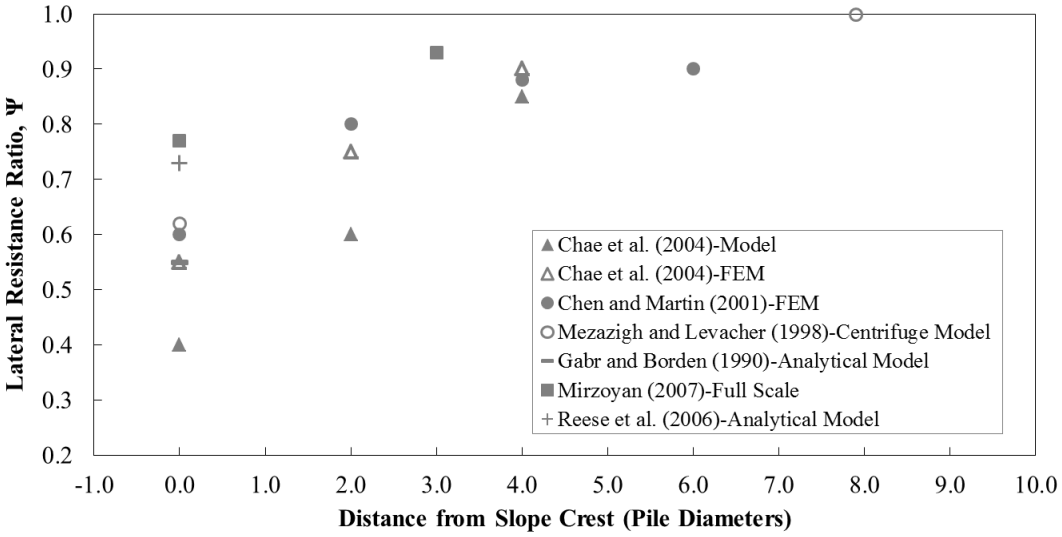

Figure 2-21. Comparison of resistance ratios presented by researchers as a function of distance from a slope crest

Based on the findings found in this literature review, full-scale test results for piles located near a cohesionless slope are limited. The majority of the methods are analytical or scaled models and the findings from the results are scattered. Many of these methods are used in full-scale predictions but have not been validated. To account for these research gaps, a full-scale testing program was conducted on piles located in or near a cohesionless slope crest with the objective of understanding full-scale lateral pile response.

3. SITE DESCRIPTION AND SOIL PROPERTIES

3.1 Introduction

This full-scale research project was conducted at the Geotechnical Engineering Field Research Site (GEFRS) located in Corvallis, Oregon. The testing site is on the Oregon State University campus 0.1 miles west of the SW 35th Street and Jefferson Street intersections. This site was chosen to carry out full scale tests because of the extensive site investigations conducted over the past 40 years (Dickenson, 2006). A map of the testing location and an aerial photograph of the testing site are shown in **Figure 3-1** and **Figure 3-2**, respectively.

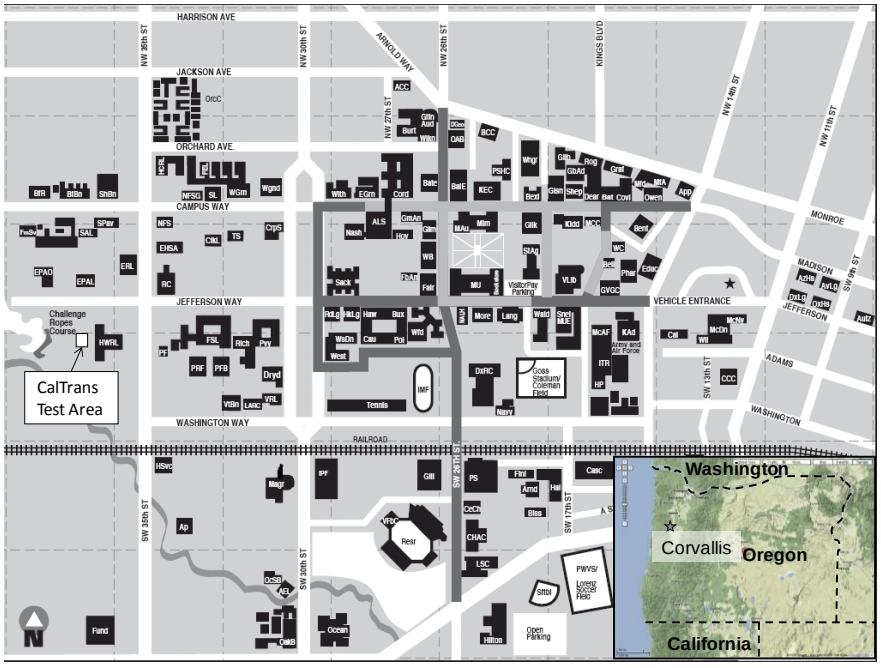

Figure 3-1. General site location in Corvallis, Oregon (adopted from OSU website 2008, Google Map, 2008)

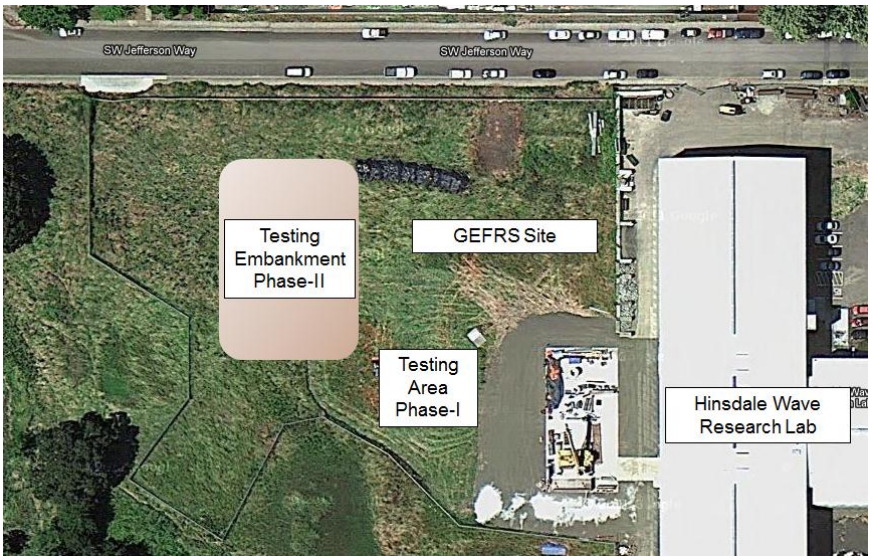

Figure 3-2. Aerial view of GEFRS site (Google Map, 2012)

3.2 **Native Soil Conditions**

The lateral load tests presented in this report are part of the second phase of a larger lateral load testing series. The effects of a cut slope and batter angle on the lateral capacities of piles in cohesionless soil was the scope of the second phase. Testing for phase one was also conducted at the GEFRS to examine similar effects in cohesive soils and was carried out by Nimityongskul (2010).

The in-situ or native soil conditions are constant across the GEFRS site from examination of cross sections created by previous borings in the area as shown Appendix A. As summarized by the GEFRS Report (Dickenson, 2006), the top 10ft of the site consists of stiff to very stiff cohesive soils underlain by a 3ft layer of dense, poorly graded sand and silt. A stratum of medium stiff sandy silt lies between the depths of 13ft to 18ft. The following 5ft of soil consists of

well-graded sand with seams of silt and gravels. This is underlain by very stiff, highly plastic blue-gray clay to depths greater than 70ft. The water table typically fluctuates between 3ft to 7ft below the ground surface. Soil property information including index texts, SPT, and triaxial data from the GEFRS Report is located in Appendix A.

3.3 **Cohesionless Soil Embankment**

The native surface soils consist of clays to silty clays, therefore an acceptable cohesionless material was needed to carry out lateral load experiments at the GEFRS location. A cohesionless structural backfill material was delivered to the site. With this material an embankment was constructed to an elevation of 10 ft above the native surface with a 2H:1V test slope. This elevation was chosen because the majority of lateral pile resistance is developed in the top 5-10 piles diameters (Reese and Van Impe, 2001). Note that the diameter for the test piles for this project equaled 12 inches.

3.3.1 **Cohesionless Soil Properties**

A cohesionless soil was processed by a local aggregate supplier to match the Caltrans structural backfill gradation specification (Caltrans, 2006) to construct the embankment. **Table 3-1** summarizes the gradation requirements of this Caltrans specification with an added fines constraint. This constraint required

the material to have less than 12% fines passing the number 200 sieve. **Figure 3-3** presents the final gradation curve for the material used during testing. This well-graded material had a coefficient of uniformity (C_u) of 41.0 and a coefficient of curvature (C_c) of 4.8. **Table 3-2** shows equivalent percent passing grain size diameters for the testing material. With an average of just less than 10% fines, the Unified Soil Classification System (USCS) classifies this soil as a well-graded sand (SW).

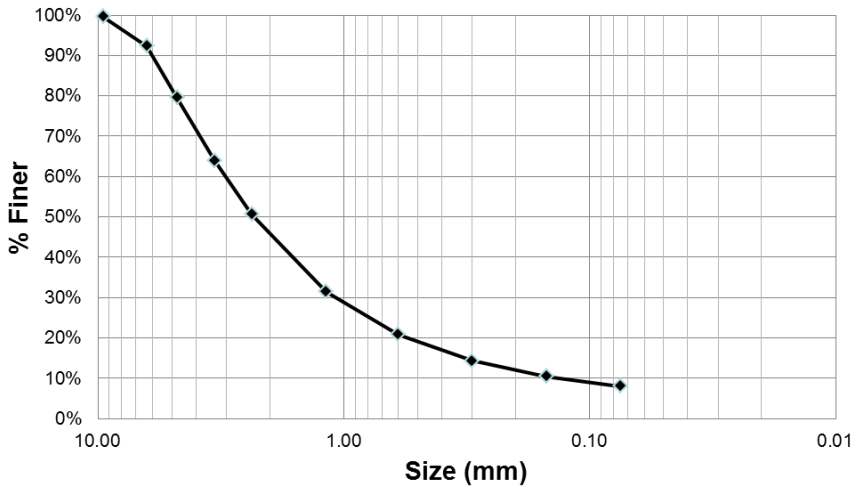

Figure 3-3. Gradation curve of the cohesionless soil

Table 3-1. Standard specifications for granular backfill material with added fines constraint (Caltrans 2006)

Sieve Size	Percent Passing (%)
3 "	100
No. 4	35-100
No. 30	20-100
No. 200	0-12

Table 3-2. Particle diameter based on percent finer

Percent Finer (%)	Diameter (mm)
D_{60}	3.33
D_{50}	2.79
D_{30}	1.14
D_{10}	0.08

3.3.2 **Embankment Construction**

The embankment was constructed in 8 inch compacted lifts in accordance to Caltrans Standard Specifications 19-3.06 (2006) to a final elevation of 10ft above the native ground surface. Each lift had a relative compaction of not less than 95% according to Caltrans Test 216 (Method of Test for Relative Compaction of Untreated and Treated Soils and Aggregates), which is a wet density specification. The maximum adjusted wet density for the embankment material was 2.12 g/cm^3 or 132 lb/ft^3 according to Caltrans Test 216 procedures. The test results for Caltrans Test 216 are located in Appendix B.

During placement and compaction, nuclear density gauge testing was conducted to confirm the 95% relative compaction (of 132 lb/ft^3) specification was achieved. This specification is typical for backfill material placed below a bridge abutment according to Standard Specifications 19-3.06 (Caltrans 2006). Four nuclear density readings meeting or exceeding the relative compaction requirement were achieved for each lift and the results can be found in Appendix B. From the nuclear density results the in-situ embankment material had an

average unit weight of 127 pcf with a water content between six and ten percent. A summary of the nuclear density gauge information is shown in Appendix A. For comparison of the results from Caltrans Test 216, a modified proctor test was also conducted on the embankment material and found a maximum dry density of 135 lb/ft^3 at a water content of 9.0%, as presented in **Figure 3-4**. The constructed location of the embankment on the GEFRS testing site is shown in **Figure 3-5**. The footprint of the embankment was 117 ft by 90 ft with a total volume of 2550 cubic yards. The test slope was cut to 2 H: 1V or 26.6°.

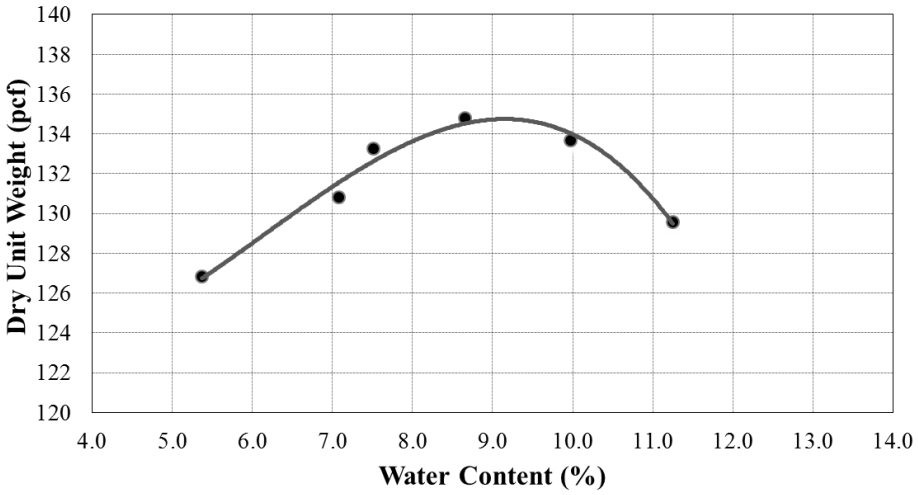

Figure 3-4. Modified proctor of the cohesionless embankment soil

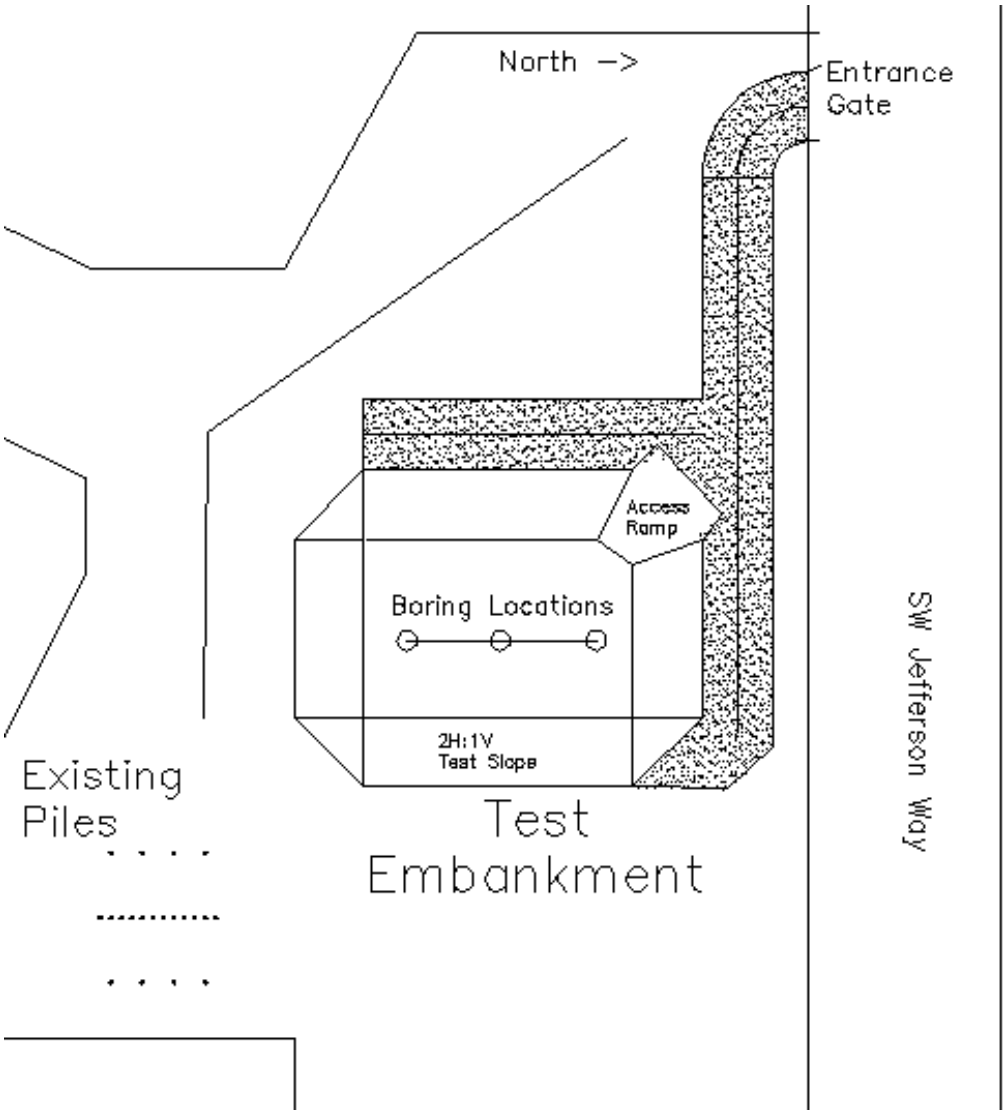

Figure 3-5. Embankment location on the test site

3.3.3 **In-Situ Soil Investigation**

An in-situ soil investigation was carried out on September 14, 2011. Three mud rotary borings were drilled to a depth of 30ft, 10ft through the embankment and 20ft into native soils. The borings were spaced equidistant through the middle of the embankment running north to south. Split spoon

samples and standard penetration tests (SPT) were conducted at 2.5 ft intervals in the top 10ft. Alternating split spoon and Shelby tube samples were performed for the remainder of each boring at 5 ft sampling intervals.

Table 3-3 shows the SPT blow counts for each test in the cohesionless embankment. The uncorrected averaged blow counts ranged between 30 and 35. Using correlations (Peck et al., 1974 and Schmertmann, 1975) from the SPT data, an averaged internal friction angle of 43 degrees is used for the cohesionless embankment material. The boring logs for the bottom 20 ft of each boring (in native soils) are consistent with the boring logs from previous soil investigation (Dickenson, 2006 and Nimityongskul, 2010) and are considered to have the same soil properties and depths in this analysis. Therefore, the generalized soil profile for this study consists of 10 ft of dense cohesionless embankment material underlain by the native subgrade as described in the previous section. A request to conduct cone penetration tests (CPT) through the embankment was not fulfilled by contractors because of the risk of damaging testing equipment.

Table 3-3. Uncorrected SPT blow counts in the cohesionless embankment

Depth (ft)	Boring 1	Boring 2	Boring 3	Average
2.5	26	30	32	30
5	36	36	29	34
7.5	35	37	32	35

Test piles penetrate through the embankment to depth of 16ft below native ground elevation (26ft of total embedment length). The soil properties of the top layers of native soils are therefore considered in the models developed in this study. A generalized profile, shear strength, water contents, cone penetration test (CTP) tip resistance, and SPT blow counts of the native are shown in **Figure 3-6**. This is data obtained from the boring logs conducted for this study and a compilation of four exploratory boreholes, three CPT test, and two Dilatometer (DMT) boreholes conducted by Nimityongskul (2010). These tests were all conducted within 200ft of the cohesionless embankment. The undrained shear strength obtained from unconsolidated undrained (UU) triaxial test averaged 1600 psf.

An assumption was made that consolidation from embankment placement in the native cohesive soils did not affect the stress and strength of these soils. The effects of new hydrogeological conditions were also not considered.

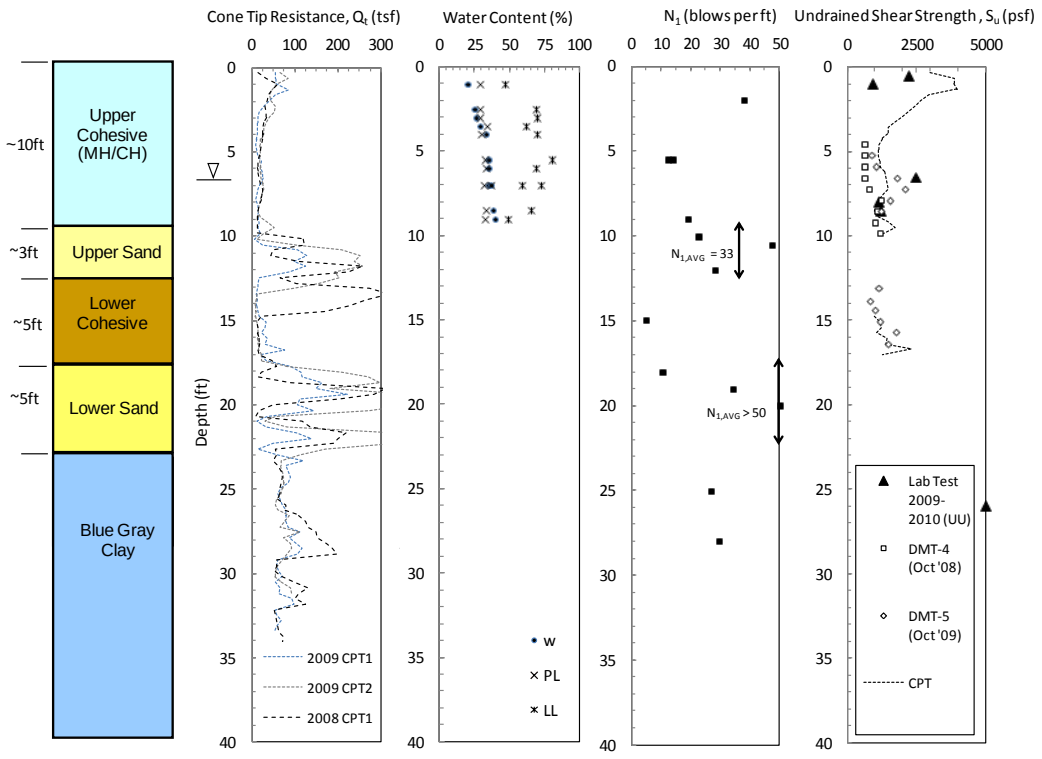

Figure 3-6. Summary of site specific explorations data (After Nimityongskul, 2010)

3.4 **Summary**

Native soil conditions at the Geotechnical Engineering Field Research Site located in Corvallis, Oregon. The scope of this project specifies testing in cohesionless soils therefore well-graded sand (SW), as classified by the USCS, was transported to the testing site. The average fines content was less than ten percent. The friction angle of cohesionless backfill material was about 43° using empirical estimates. An embankment was constructed with this material in 8 inch lifts to 95% relative compaction in accordance to Caltrans specifications to a height of 10 ft. A test slope of 2H:1V was cut in the embankment. Uncorrected

blow counts ranged between 30 and 35 in the cohesionless material. A more in depth review of native soil conditions are summarized by Dickenson (2006) and Nimityongskul (2010).

4. TESTING SET-UP

4.1 Introduction

Lateral load testing was carried out on ten piles at the geotechnical engineering field research site at Oregon State University. Piles were installed at various locations near a test slope to analyze the effects on lateral capacity. Each pile was instrumented and loaded in a similar manner.

4.2 Testing Layout

The testing program carried out during this project involved ten lateral load tests to analyze the effects of soil slope and batter angle in cohesionless soils. **Table 4-1** summarizes the location and orientation of each test pile. A plan and cross sectional view for the pile testing and embankment arrangement is shown in **Figure 4-1**. Five piles were driven near or in the 2H: 1V test slope. These piles were located 8D, 4D, 2D, 0D, and -4D from the slope crest where D is pile diameter. Also, five piles were located on the opposite side of the embankment with sufficient distance (greater than 15D) from the back slope to ensure the lateral capacities were not influenced. These tests represent the baseline piles and battered piles in horizontal ground conditions.

Table 4-1. Summary of testing program and pile orientation

Test Pile	Soil Type	Test Type	Batter Angle (θ)	Slope (α)	Distance from Crest (t/D)
P-1	Cohesionless	Baseline	---	---	---
P-2					
P-3		Battered	14°	---	---
P-4			-14°		
P-5			26.5°		
P-6		Near slope or In slope	---	2H:1V 26.5°	2
P-7					4
P-8					8
P-9					0
P-10					-4

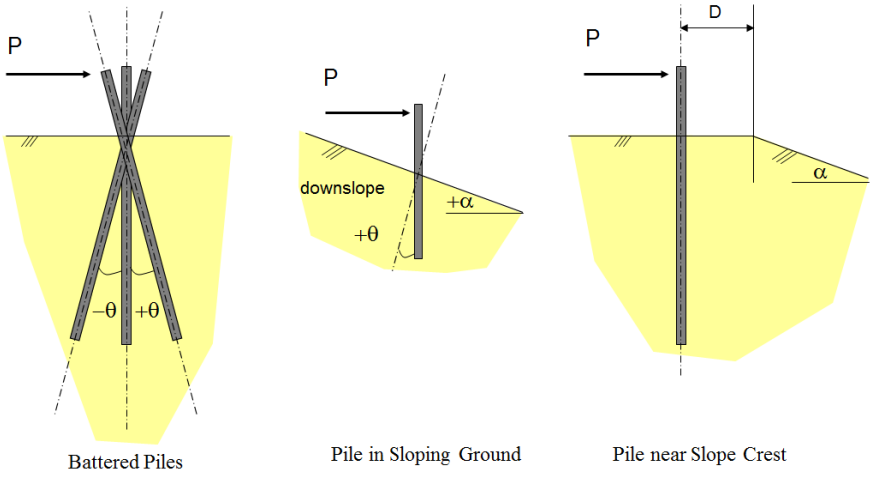

Battered Piles Pile in Sloping Ground Pile near Slope Crest

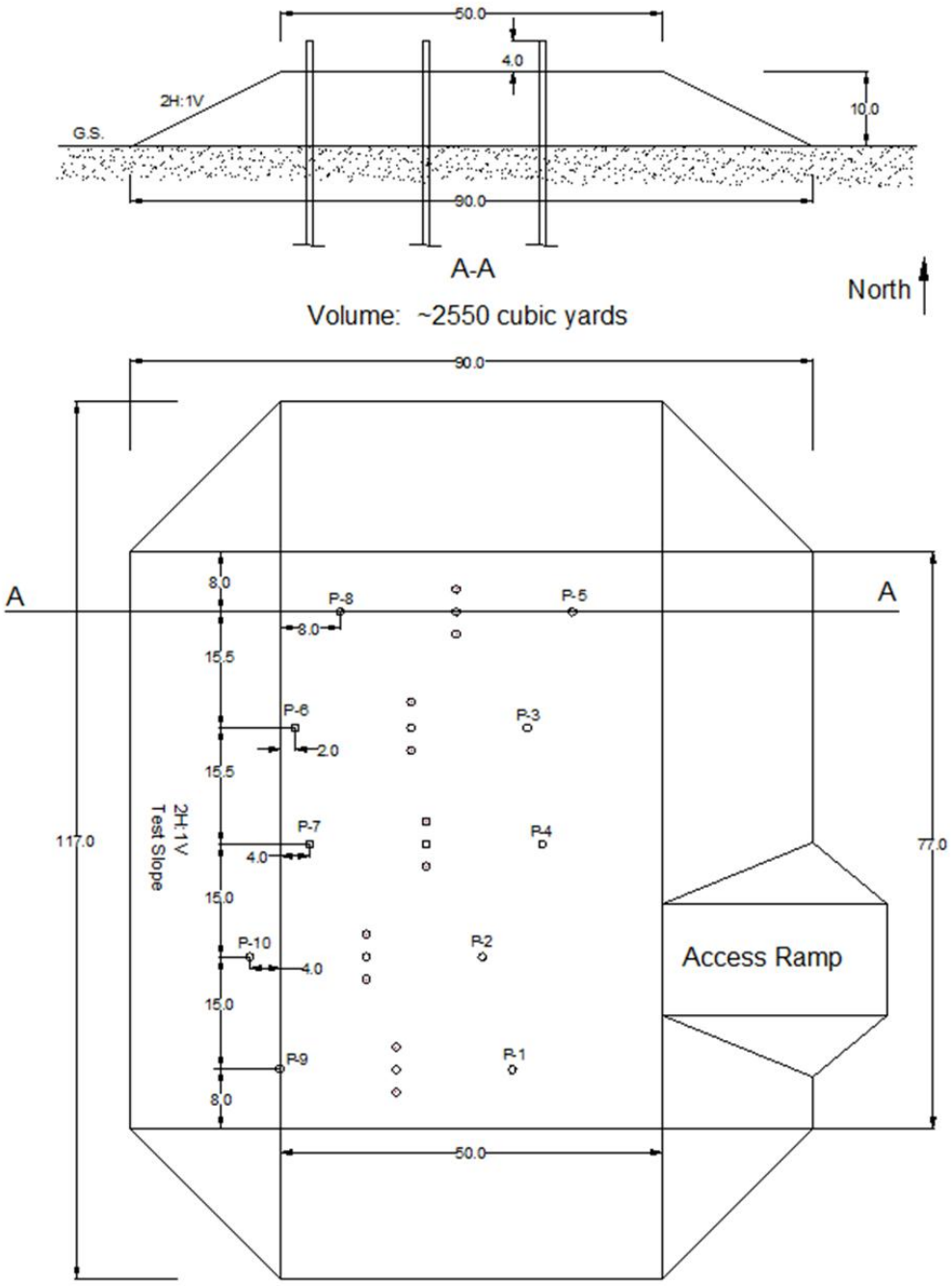

Figure 4-1. Plan and cross-sectional views of cohesionless embankment

Fifteen reaction piles were installed in groups of three along the center of the embankment. Reaction piles are used to support or resist lateral movement of the testing equipment during lateral loading. A transfer beam tied the group of reaction piles together with a 500-kip capacity hydraulic actuator applying lateral load to the test piles. Lateral loads were applied by the hydraulic actuator 3 ft above the ground surface. Temporary support beams rested between the hydraulic actuator and the ground to ensure this loading height. The hydraulic actuator was connected to the test piles with steel plates compressing wooden transfer blocks around the pile. The wooden blocks were used to distribute the load across the pile to avoid local pile deformations. This testing layout is shown in **Figure 4-2** The test setup for the battered piles (P-3, P-4, and P-5) was slightly different from other tests and is discussed more in depth in chapter 5. **Figure 4-3** shows a diagram of a typical testing set up, reaction pile system, and hydraulic actuator.

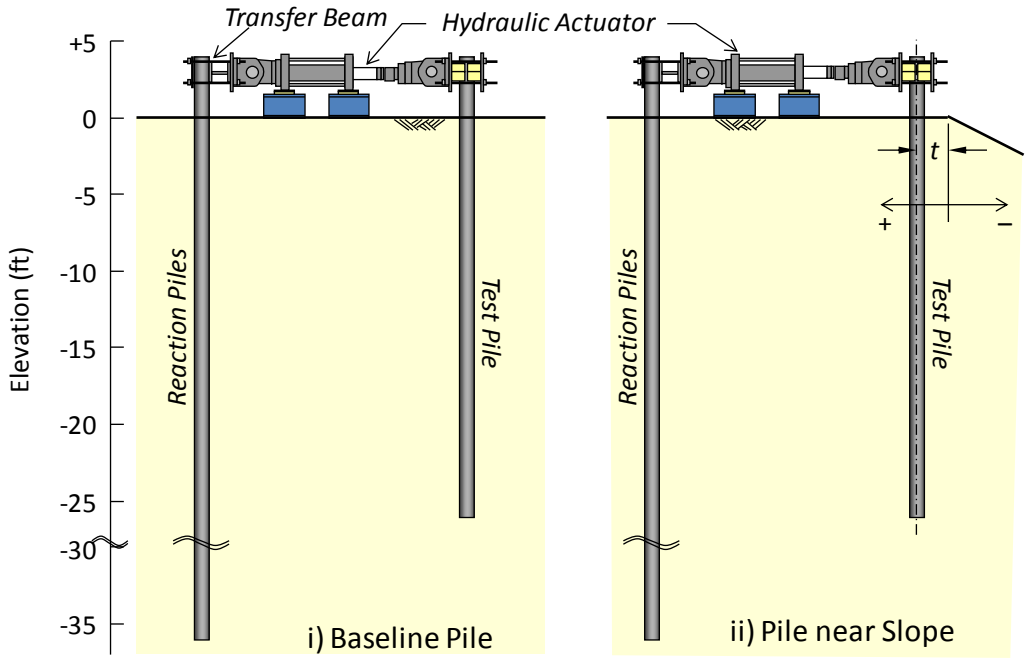

Figure 4-2. i) Baseline pile test setup ii) Near slope testing setup (after Nimityongskul 2010)

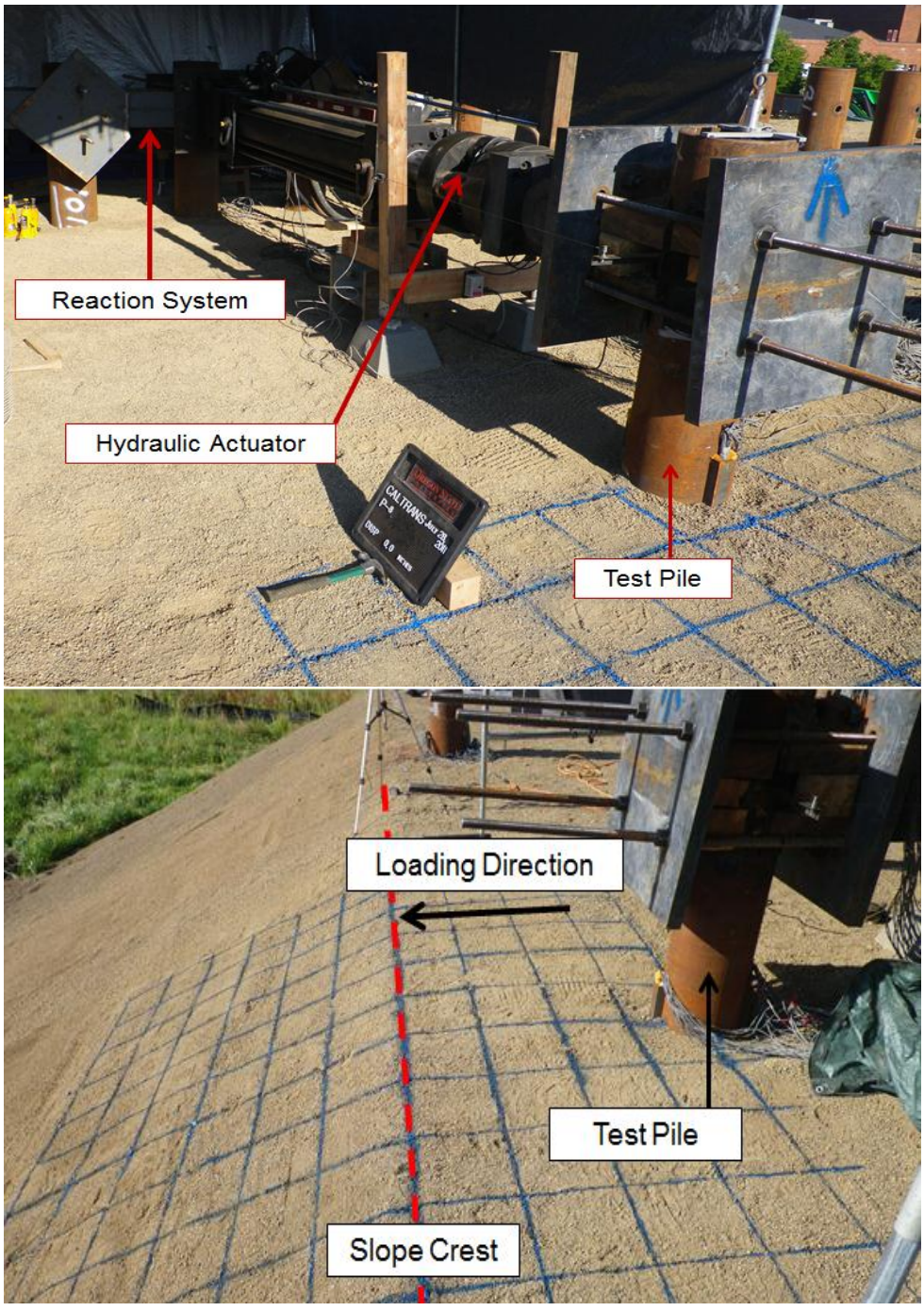

Figure 4-3. Typical test setup

4.3 **Pile Installation**

Test piles P-1 through P-10 were installed through the cohesionless embankment between June 6 and 7, 2011. All test piles were driven closed-ended to allow for insertion of instrumentation. The piles were driven using an APE D19-42 diesel impact hammer with a rated energy of 47,300 ft-lbs at a maximum stroke of 146 inches. Each test pile was 30 ft in length and driven to a depth of 26 ft below the embankment surface. The exposed 4 ft of pile provided adequate room to connect testing equipment. A pile length of 30 ft in length was used to ensure the piles acted as long piles with fixed ends during testing. A pile is considered fixed when no rotation occurs at the base of the pile during lateral pile head movement. During this research it was important that the piles were fixed because this boundary condition was applied to the analysis model.

Pile driving logs for a selection of piles are shown in **Figure 4-4**. Pile P-10 was driven into the slope at an elevation 2 ft below the embankment surface. During driving, piles P-3, P-4, and P-10 were driven with a slight rotation where the strain gauges were slightly off from perpendicular (10° to 20°) with the testing slope. This error was taken into account during data analysis. The effects from installation on testing soil conditions and pile sections were assumed similar for each pile during analysis, because all piles were driven in comparable condition with the same equipment.

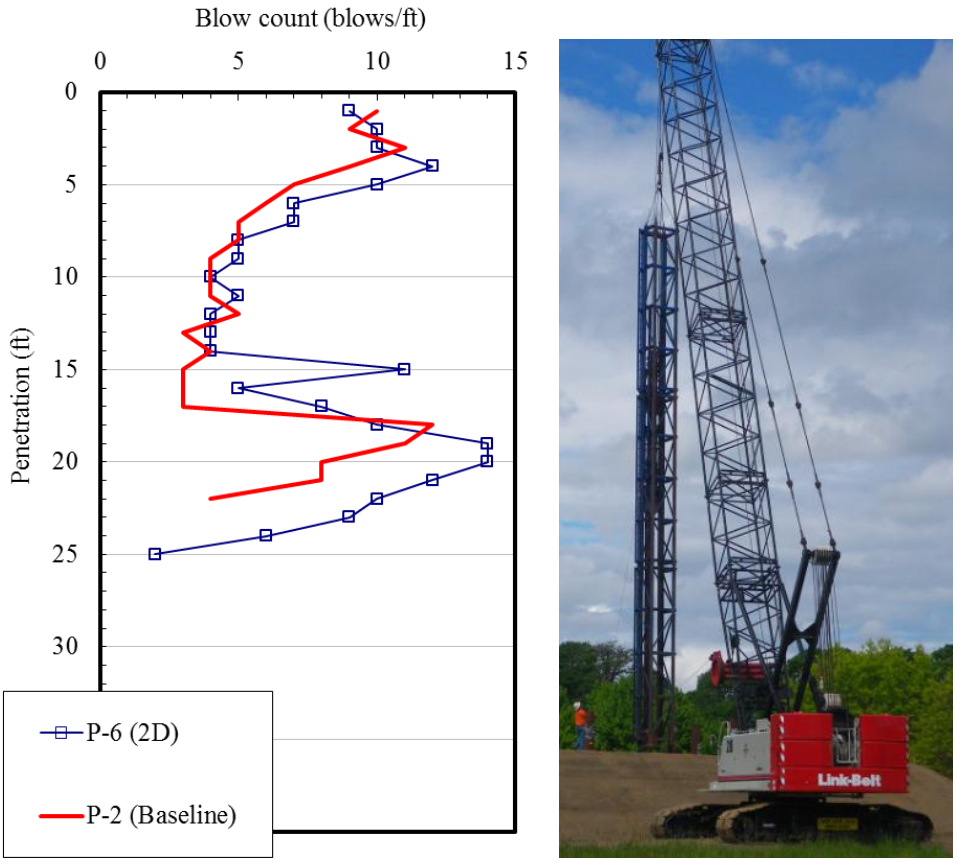

Figure 4-4. Example pile driving logs for baseline Pile P-1 and 2D Pile P-6

4.4 **Pile Type and Calibration**

All tests were conducted on steel pipe piles with an outer diameter of 12.75 inches, a wall thickness of 0.375 inches, and an inner diameter of 12.0 inches. Each pile met the requirements of the ASTM 252 Grade 3 specifications. This pile section was also selected, in part, because it is a standard size presented in the Caltrans Bridge Design Specifications for lateral pile resistance. The materials inspection certifications for each pile are located in Appendix B. The average yield strength of the test piles was between piles is 71ksi and 81ksi as provided by the manufacturer certification reports. As shown in **Figure 4-5**,

C3x4.1 steel c-channels were welded on opposite sides the test piles to protect the strain gauges during pile driving.

Nimityongskul (2010) conducted a calibration test on the pile with c-channel member to measure the structural properties and verify strain gauge performance before pile installation. The three point loading set up with cross sections is shown in **Figure 4-6**. The section modulus obtained from this calibration test was 61.6 in^3. A flexural rigidity (EI) of 84,450 $k\text{-}ft^2$ was used for the test piles during analysis. The effective yielding moment of the test piles is between 365 kip-ft to 416 kip-ft. This is based on the section modulus obtained from the calibration test and the yield strength of the test piles. A post yielding bending stiffness of 5% of the elastic stiffness was chosen for the analysis in this study.

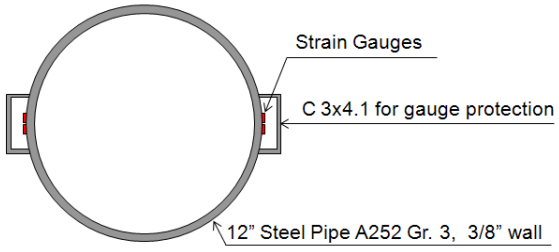

Figure 4-5. Cross section of test pile (after Nimityongskul 2010)

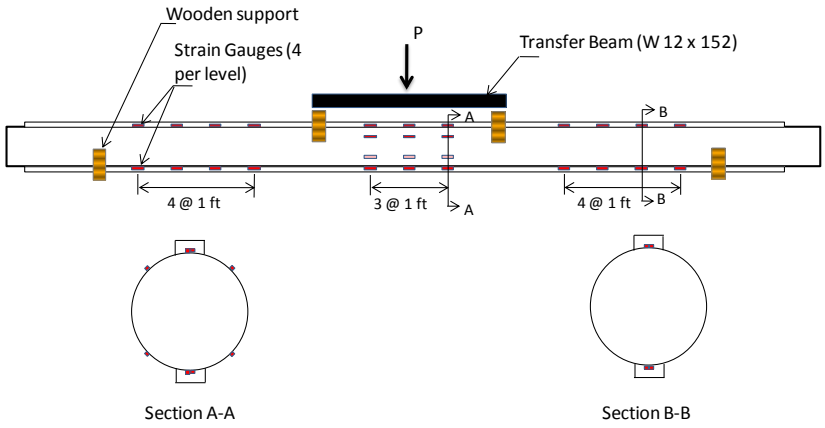

Figure 4-6. Calibration test of instrumented pile (after Nimityongskul 2010)

4.5 **Instrumentation**

Four types of instrumentation were utilized to collect data during lateral load testing. Strain gauges were installed at 16 levels along the length of each pile. Two gauges were fixed at every level on each side of the test piles to record tension and compression during lateral loading. The strain gauges were spaced at 1ft intervals for the top ten levels and increased to 2 ft and 4ft spacing at increasing depth. The c-channel sections protected the 64 strain gauge during pile driving. After installation but prior to testing, 13 tiltmeters were installed in the center of the pile to known depths to measure pile rotation during testing. **Figure 4-7** presents a cross section of a typical test pile with location of the strain gauges and tiltmeters.

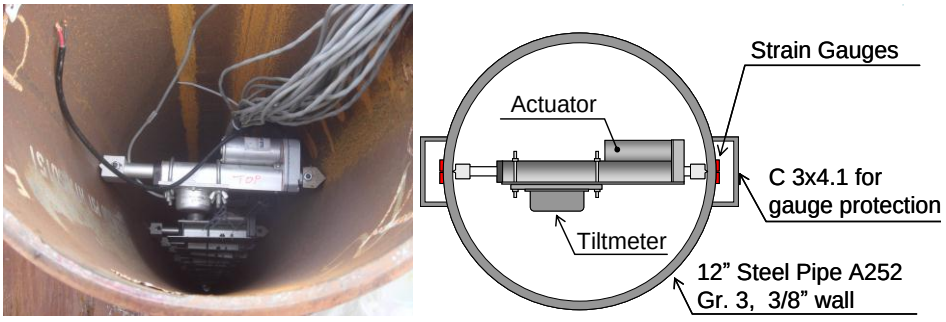

Figure 4-7. Cross-section view of test pile showing tiltmeter arrangement (after Nimityongskul, 2010)

Linear string potentiometers were connected to either side of the test pile at the loading elevation to measure lateral pile head displacement. A third linear string potentiometer was also placed near the ground surface. A reference frame independent from the loading system was used to mount these potentiometers. This ensured only the movement of the test pile was captured and not the lateral movement of the reaction system. Four load cells were incorporated into the hydraulic actuator to measure the applied lateral load. **Figure 4-9** shows the locations of the instrumentation with depth on the test piles. All testing data was digitally recorded at 0.5 second intervals with a data acquisition system.

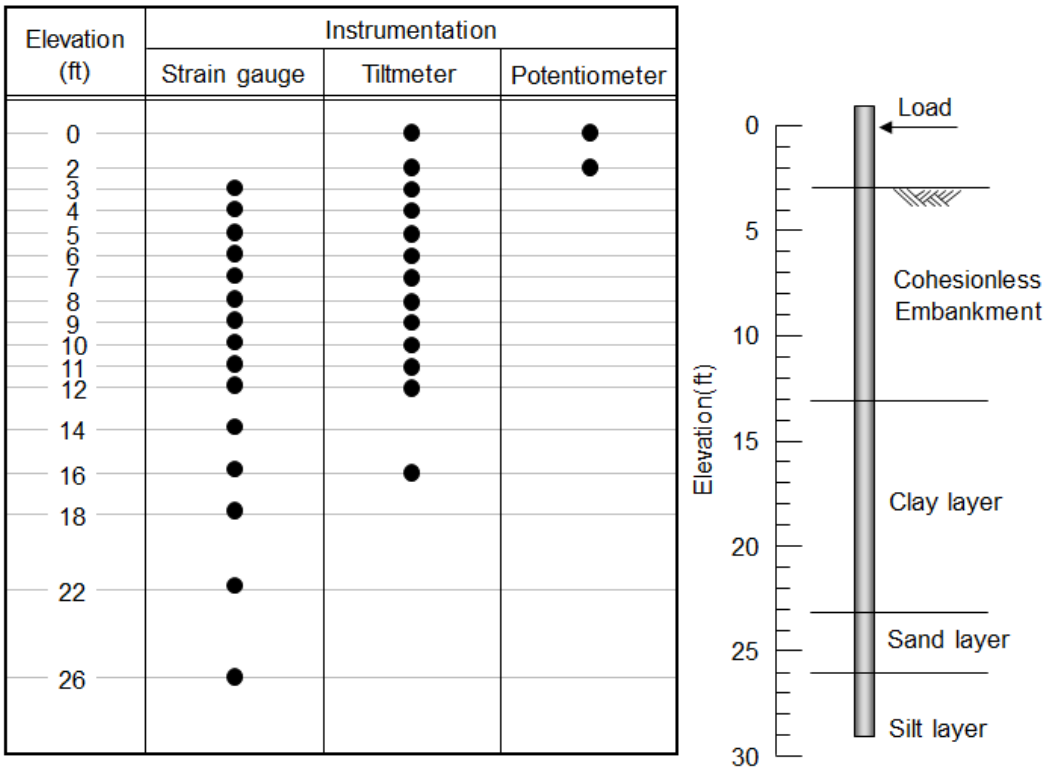

Figure 4-8. Summary and location of test pile instrumentation

4.6 **Lateral Loading Procedure**

A short term static loading condition was applied during all lateral load tests in which a 500 kip hydraulic actuator was extended at rate of 0.1 inch/minute. This actuator ramp rate is considerably slower than other monotonic lateral load test in sand; however this rate was selected to be consistent to tests conducted by Nimityongskul (2010) in the first phase of this project. A pile head loading rate of approximately 0.075 inch/minute was observed during testing due the displacement of the reaction pile system in the opposing direction. This rate was

also considered slow enough for pore water pressure dissipation during testing in the cohesionless material.

During the design phase of this project, initial predictions were conducted to estimate the load-displacement, moment, curvature, and p-y curves using LPILE Plus version 5.0 (Reese et al., 2004). This analysis was conducted using predicted cohesionless soil properties and the in-situ native soil conditions. Target displacements of 0.1, 0.25, 0.5, 0.75, 1, 1.25, 1.5, 1.75, 2, 2.25, 2.5, 3, 3.5, 4, 4.5, 5, 6, 7, 8, 9, 10 inches were chosen during lateral load testing. The hydraulic actuator was held at these target displacements for 5-10 minutes to allow the soil-pile system to reach equilibrium. **Figure 4-9** shows the loading protocol used during testing. In this figure the displacement ductility is based on the predicted point of plastic yielding in respect to the lateral loading rate at the pile head.

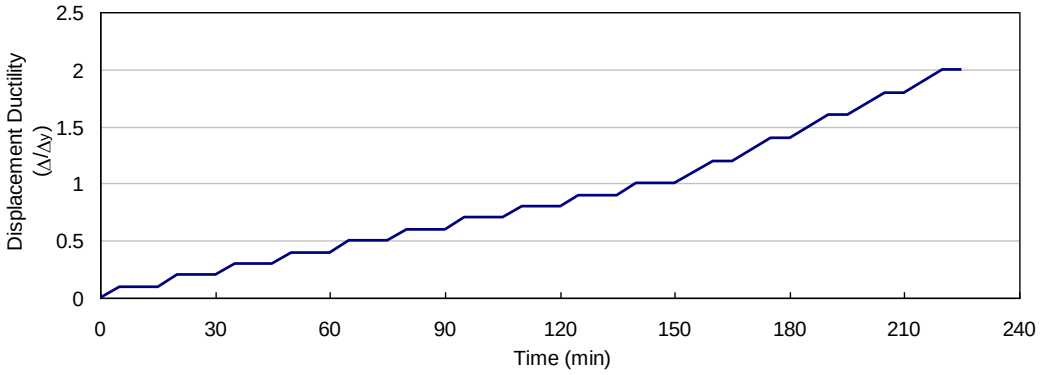

Figure 4-9. Load protocol for lateral load tests arrangement (after Nimityongskul 2010)

4.7 **Summary**

Ten 1ft diameter, 30ft long steel pipe piles were driven into a cohesionless embankment in the summer of 2011. Five piles were located in proximity to the 26.6° test slope located at -4D, 0D, 2D, 4D and 8D from the slope crest where positive D is the distance behind the slope crest. Three battered piles were installed with positive and negative batter angles. Two baseline piles were driven in level ground to use for comparison of results. A calibration test was conducted on a pile with c-channel members to obtain accurate section properties. Each pile was instrumented with strain gauges, tiltmeters, linear string potentiometers, and load cells.

5. LATERAL LOAD TESTING

5.1 Introduction

Between July and September of 2011, ten lateral load tests were carried out to study the effects of soil slope and batter angle on the performance of piles. A brief description of the observations made during load tests and photographs are provided in the following sections. Throughout the following sections the non-battered test piles will be called the baseline piles (P-1, P-2), 8D pile (P-8), 4D pile (P-7), the 2D pile (P-6), 0D pile (P-9), and -4D pile (P-10) as previously summarized in **Table 4-1**.

5.2 Baseline and 8D Load Tests

5.2.1 Baseline Test Piles (P-1 and P-2) and 8D Pile Observations

The second baseline load test, pile P-2, was carried out at the test site on August 10, 2011. One foot square gridlines were painted in front of each pile to analyze the ground deformations during lateral pile movement**. Figure 5-1** shows observations made during the second baseline pile test. Some slumping of the soil occurred behind the pile, a large gap also formed in the cohesionless soil. This gap is most likely due to apparent cohesion from capillarity effect between soil particles. Ground heaving in front of the pile was observed and increased with increased displacement. Large cracks formed at various angles in front of the pile

and propagated out about 4ft. Smaller cracks also formed on both sides of the pile and increased in size and width with an increase in displacement.

The first baseline load test, pile P-1, was conducted on July 1, 2011. This load test encountered a problem midway through lateral loading. At a displacement of 3.5 inches the connecting frame between the hydraulic actuator and pile slipped and rotated downward. This induced an axial load into the pile during testing. The test was immediately stopped and the pile was unloaded. The connection frame was realigned and the test was completed to a final pile head displacement of 8.0 inches. During testing there was also a slight loading oscillation from the actuator causing a small amount of scatter in the load-displacement data. The second baseline test was conducted successfully therefore the results and analysis from the first baseline are not included in this report. The connecting frame and actuator oscillation difficulties were resolved and were not an issue for the remainder of the tests.

The lateral Load test for the 8D pile was carried out on July 28, 2011. **Figure 5-2** shows observations made during lateral load test of the 8D pile. Several minor cracks formed in the level ground around the 8D pile. No cracking on the slope was observed throughout the duration of the load test, with a final pile head displacement of more than 9 inches. Ground heaving in front of the pile was observed similar to that observed in the baseline pile load tests.

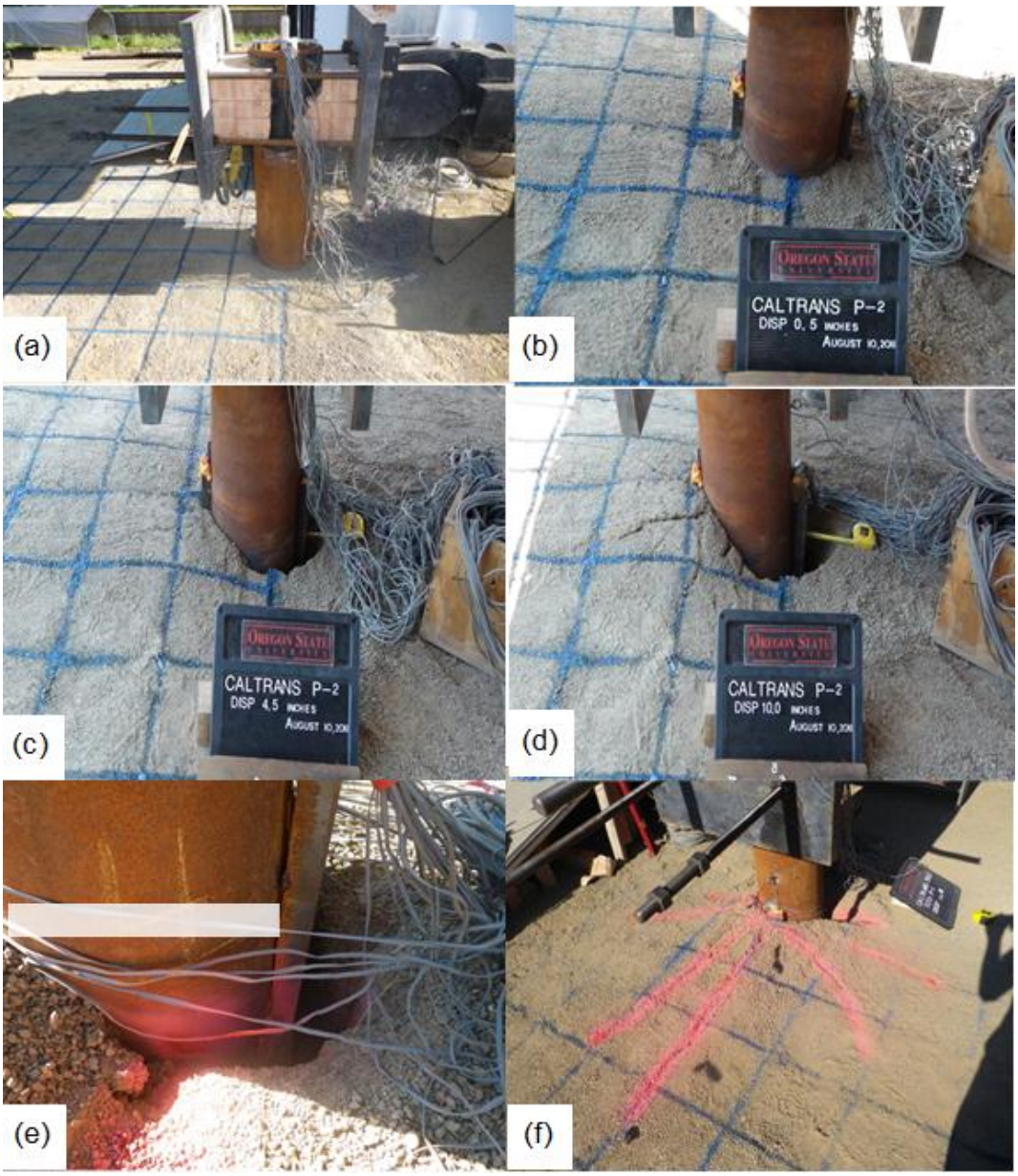

Figure 5-1. Observations during load test of first and second baseline piles a) Pile before loading b) Pile at 0.5" of displacement c) Pile at 4.5" of displacement d) Pile at end of testing e) Gap formation behind pile f) Heave and cracking in front of pile

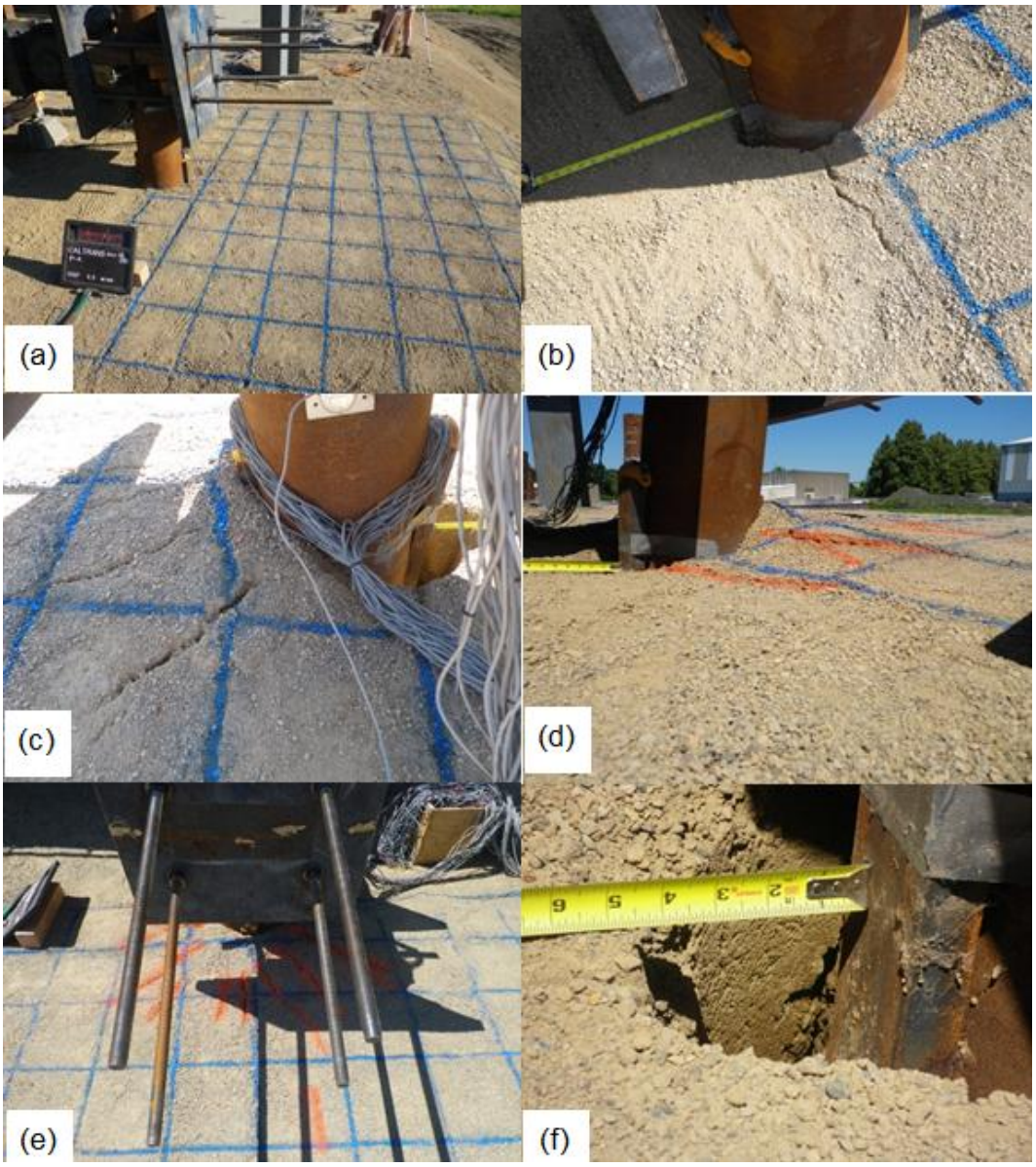

Figure 5-2. Observations during lateral loading testing of pile P-8 (8D) a) Pile before loading b) Pile at 0.5" of displacement c) Pile at 5.0" of displacement with cracking d) Soil heave at end of testing e) Soil cracking at end of testing f) Gap formation behind pile

5.2.2 **Load Displacement Curves**

The load-displacement curves for the baseline and 8D piles are shown in **Figure 5-3**. For the 8D pile, the load-displacement curve was almost identical to the baseline pile. The 8D pile was slightly stiffer than the baseline between 1.0 inch and 4.0 inches of displacement, but still considered to be comparable curves. Both piles had a maximum lateral capacity of approximately 87 kips at 8.0 inches of displacement. The jump in displacement at 2.0 inches and a load of 40 kip is a result of a researcher slightly bumping the potentiometer causing a quick spike in displacement. This displacement was not applied to the pile.

Figure 5-4 compares the curvature profiles for the second baseline pile and the 8D pile. The curvature profile was obtained by averaging the strain data collected on both sides of the pile and dividing by the neutral axis distance. This profile confirms the test piles behaved as flexible long piles under lateral loading because negligible curvature was observed below a depth of 17ft.

The load-displacement curves and the curvature profiles for the baseline and 8D piles are almost identical, and it is concluded that the effects of slope are insignificant on piles located 8D or further from the slope crest. Therefore, further analysis of the 8D pile was not included in this report and only the baseline results are discussed.

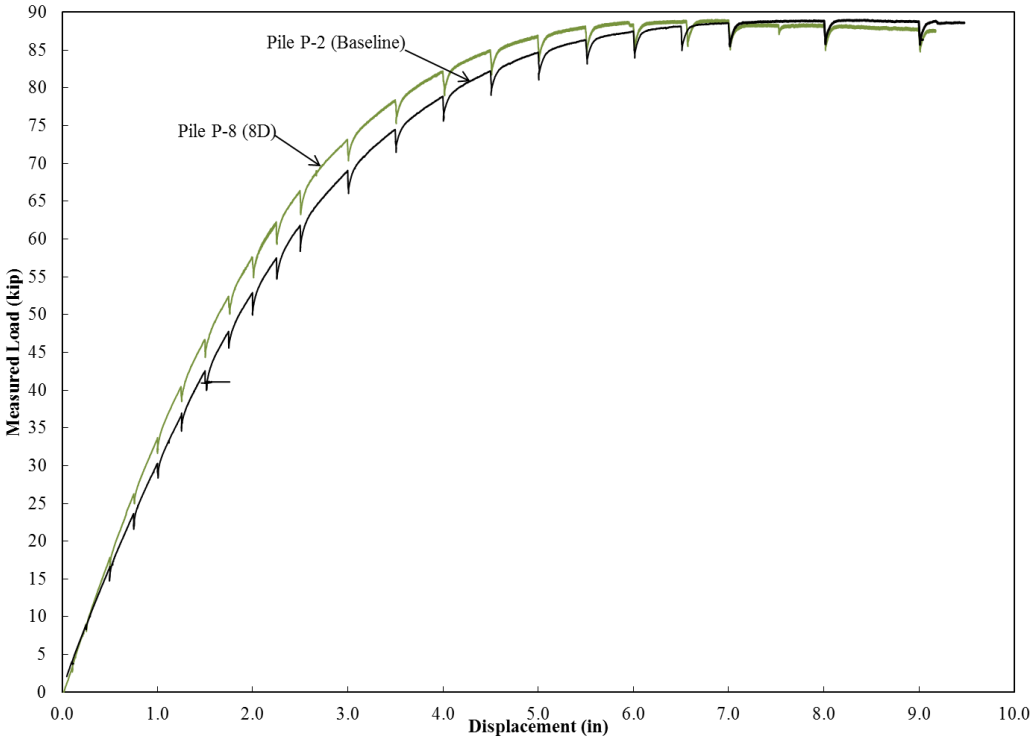

Figure 5-3. Comparison of load-displacement curves between the baseline pile (P-2) and the 8D Pile (P-6)

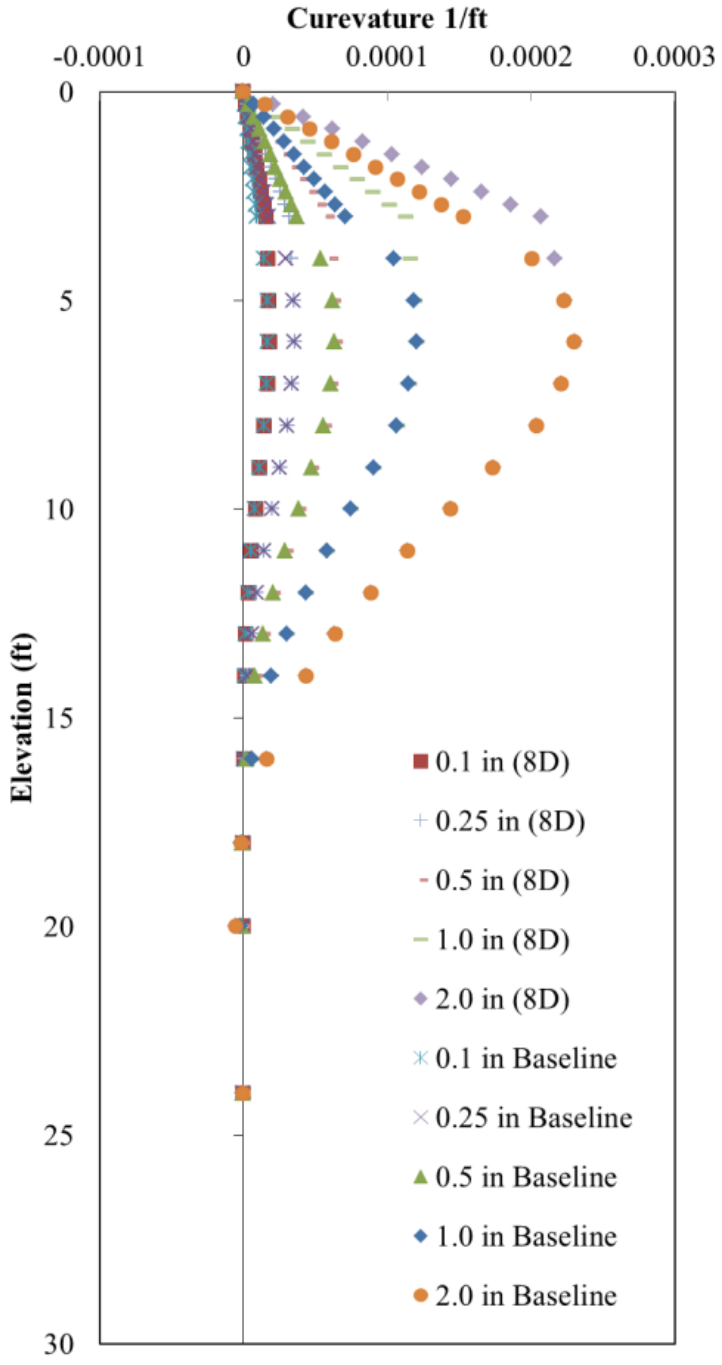

Figure 5-4. Comparison of the curvature data for the baseline pile and 8D Pile

5.3 **4D Load Test Observations and Load Displacement Curve**

The 4D pile load test was conducted on July 22, 2011. **Figure 5-5** shows observations made during lateral load test of the 4D pile. At a displacement of 1.0 inch, the first minor crack was observed moving outward of a 45 degree angle from the pile and appeared to be the initial formation of a passive wedge. Also, large cracks formed perpendicular to the loading directing at the pile base. The cracking pattern on both sides of the pile was similar. The test was ceased at a final pile head displacement of 10 inches. Passive wedge cracking was noticeable on the slope at pile head displacements greater than 7 inches. A gap formed behind the pile during testing.

Figure 5-6 presents the load-displacement curve for the 4D pile. The initial stiffness, up to a pile head displacement of 2.5 inches is similar to the initial stiffness of the baseline curve. Thereafter, the stiffness and load are lower to a final displacement of ten inches. At lower displacements, the load was similar to the baseline pile test. This demonstrates that the proximity of the slope had little effect on the lateral capacity at 4D from the crest for displacements less than 2.5 inches. The peak capacity was reached at 78 kip at a pile head displacement of 5.5 inches through the end of the load test. This capacity was less than the baseline demonstrating an effect from the slope at high displacements, above 2.5 inches of displacement at the point of loading. The jump

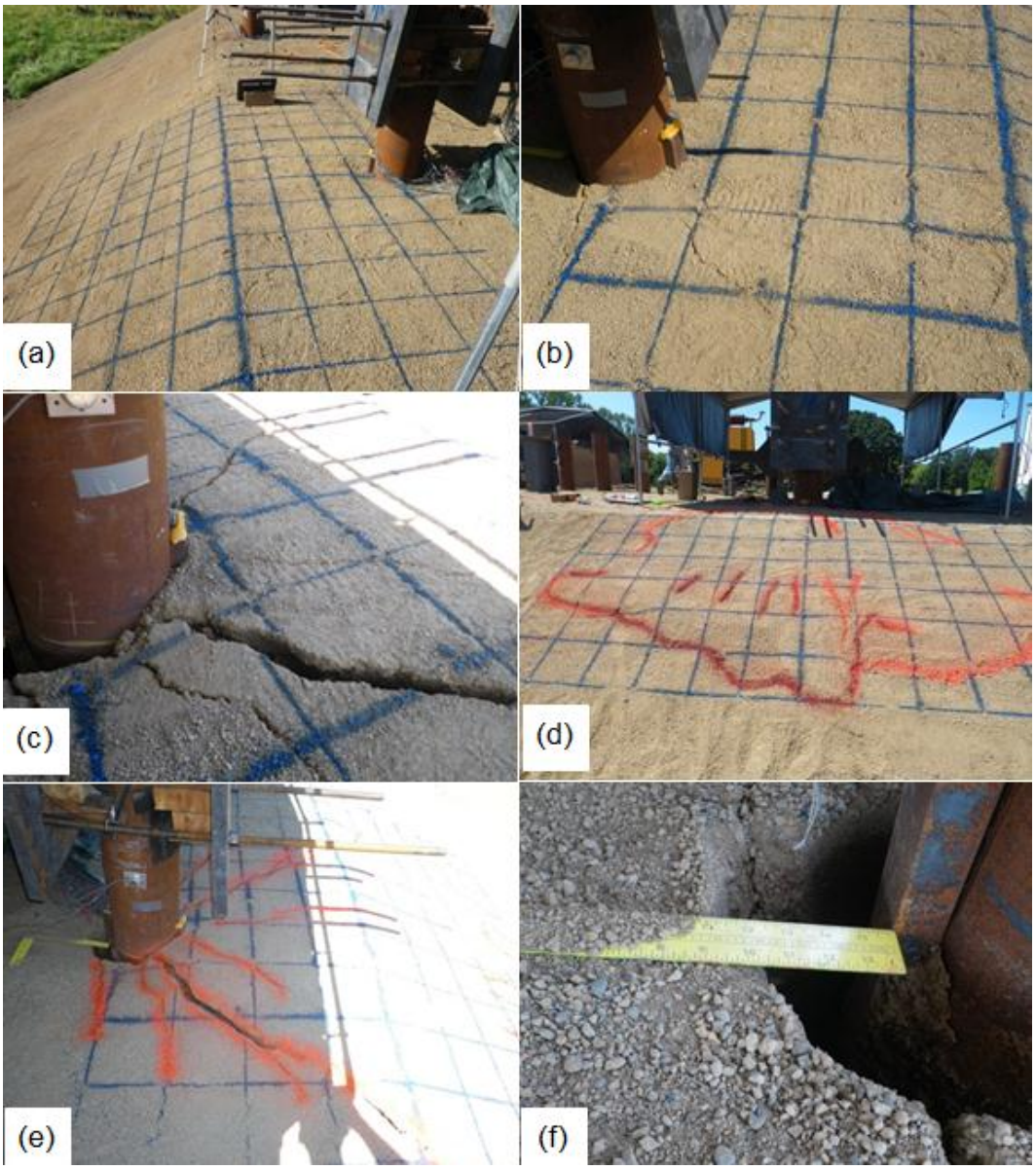

Figure 5-5. Observations during lateral loading testing of pile P-6 (4D)
a) Pile before loading b) Pile at 3.5" of displacement with large cracking c) Pile at 8.0" of displacement with passive wedge cracking d) Passive wedge cracking on slope e) Passive wedge movement in front of pile f) Gap formation behind pile

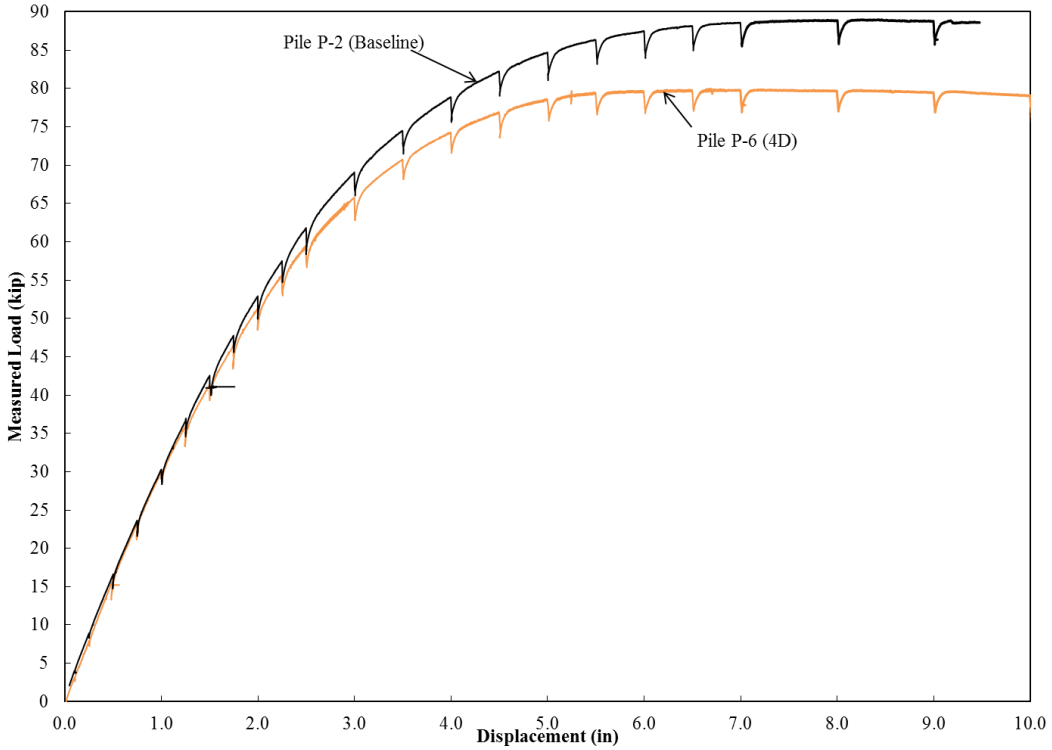

Figure 5-6. Comparison of load-displacement curves between the baseline pile (P-2) and the 4D Pile (P-7)

5.4 **2D Pile Load Test Observations and Load Displacement Curves**

The 2D pile load test was conducted on July 19, 2011. **Figure 5-7** depicts the modes of soil failure around the test pile. A large crack observed during the beginning of testing was near the side of the pile propagating out perpendicular on either side. The next significant cracking occurred with an angle of 35 degrees perpendicular to the loading. These cracks appeared to be the initial movement of a passive soil wedge. At the end of the tests the cracking patterns around the pile were slightly off from symmetrical in respect to the direction of loading. At a pile

head displacement of 2.0-3.0 inches a large passive soil wedge movement was observed on the slope. This wedge propagated at approximately a 30-35 degree angle from the pile. The wedge formation was six pile diameters long and propagated three feet (vertically) down the slope as seen in **Figure 5-7**. An offset of up to three inches was seen between gridlines where the soil wedge had moved outward from the original position. Less heave occurred in this test compared to the baseline, but considerably more cracking was seen. A large gap also formed behind the pile.

Figure 5-8 presents the load-displacement curve for the 2D pile. The initial stiffness, up to a pile head displacement of 2.5 inches, is similar to the baseline curve. Thereafter, the stiffness and load are lower up to a final displacement of 10 inches. The load displacement curve is almost identical to the 4D pile at all displacement. This demonstrates that the proximity of the slope had little effect on the lateral capacity for displacements less than 2.5 inches. The capacity of 78 kips was reached around a pile displacement of 5.5 inches. This magnitude was lower than the baseline demonstrating the effects of the slope at higher displacements, above 2.5 inches.

Figure 5-7. Observations during lateral loading testing of pile P-5 (2D) a) Pile before loading b) Pile at 1.5" of displacement with cracks forming c) Pile at 8.0" of displacement with passive wedge cracking d) Passive wedge movement on slope e) Passive wedge movement in front of pile at end of testing f) Gap formation behind pile

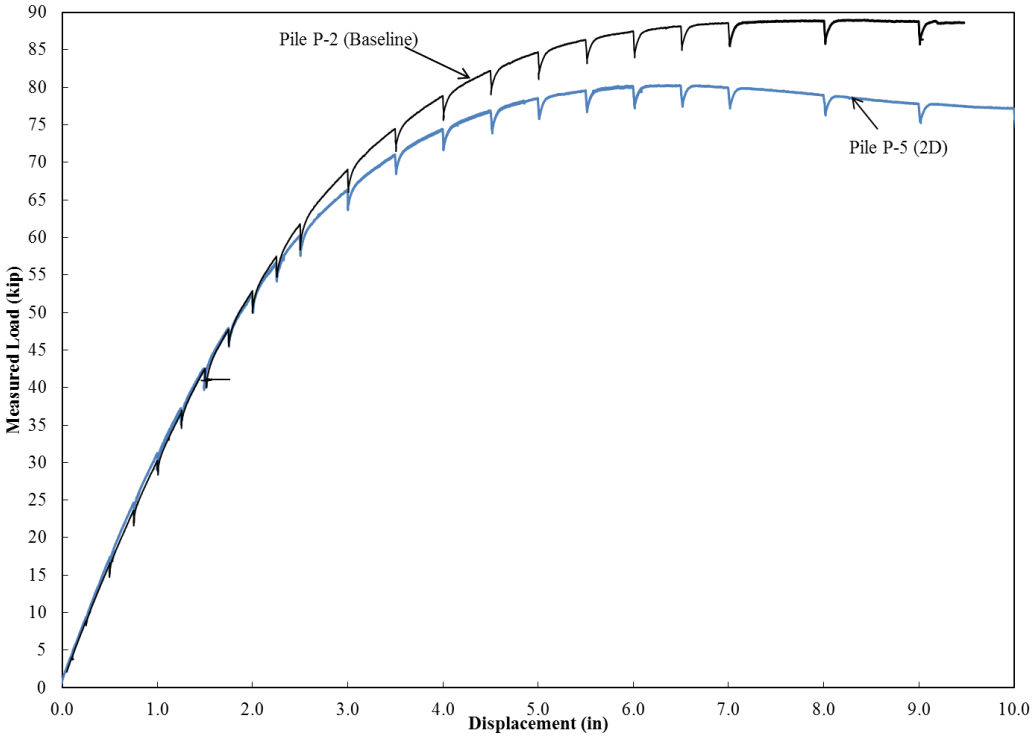

Figure 5-8. comparison of load-displacement curves between the baseline pile (P-2) and the 2D Pile (P-6)

5.5 **0D (Crest) Pile Load Test Observations and Load Displacement Curves**

The 0D pile (on the slope crest) load test was conducted on July 12, 2011. **Figure 5-9** shows the cracking and ground heaving that occurred. The first major crack was observed at a pile head displacement of 1.25 inches propagating out at a 30 degree angle. At 3.0 inches of pile head displacement, these cracks moved out 4 ft onto the slope on either side of the pile and was the initial signs of passive wedge movement. The cracking consisted of cracks perpendicular to loading at the base of the pile and cracking within the passive wedge. At displacements

great than 4.5 inches, it was apparent that the soil wedge was moving outward with increased load. The grid line pattern began to move downslope relative the lines outside of the passive wedge. By the end of the test a large passive wedge had formed on the slope and the majority of the cracking occurred within this area.

Figure 5-10 presents the load-displacement curve for Pile P-9 (0D). The initial stiffness was lower than the baseline. The stiffness remained lower throughout the duration of the test. At displacements of 0.25, 0.5 and 1.0 inch the lateral load was 5.5 kips, 10.5 kip and 21.8 kips, respectively. When compared to the baseline, this demonstrates that the proximity of the slope had a significant effect on the lateral capacity for all pile head displacements. The peak capacity was 65 kip at a pile head displacement of 7.0 inches. This ultimate resistance was 22 kips less than the baseline peak.

Figure 5-9. Observations during lateral loading testing of pile P-9 (0D)
a) Pile before loading b) Pile at 5.0" of displacement with cracks forming c) Pile at 10.0" of displacement with passive wedge cracking d) Passive wedge movement on slope at end of testing e) Passive wedge movement at end of testing f) Gap formation behind pile

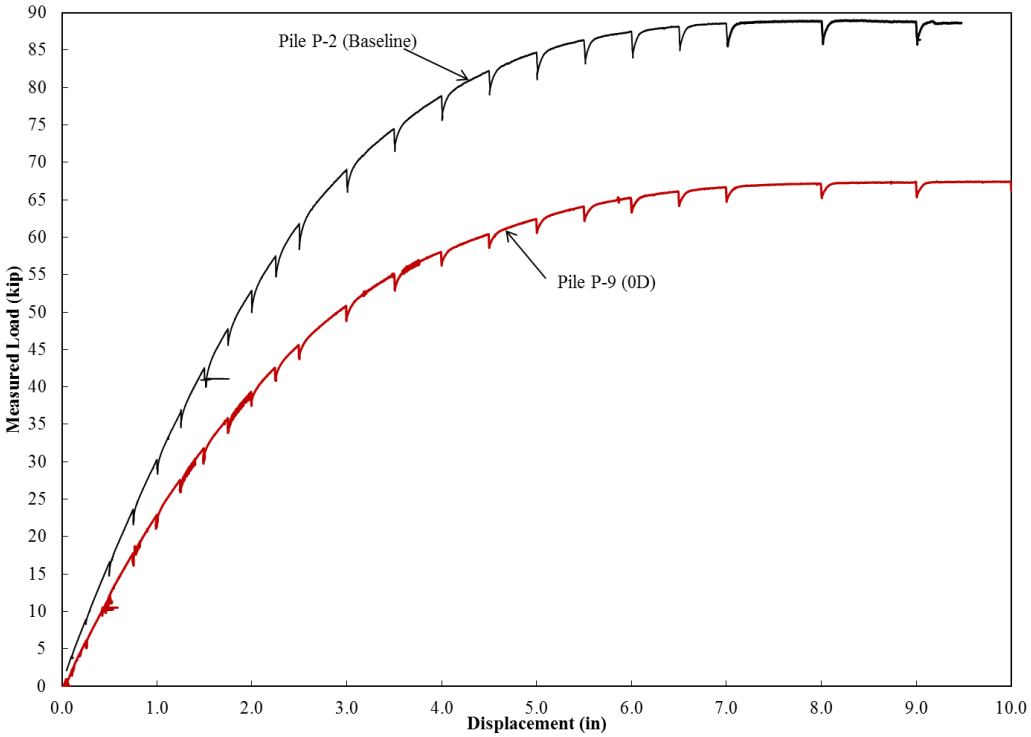

Figure 5-10. Comparison of load-displacement curves between the baseline pile (P-2) and the 0D Pile (P-9)

5.6 -4D Pile Load Test Observations and Load Displacement Curves

The lateral Load test for the -4D Pile (P-10) was conducted on August 19, 2011. **Figure 5-11** presents observations made during lateral load testing of the -4D pile. Note that the jump in displacement at 3.0 inches and 32 kips is a result of the string potentiometer being pumped. This was not displacement in the pile. Ground cracking was first observed perpendicular to loading at the base of the pile similar to the 0D and 2D tests. At displacements greater than 4.0 inches, it was apparent that the soil wedge was moving outward with increased load. By

the end of the test a large passive wedge had formed on the slope similar to the 0D and 2D piles.

Figure 5-12 presents the load-displacement curve for the -4D Pile. The stiffness was lower than the baseline at all pile head displacements. The lateral capacity was significantly less than the baseline pile and 0D tests. The pile location in the slope had a significant effect on the lateral capacity throughout the entire lateral displacement range. The peak capacity was 51 kips around a pile head displacement of 7.0 inches.

Figure 5-11. Observations during lateral loading testing of pile P-10 (-4D) a) Pile eat 0.5" of displacement b) Pile at 5.0" of displacement c) Pile at 10.0" of displacement with passive wedge cracking d) Passive wedge movement on slope

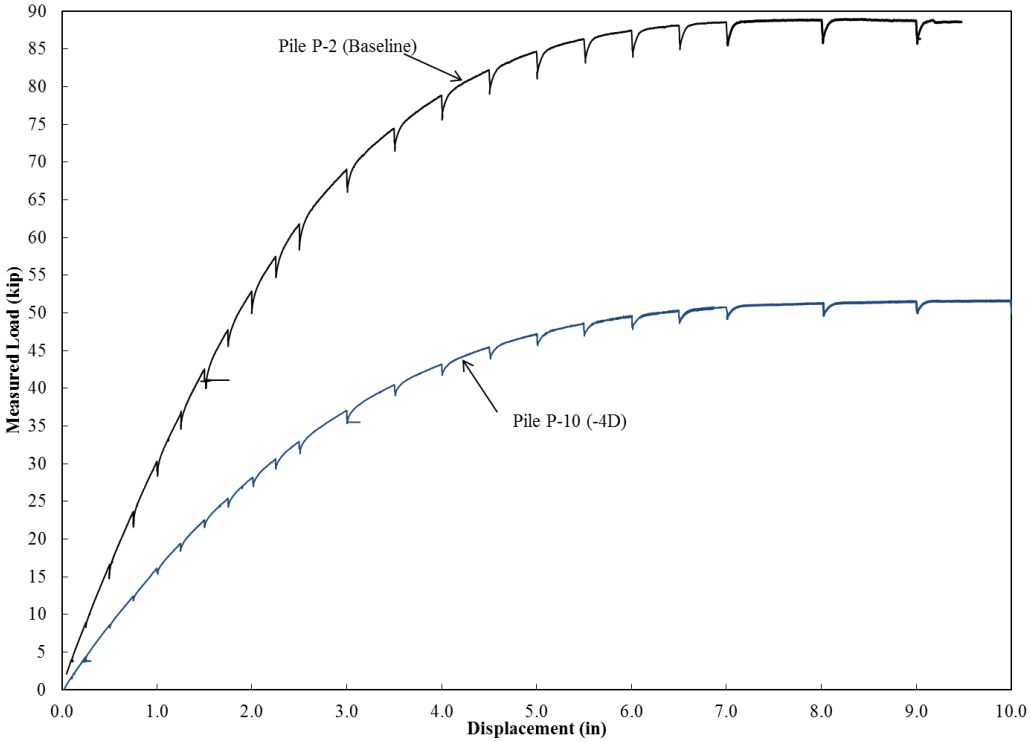

Figure 5-12. Comparison of load-displacement curves between the baseline pile (P-2) and the -4D Pile (P-10)

5.7 Pile Curvature and Rotation

Appendix B presents the curvature and rotation profiles at various pile head displacements. The rotation profiles were obtained from the tilt sensor data. This data was used to verify the accuracy of the strain gauge data. The curvature profiles were obtained by averaging the strain data collected on both sides of the pile and dividing by the neutral axis distance. The point of maximum curvature in the test piles ranged between 3ft to 5ft below the ground surface. As the piles were located closer to the crest slope the depth to maximum curvature slightly increased.

5.8 Battered Pile Test Observations and Load Displacement Curves

The purpose of the battered pile tests was to compare the performance of battered piles to near slope piles because in some design assumptions (i.e. Reese et al., 2004), battered piles are treated as if it was equivalent to piles on a slope. According to this assumption a vertical pile loaded down slope with an angle, θ, would have the same lateral response as a positively battered pile with a batter off of vertical of the same angle.

Three battered piles were tested in horizontal conditions, batted at -14, +14, and +26 degrees from vertical. A negative batter angle corresponds with a pile battered in the loading direction and, inversely, a positive angle is battered against the loading direction. The test setup for the three battered pile tests differed from the vertical tests to ensure slipping would not occur between the pile and the transfer frame. The new loading frame consisted of a steel loading plate welded vertically to the battered pile to ensure a lateral load was applied by the actuator as shown in **Figure 5-13A**. The head of the pile was still free to rotate satisfying the required free head conditions.

The lateral load test for the -14 degree battered pile (P-4) was conducted on September 8, 2011. **Figure 5-13** shows observations made during lateral load testing of pile P-4 and the new load transfer set up. A small amount of heave occurred during the testing directly in front of the pile. A small gap formed

behind the pile during testing. The majority of the cracking was smaller than the baseline cracking and fanned out around the front of the pile in the region of heaving. This area was within a 2 ft radius of the pile.

The lateral load test for the +14 degree battered pile (P-3) was conducted on September 18, 2011. **Figure 5-14** shows observations made during lateral loading. During this test, heaving occurred over a broader area when compared to pile P-4. The heave was noted at five pile diameters directly in front of the pile at the end of testing. Larger cracking (compared to the -14° test) occurred during this battered pile test. Cracking occurred around the front of the pile with the largest cracks propagating directly out and perpendicular to the load direction. These cracks were up to 2 inches wide and 3 pile diameters in length.

The lateral Load test for the +26 degree battered pile (P-5) was conducted on August 26, 2011. **Figure 5-15** shows observations made during this lateral load test of pile P-5. Heaving was significant during this test, the largest amount of heave out of the ten piles tested in this study. Heaving was apparent 7 ft directly in front of the pile by the end of testing. A very large crack, 3’ inches wide, formed directly in front of the pile in the area of most heave. Slumping of the material was seen in front of and behind the pile. Cracking was observed at greater distances (7 pile diameters) from the test pile compared to the baseline and other battered tests.

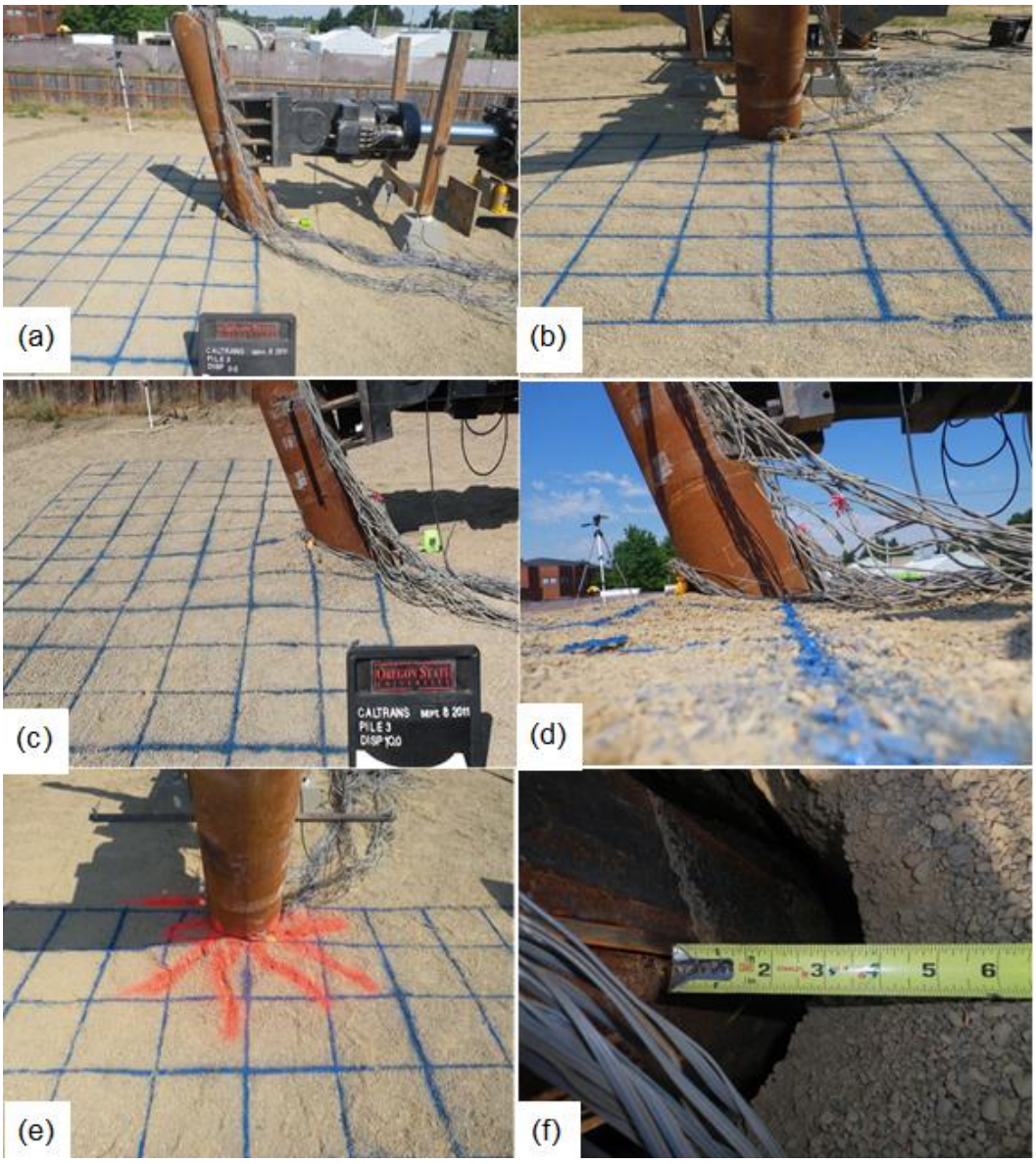

Figure 5-13. Observations during lateral loading testing of Pile P-4 (-14 Batter) a) Pile before loading b) Front of pile before loading c) Pile at 10.0" of displacement d) Soil heave at end of testing e) Soil cracking at end of testing f) Gap formation behind pile

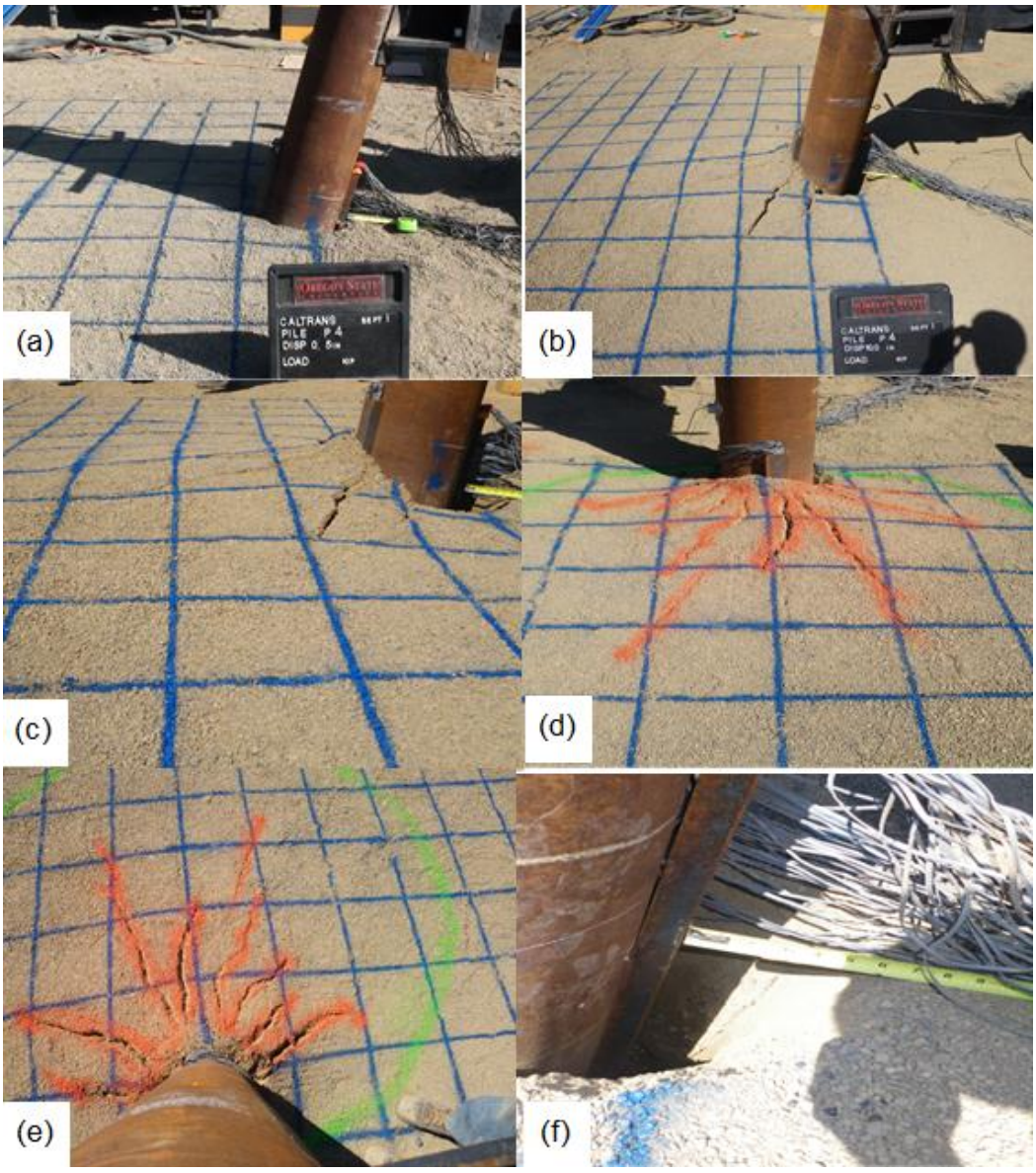

Figure 5-14. Observations during lateral loading testing of Pile P-3 (+14 Batter) a) Pile before loading b) Pile at end of testing c) Soil heave at end of testing d) Soil heave at end of testing e) Extensive cracking and heave f) Gap formation behind pile

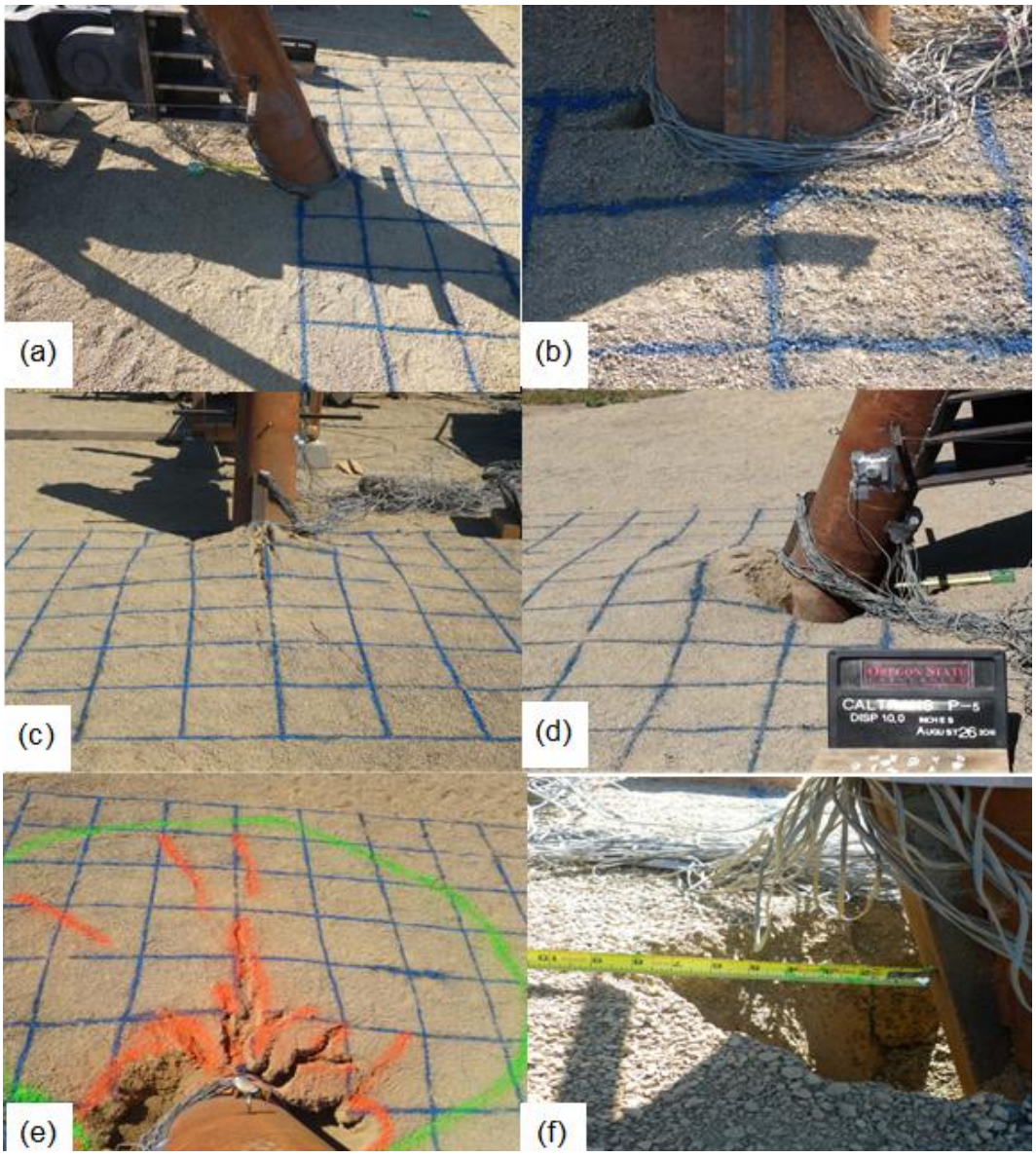

Figure 5-15. Observations during lateral loading testing of Pile P-5 (+26 Batter) a) Pile before loading b) Front of pile before testing c) Soil heave and cracking at end of testing d) Soil heave at end of testing e) Extensive cracking f) Gap formation behind pile

5.9 **Battered Pile Load-Displacement Curves**

The load-displacement curves for the three battered pile tests (P-3, P-4, and P-5) are presented in **Figure 5-16** along with the baseline and -4D curves for comparison. Pile P-4 with a -14° batter angle (battered in same direction as loading) had the highest stiffness of all piles tested in this study. The capacity was also significantly higher with a peak load of 113 kips compared to 87 kips for the baseline pile. The greater load and stiffness is likely due to the direction of movement of the soil failure mechanism. This negatively battered pile, when loaded laterally, forces the passive soil wedge to move laterally and in a downward direction. This downward movement of the wedge interacts with deeper and presumably stiffer soils and results in the increased resistance.

Pile P-5 with a positive batter angle of 26° (battered in the opposite direction of loading) was initially stiffer (up to a displacement of 2.5 in) than the baseline pile. At higher displacements the stiffness and load quickly decreased with a final capacity of 81 kips, 6 kips less than the baseline. This reduction is likely due to the upward movement of the passive soil wedge. According to Reese *et al*. (2004), battered piles are treated as if it was equivalent to a pile on a slope with a similar angle. Therefore, predictions suggest that the load displacement curves of pile P-5 would be similar to pile P-10, which was tested on a 26° or 2H:1V slope. Comparing the curves on **Figure 5-16**, the battered pile had a significantly higher capacity and the stiffness was greater throughout the entire range of

displacements. The trend does not fit the suggestions that a batter angle and slope of similar angle act in the same mechanism. Pile P-3 (14° positive batter) had the lowest stiffness of the tested battered piles and was also lower than the baseline pile. The maximum capacity of pile P-3 was 78 kip.

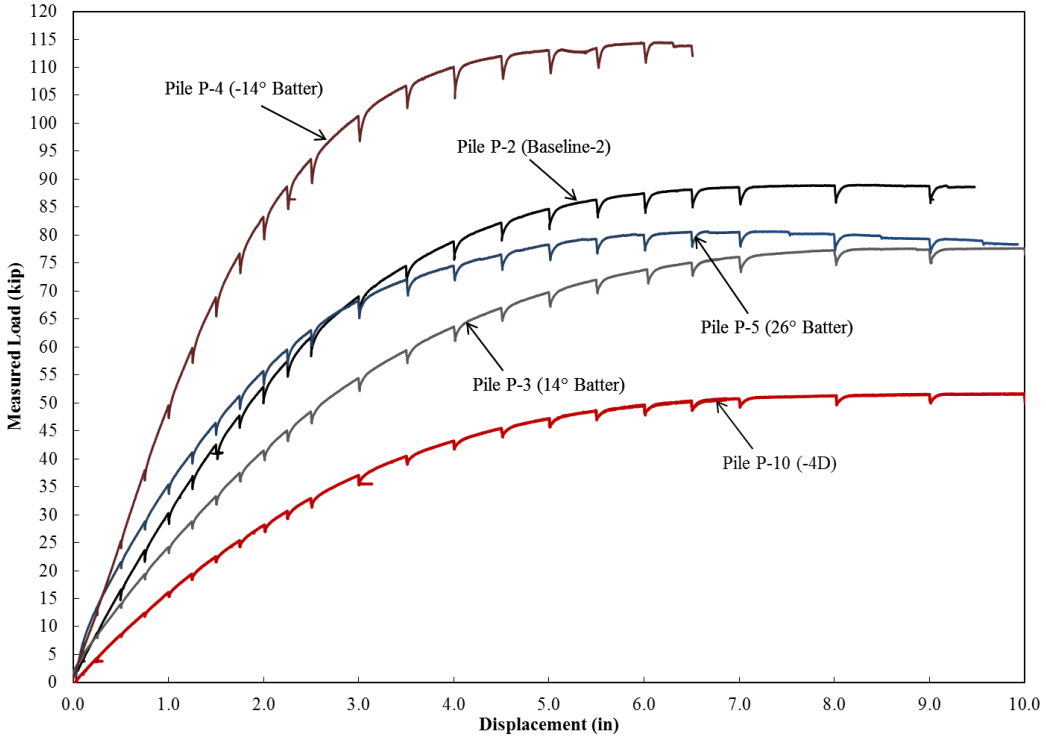

Figure 5-16. Comparison of load-displacement curves between the baseline Pile (P-2), Pile P-10 (-4D) and battered piles

Figure 5-17 presents the LPILE predictions for all battered piles and the baseline pile load displacement curves. The predicted load displacements for pile P-3 (+14°) and P-4 (-14°) follow the same trend as the full-scale results (**Figure 5-16**), with Pile P-4 reaching higher loads than the baseline and Pile P-3 with lower loads than baseline. Overall, LPILE predictions of stiffness and loads are conservative, but accurately predict the trends observed in full-scale results.

Pile P-5 (+26°) has a much higher than predicted stiffness and load where it was predicted to have to lowest of all battered tests. A conclusion was made from analyzing the load displacement data from this battered pile that the testing equipment was near its limitations to laterally load a pile with this steep batter angle. According to the United States Army Corps of Engineers (USACE, 2005) a pile should rarely be battered at an angle greater than 20° and never greater than 26°. The results from the full-scale test are likely inaccurate, due to testing a pile at this upper batter angle limit. The unexpectedly high stiffness and load are likely due to unintended axial loading.

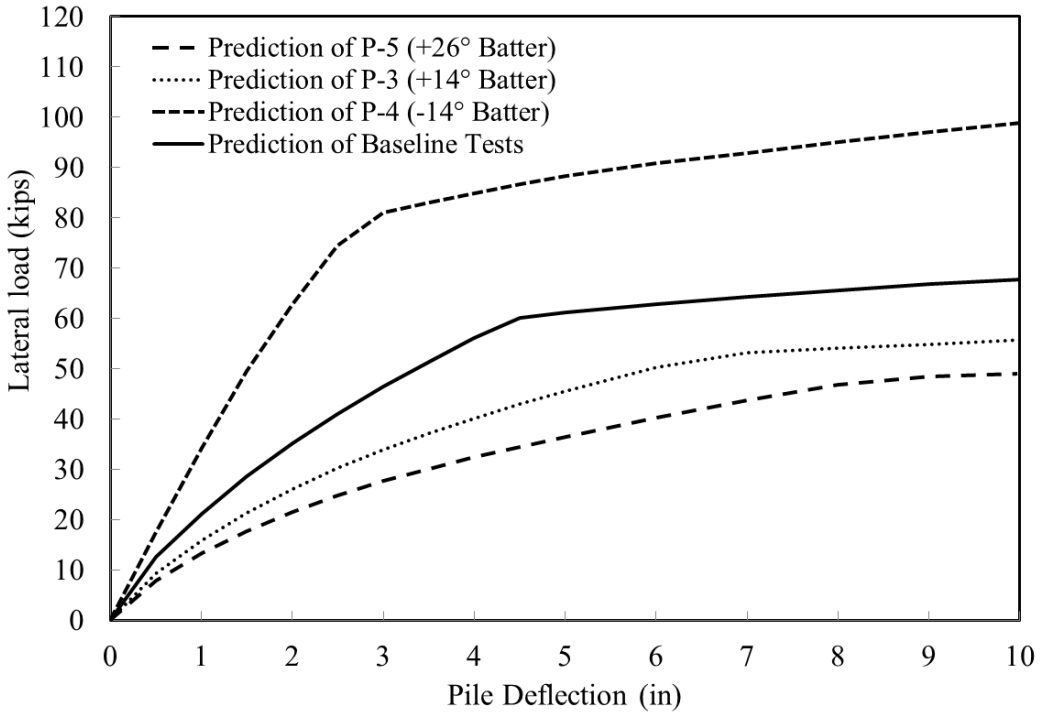

Figure 5-17. LPILE predictions for the battered pile load tests with the baseline prediction

5.10 Factors Effecting Testing Results

Special care was taken throughout testing to ensure testing conditions were as consistent as possible between each load test. With full-scale testing many outside factors can influence the results. For this research experiment these factors include: weather, construction details, soil conditions, equipment compliance and malfunction, and human error.

Changing weather conditions may have had an influence on the overall results. These factors include temperature and moisture. The total amount of rainfall throughout the period of testing was 1.26 inches. The greatest amount of

rain occurred between the 0D and 2D load test where almost 1.0 inches of rain fell. There was a day of dry weather before testing of the 2D pile. The number of days with precipitation was 5 days during the course of testing and the average high was between 66 and 89 degrees Fahrenheit. The weather most likely had limited effects on testing results. The rain before the 2D test likely had the largest weather related effects on testing. During testing, the depth to moisture in the embankment was typically between 2”-5” below the surface. The precipitation data and average high temperatures between each test are shown in **Table 5-1**.

Table 5-1. Precipitation and temperature data during lateral-load testing

Pile	Orientation	Test Date	Precipitation Between Tests (in)	Average High Between Tests (°F)
P-1	Baseline	7/1/2011	-	-
P-9	0D	7/12/2011	0.27	79
P-6	2D	7/19/2011	0.99	72
P-7	4D	7/22/2011	0	75
P-8	8D	7/28/2011	0	78
P-2	Baseline	8/10/2011	0	81
P-10	-4D	8/19/2011	0	81
P-5	26° Batter	8/26/2011	0	82
P-3	14° Batter	9/1/2011	0	N/A
P-4	-14° Batter	9/8/2011	0	85

Care was taken to restrict movement of testing equipment in front of testing piles when possible. The weight of the testing equipment may have slightly densified the soil around the level ground piles resulting in a slight increase in soil stiffness. This is not considered to have a major effect on the test

results because the embankment was constructed at a relatively high compaction to begin with. Testing equipment was not taken in front of the near slope piles.

The cohesive soils below the testing embankment likely experience consolidation after placement of the embankment resulting in added axial load on the test pile but likely had little effect on the lateral loading results. Even though nuclear density gauge testing was conducted to verify the density of the cohesionless embankment during construction, it is likely the density in the embankment may have varied slightly resulting in variations in soil stiffness.

5.11 **Cracking and Shear Failure Angle**

According to Reese et al. (2006) the shear failure angle of a passive soil wedge in cohesionless soils ranges between ϕ and $\phi/2$ and states that angle is dependent on the soil density. Higher density leads to a higher friction angle, ϕ, and therefore a larger shear failure angle, Ω. **Figure 5-18** shows the passive wedges from the full-scale tests ranged between 24° and 39°. This angle increased with greater distances from the slope crest. A recommendation of 70% of ϕ was found for the shear failure angle in dense cohesionless material. The cracking patterns observed for all tests were drawn in AutoCAD with 1 ft square gridlines. These are shown in **Figure 5-19** through **Figure 5-23**.

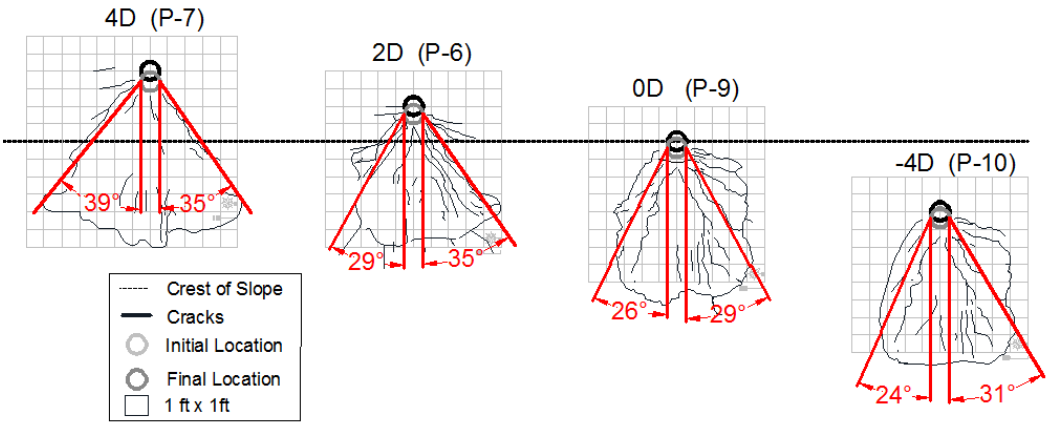

Figure 5-18. The shear failure angle, Ω, for the near slope tests

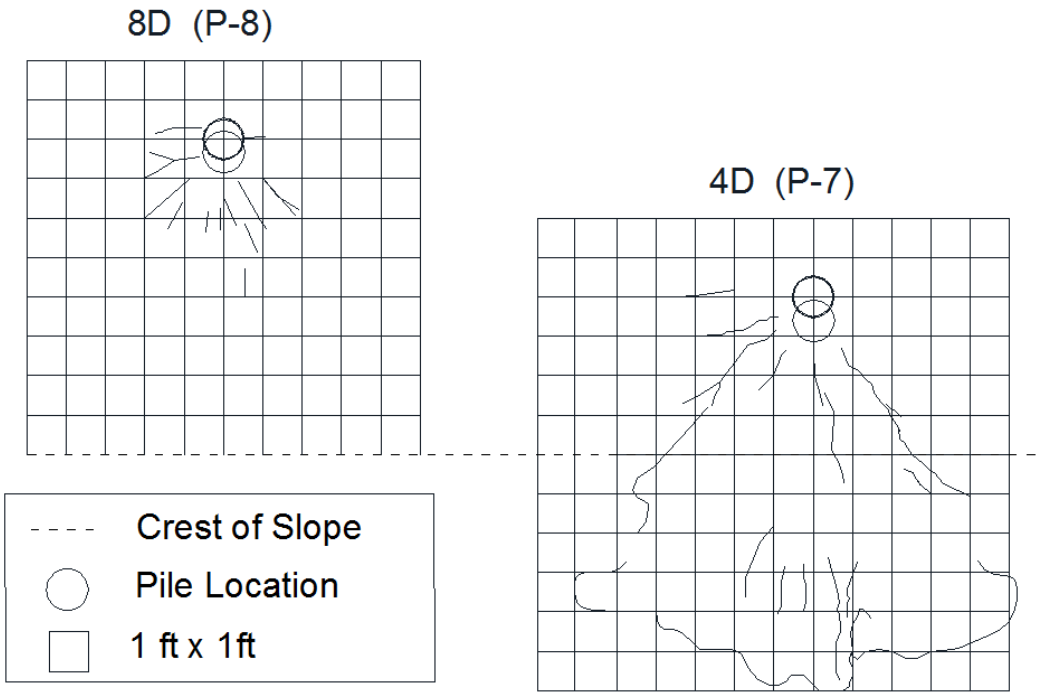

Figure 5-19. Cracking patterns for the 8D and 4D test piles

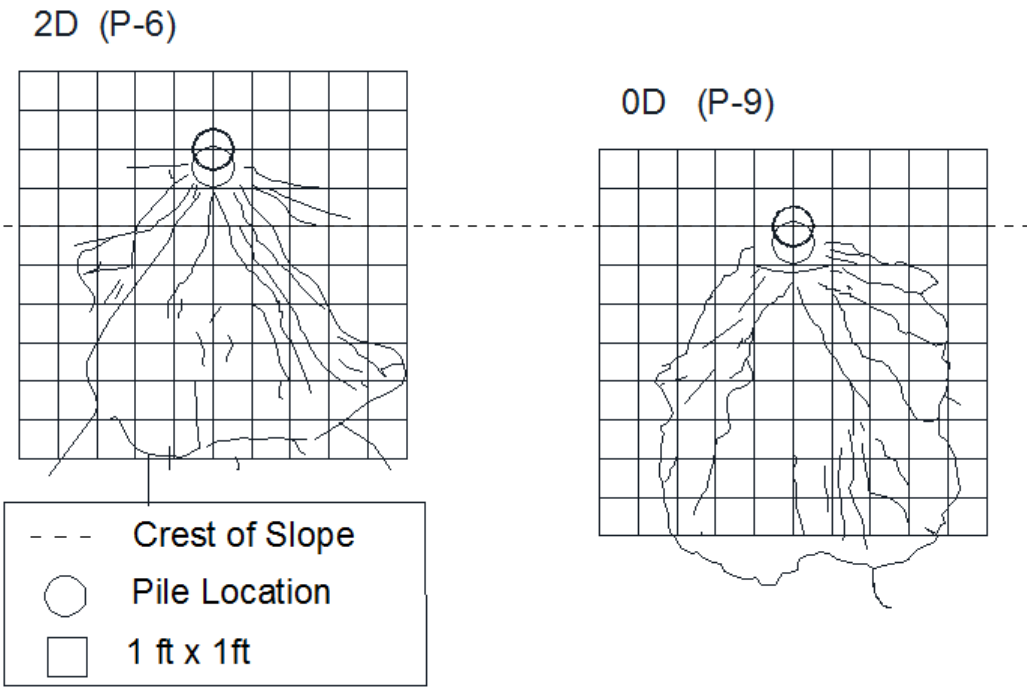

Figure 5-20. Cracking patterns for the 2D and 0D test piles

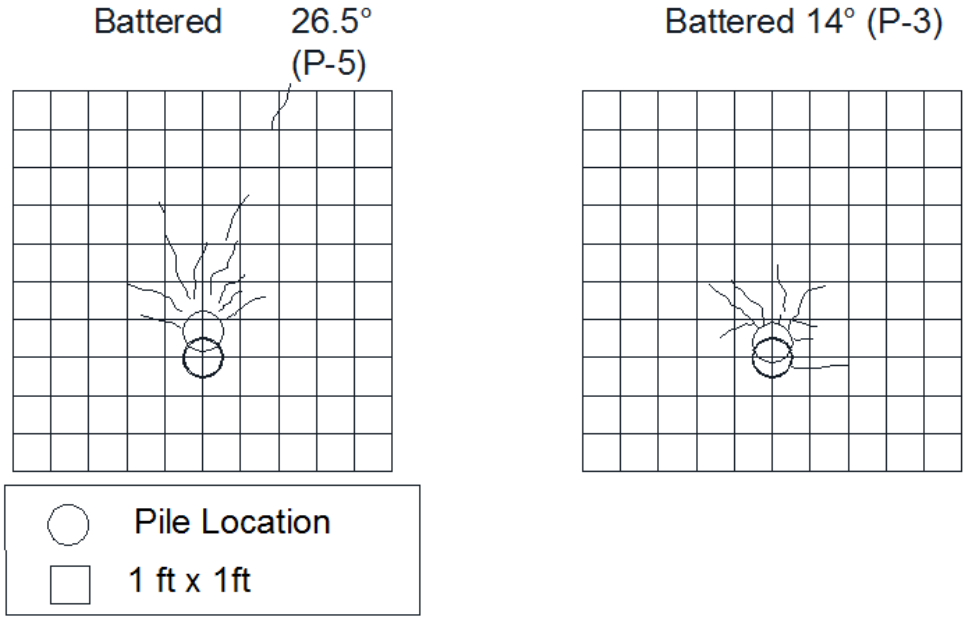

Figure 5-21. Cracking patterns for the +26° and +14° battered test piles

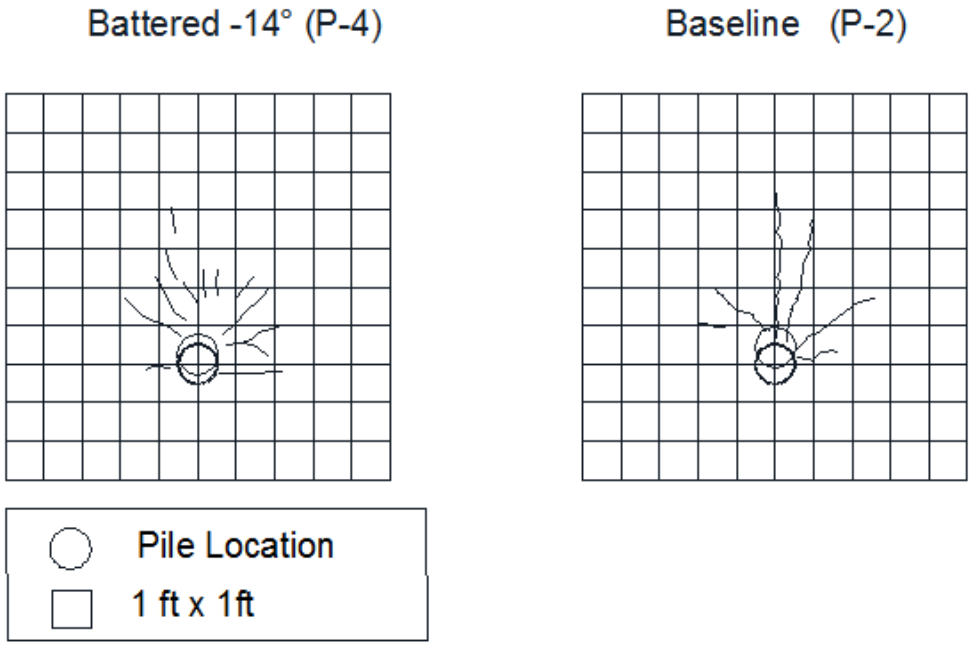

Figure 5-22. Cracking patterns for the baseline and -14° battered piles

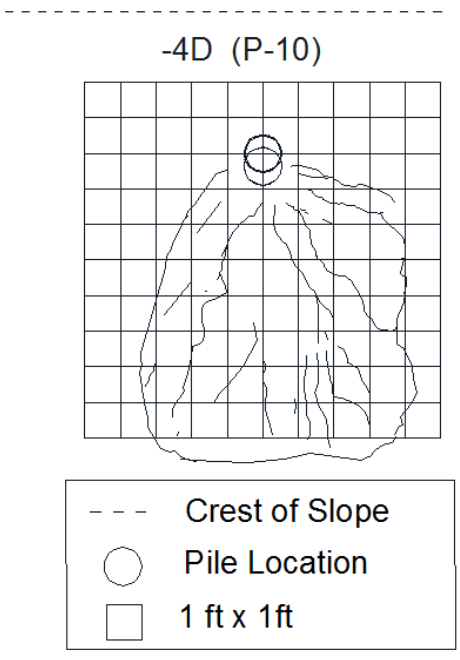

Figure 5-23. Cracking patterns for the -4D (on slope) pile

5.12 **Summary**

Ten full scale lateral load tests were carried out on two baseline piles, four piles near sloping ground, one pile on a slope, and three battered piles. Major observations include heaving of the ground in front of the pile for the baseline pile tests, 8D test, and the three battered tests. A gap formed behind all test piles as well as cracking of the ground surface near the pile. An analysis of test results of each pile is presented in Chapter 6.0.

The laterally loaded piles in proximity to a slope (4D, 2D, 0D, -4D piles) formed visible passive soil wedges. It is concluded that this type of soil failure occurred because of the removal of soil volume in front of the pile allowing for the wedge to overcome resistance and move out laterally. The closer the proximity to the slope the sooner (at lower loads and displacements) the passive wedge cracking formed on the ground surface. Heaving was more evident in the baseline, battered, and 8D tests as pile head displacements increased. For the majority of the tests, cracks formed near the pile along a line perpendicular to the loading direction. The shear failure angle of the passive wedges ranged between 24° and 39° with an average of 70% of ϕ.

Load displacement curves for near slope tests indicate that slope has a significant impact on the lateral capacity of piles. **Figure 5-24** displays all non-battered load displacement curves. For the 0D and -4D piles the slope had a significant effect for all ranges of pile head displacements. For the 2D and 4D

piles the slope had little to no effect for displacements less than 2.5 inches. Piles eight diameters or greater from the crest show no impact. Pile P-3 (+14°) and Pile P-4 (-14°) followed predicted trends from LPILE but had higher than expected lateral loads. The results from battered Pile P-5 (+26°) were not conclusive due to the attempt to test a pile with an excessively high batter angle. The shear failure angle of the passive soil wedges averaged 70% of the friction angle. With full-scale testing many outside factors can influence the results including: human error, weather, construction details, soil conditions, and equipment compliance, and malfunction.

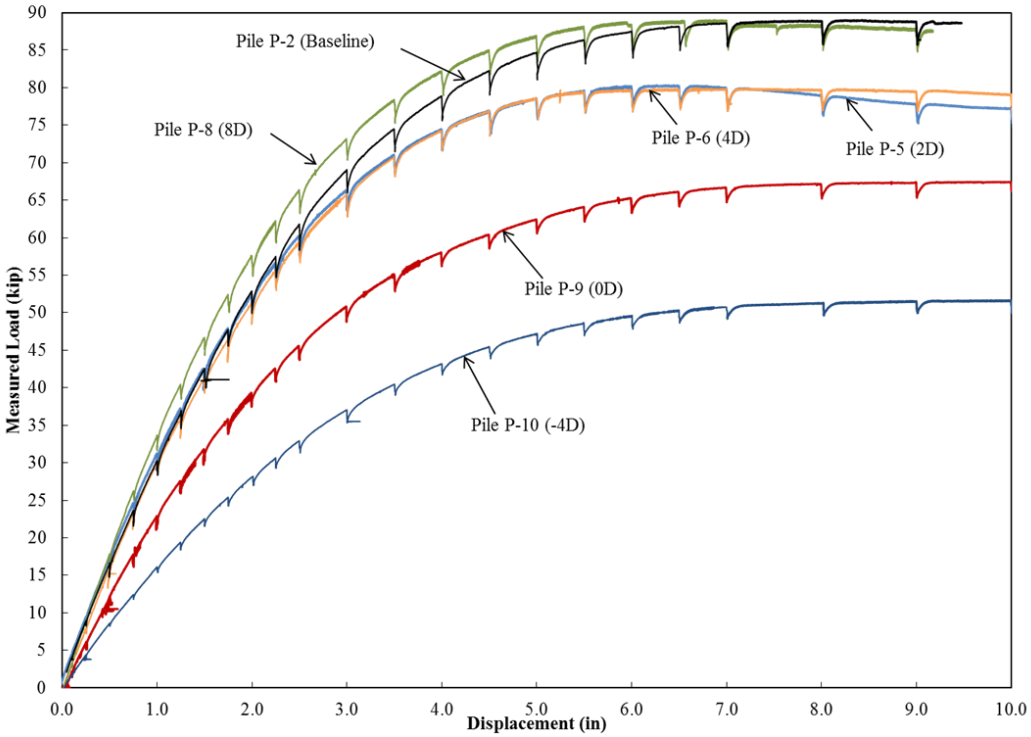

Figure 5-24. Comparison of all non-battered load-displacement curves

6. ANALYSIS OF LATERAL LOAD TEST RESULTS

6.1 Introduction

Using the data obtained from full-scale experiments the soil-pile interaction was back-calculated for each test. This back-calculation provides moment, deflection, rotation, soil reaction, and ultimately *p-y* curves along the profile of each test pile. The effects of soil slope on the soil reaction, *p*, at given displacements, y, was then compared.

6.2 Early Pile Yielding

During the design phase of this project, initial predictions and calculations were conducted to estimate the load-displacement, moment, curvature, and *p-y* curves. This analysis was conducted using predicted soil properties. These predictions were a unit weight of 125 pcf, friction angle of 42°, and an initial coefficient of subgrade reaction of 225 pci. The soil properties from the native soil conditions below the embankment were input in this prediction. Based on these properties, an idealized soil profile was created in LPILE Plus version 5.0 (Reese et al., 2004). The analysis was conducted using available standard sand p-y curves (Reese et al., 1974 and API, 1987) in LPILE 5.0.

The design of the required pile section was selected for the lateral load testing with this output data. As discussed previously, the geometry of the test pile was that of a standard 1-ft inner diameter steel pipe with a wall thickness of

0.375 inch and a length of approximately 30 ft. This pile section was also selected, in part, because it is a standard size presented in the Caltrans Bridge Design Specifications for lateral pile resistance.

During back-calculation of the p-y curves for the lateral load tests conducted in the cohesionless soil, it was discovered that the selected pile section began to yield plastically at pile displacements lower than that predicted. Pile yielding occurred at a pile head displacement of 1.5 inches in the baseline pile and at displacements up to 5.0 inches for piles closer to the crest of the slope. The point of plastic yielding was determined by examining the strain and moment profiles for each pile. The point of yielding for the test piles occurred at 3 ft to 6 ft below ground surface.

Back-calculated p-y curves are shown as solid lines at locations where the strain data used in analysis was within the elastic range for the pile section. The dashed lines (with shown calculated data points) are the computed p-y curves past the point of plastic yielding. This portion of the p-y curves should not be considered accurate as the methods used for back-calculations of these p-y curves is not developed for analyses outside of the elastic range based on the method used for back-calculation.

The back-calculation results for the baseline pile (P-2) data in the elastic range resulted in higher than predicted soil reaction (p) at similar displacements (y) when compared to the predicted model. The predicted soil resistances had

lower ultimate resistances than the full-scale results. This is l the reason for the plastic yielding of the test piles at lower displacements. Due to this yielding, an accurate prediction of the ultimate soil resistances could not be confidently determined. There was an adequate amount data obtained in this series of tests to investigate the effects of slope on lateral pile capacities at small piles displacements, in the range where Caltrans is most interested.

6.3 **Back-Calculation**

6.3.1 **Back-Calculation Method**

A high order global polynomial curve fitting method was used to back-calculate the soil resistance, p, and displacement, y, along the length of each test pile; similar to methods employed by Reese and Welch (1975) and Wilson (1998). Similar to methods used by Nimityongskul (2010), a sixth order polynomial function was fit to the curvature profile obtained from the strain gauge data. This curvature profile was a function of the averaged strain reading at each of the 16 locations along the depth of the pile with the neutral axis distance. **Table 6-1** presents the steps followed to obtain the moment, shear, and soil reaction profiles from the curvature profile. The moment was determined from the product of curvature profile and the flexural rigidity obtained from the beam calibration test. The shear and soil resistance profiles were calculated by differentiation and double differentiation of the moment profile, respectively.

Table 6-1. Procedure to calculate soil reaction, p, from the curvature profile

Profile	Procedure	Eqn.
1. Curvature Profile, ϕ	$\phi(z) = \frac{(\varepsilon_{c\,ave}(z) - \varepsilon_{t_{ave}}(z)) * (0.5)}{N_D}$	(5.1)
2. Moment Profile, M	$M(z) = EI * \kappa(z)$	(5.2)
3. Shear Profile, S	$S(z) = \frac{dM(z)}{dz}$	(5.3)
4. Soil Reaction, p	$p(z) = \frac{dS(z)}{dz}$	(5.4)

EI is the flexural rigidity of the pile, ε_{cave} is the averaged compressive strain, ε_{tave} is the averaged tensile strain, and N_D is the neutral axis distance, which is 12 in.

Table 6-2 shows the procedures followed to obtain the rotation and pile deflection profiles from the curvature. Integration of the curvature profile with depth results in the pile rotation. The pile deflection was determined by double integration of the curvature profile.

Table 6-2. Procedure to calculate deflection, y, from the curvature profile

Profile	Procedure	Eqn.
1. Curvature Profile, ϕ	$\phi(z) = \frac{(\varepsilon_{c\,ave}(z) - \varepsilon_{t_{ave}}(z)) * (0.5)}{N_D}$	(5.1)
2. Rotation Profile, r	$r(z) = \int \kappa(z) dz$	(5.5)
3. Pile Deflection, y	$y(z) = \int r(z) dz$	(5.6)

The top strain gauge pairs were located at the ground surface for each test pile; this was equal to 3ft below the point of loading. An assumption was made that the calculated moment at the top strain gauge decreased linearly to zero at the point of loading when fitting the sixth order polynomial curve. Other assumptions made during this analysis include (Reese et al., 1974):

1. The piles were straight with a uniform cross section.
2. The piles were isotropic and homogeneous.
3. The modulus of elasticity was the same in tension and compression.
4. Piles were not subject to dynamic loading.

A cubic spline method was also investigated to calculate the p-y curves. The results from this method were not consistent and are not presented in this report. Based on the large number of test piles (10), the high order global polynomial curve fitting method was considered the best choice based on the time of implementation and relative accuracy of the method. Yang and Liang (2007) present other methods to calculate p-y curves from strain data including an overview of the cubic spline and high order polynomial method.

6.3.2 **Back-Calculated *p-y* Curves for the Baseline Test**

The back-calculated p-y curves for the baseline pile are shown in **Figure 6-1** for the calculated range of displacements to a depth of 6ft. **Figure 6-2** presents the same p-y curves for displacements up to 1.0 inch to emphasize the

reaction at lower pile movements. The p-y curves obtained for the baseline test have pre-yielding data up to 0.8 inches of displacement. As would be expected, with increased depth the soil reaction (p) increased for a given displacement (y). The ultimate soil reaction was not obtained for this test, but a comparison of the baseline at low displacements (less than 0.8 inches) with near slope piles was possible.

Figure 6-3 and **Figure 6-4** show the results for the bending moment, deflection, and rotation profiles for varying pile head displacements. The bending moment in the latter figure (displacements of 2 inches and greater) reaches a moment of 420 kip-ft at a pile head displacement of 5 inches or greater. This bending moment is similar to the stated maximum determined in the calibration test. An inaccuracy is observed in the deflection plots at the higher displacements as a result of large variance in strain data after plastic pile yielding. The displacements and rotation profiles in **Figure 6-4** for pile head displacements of greater than 3.0 inches show significant error. The rotation profile shows movement at the base of the pile (i.e. not a fixed end) but this is not shown in the rotation data from the tilt sensors (Appendix B-15). The displacements do not match with the measured pile head movement. These results are likely due to carrying through the post-yield strain data during integration steps.

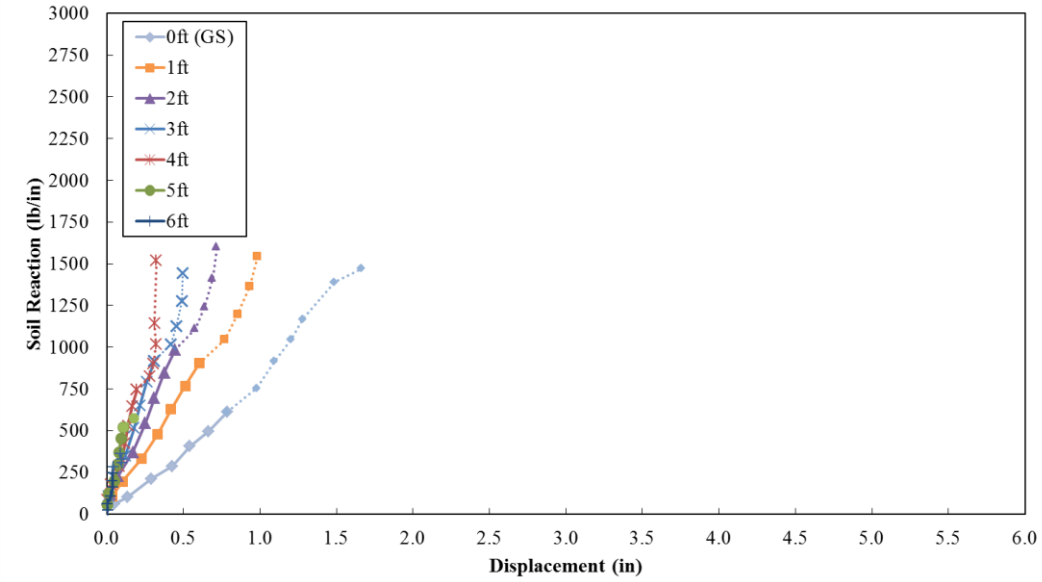

Figure 6-1. Back-calculated p-y curves for the baseline pile
note: dotted lines present data after initial pile yielding

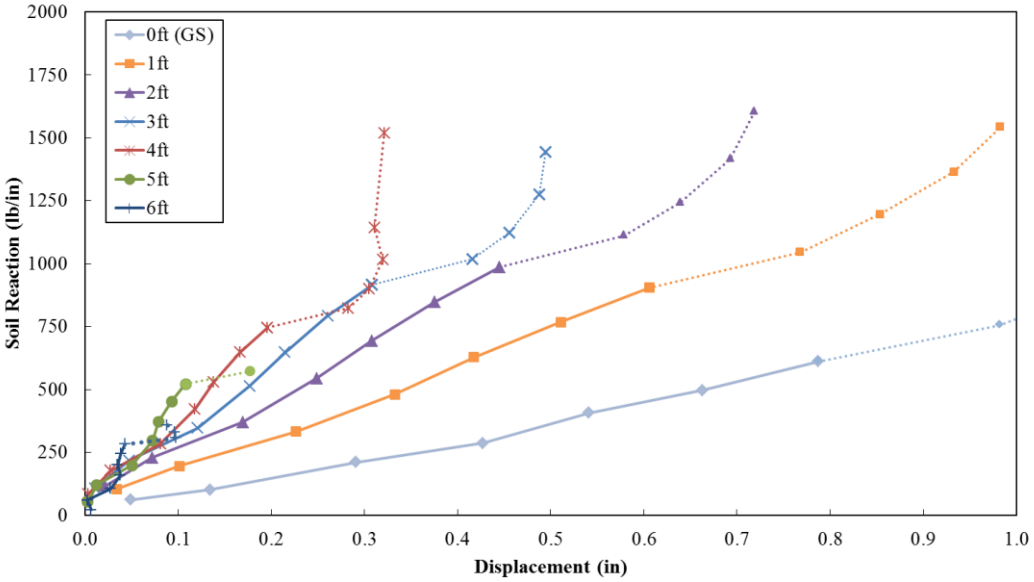

Figure 6-2. Back-calculated p-y curves for the baseline pile at lower displacements
note: dotted lines present data after initial pile yielding

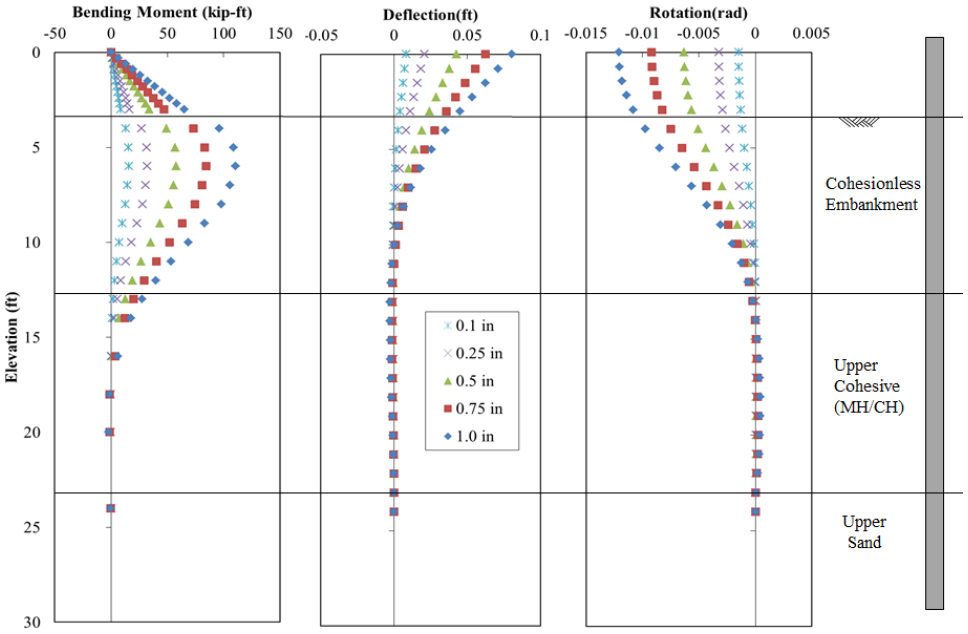

Figure 6-3. Comparison of test results for the second baseline pile head displacement of 0.1, 0.25, 0.5 and 1.0 in.

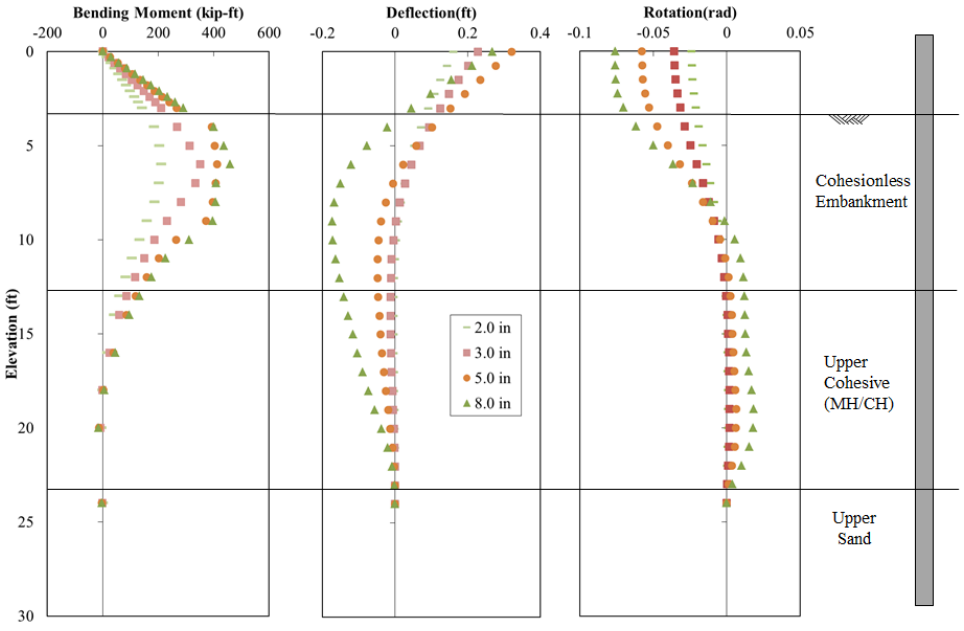

Figure 6-4. Comparison of test results for the baseline pile displacement of 2.0, 3.0, 5.0 and 8.0 in

6.3.3 **Back-Calculated *p-y* Curves for the 4D Pile**

The back-calculated p-y curves for the 4D pile are shown in **Figure 6-5** to a depth of 6ft. **Figure 6-6** presents the same *p-y* curves for displacements up to 1 inch to emphasize the reaction at lower pile movements. The p-y curves for the 4D pile has reliable data up to 0.8 inches, similar to the baseline test. The ultimate soil reaction was not obtained for this test, but a comparison to the baseline at lower displacements (less than 0.8 inches) is possible. When compared to the baseline, the soil reaction is slightly less at similar displacements near the ground surface and nearly the same at lower depths. This demonstrates that the proximity of the slope had little to no effect on the p-y curves at 4D from the slope.

Figure 6-7 and **Figure 6-8** present the results for the bending moment, deflection and rotation profiles for varying pile head displacements. The plots for the lower displacements present expected curves. The higher displacement plots present errors due to pile yielding. The bending moment in the latter figure saturates around a moment of 420 kip-ft for a pile head displacement of 5 inches and greater. The displacements and rotation profiles for pile head displacements of greater than 5.0 inches show significant error. The rotation profile shows movement at the base of the pile (i.e. not a fixed end) but this is not shown in the tilt sensor results (Appendix B-17) and is likely due to carrying through the post-yield strain data during integration.

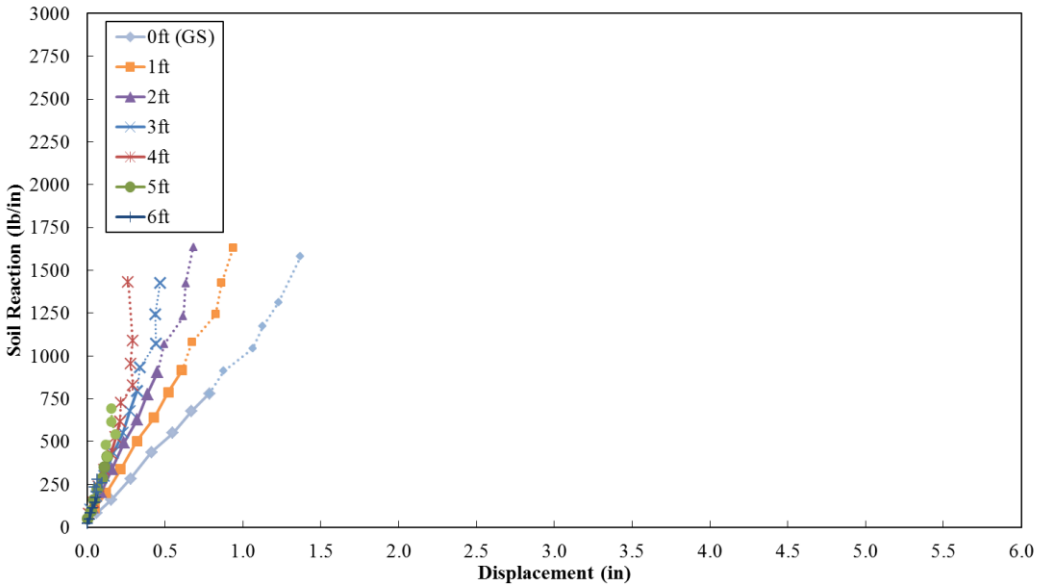

Figure 6-5. Back-calculated p-y curves for the 4D pile
note: dotted lines present data after initial pile yielding

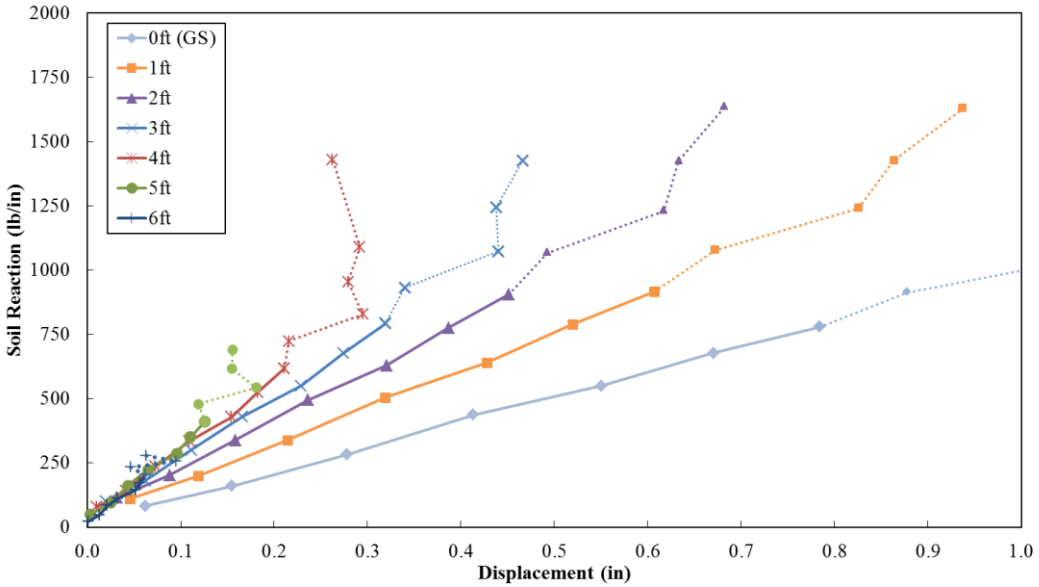

Figure 6-6. Back-calculated p-y curves for the 4D pile at lower displacements
note: dotted lines present data after initial pile yielding

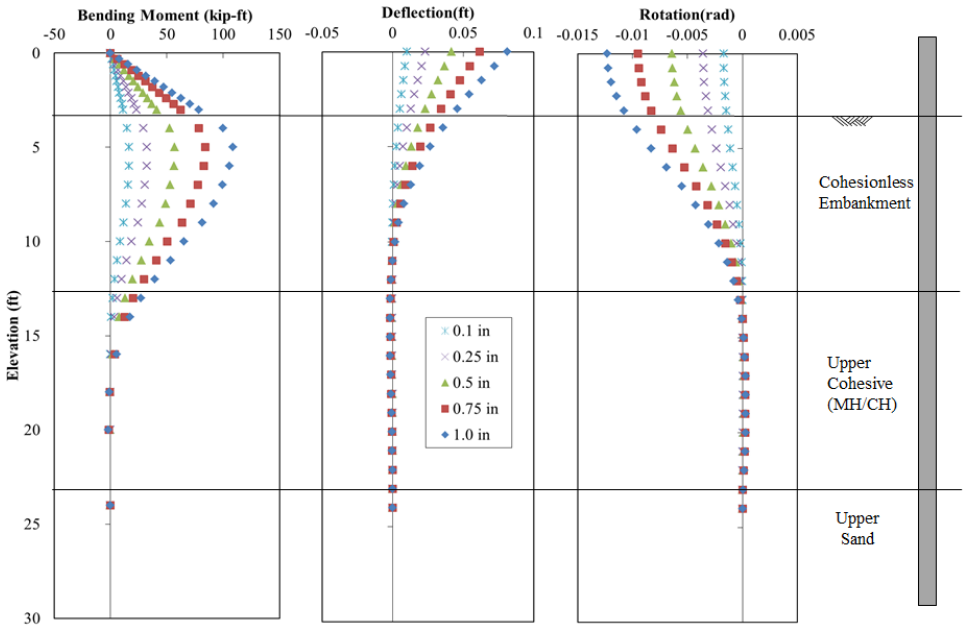

Figure 6-7. Comparison of test results for the 4D pile (p-7) for pile displacement of 0.1, 0.25, 0.5 and 1.0 in.

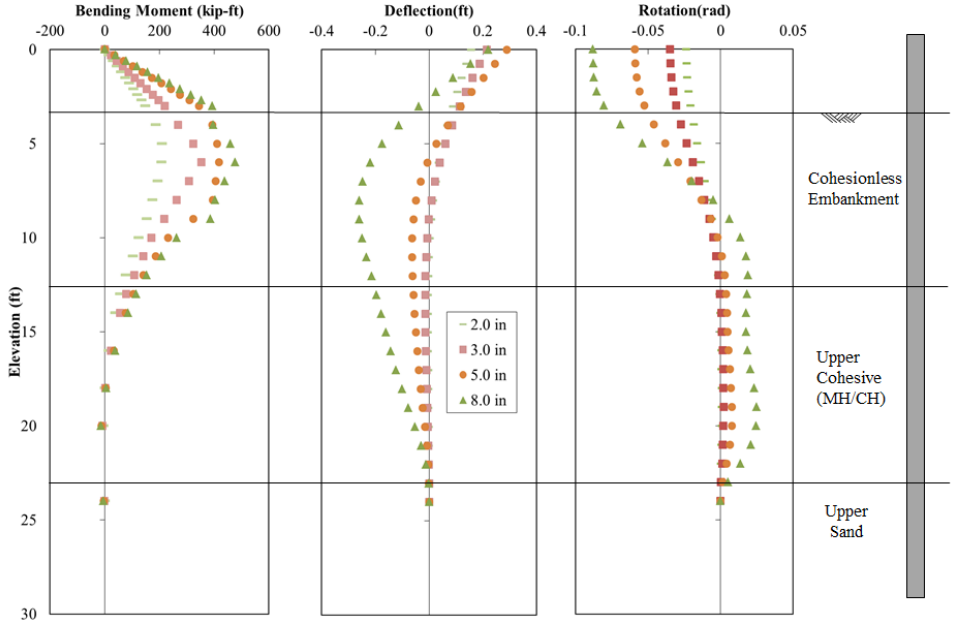

Figure 6-8. Comparison of test results for the 4D pile (p-7) for pile displacement of 2.0, 3.0, 5.0 and 8.0 in.

6.3.4 **Back-Calculated *p-y* Curves for the 2D Pile**

The back-calculated *p-y* curves for the 2D pile are shown in **Figure 6-9** for the calculated range of displacements at 1ft depth intervals. **Figure 6-10** presents the same p-y curves for displacements up to 1.0 inch to emphasize the reaction at lower displacements. The p-y curves for the 2D have reliable data up to a displacement of 1.5 inches. The ultimate soil reaction was not obtained for this test, but a comparison of displacements of less than 1.5 inches is possible. For the back-calculated p-y curves the apparent ultimate soil capacity (flat portion of the p-y curve) is past the elastic range of the pile. Therefore, these results (dashed segments) are not considered reliable. When compared to the baseline, the soil reaction (p) is considerably less at similar displacements at all depths. This demonstrates that the proximity of the slope has a significant effect on the p-y curves at 2D from the slope. **Figure 6-11** and **Figure 6-12** present the results from the analysis for the bending moment, deflection and rotation profiles for varying pile head displacements.

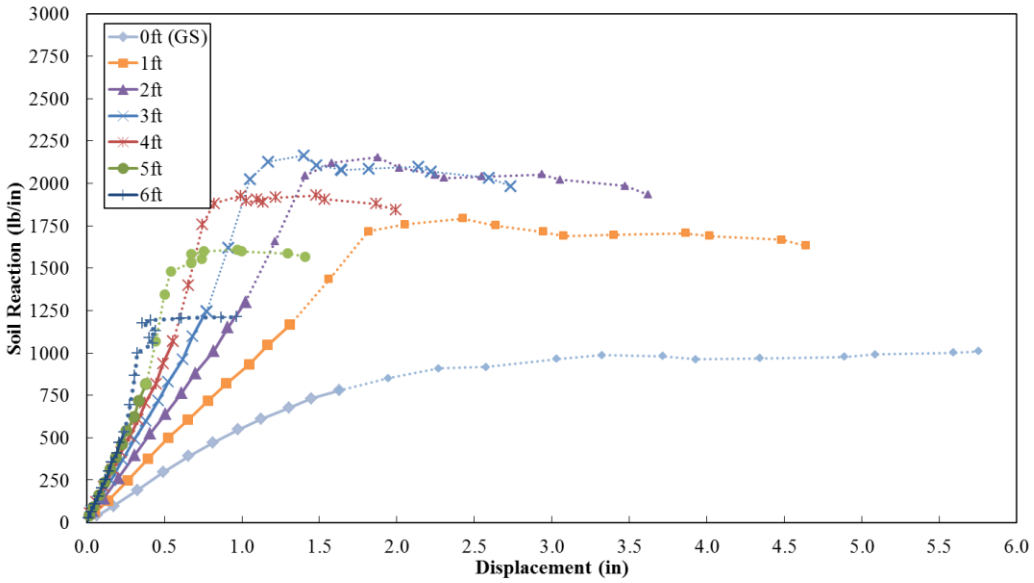

Figure 6-9. Back-calculated p-y curves for the 2D pile
note: dotted lines present data after initial pile yielding

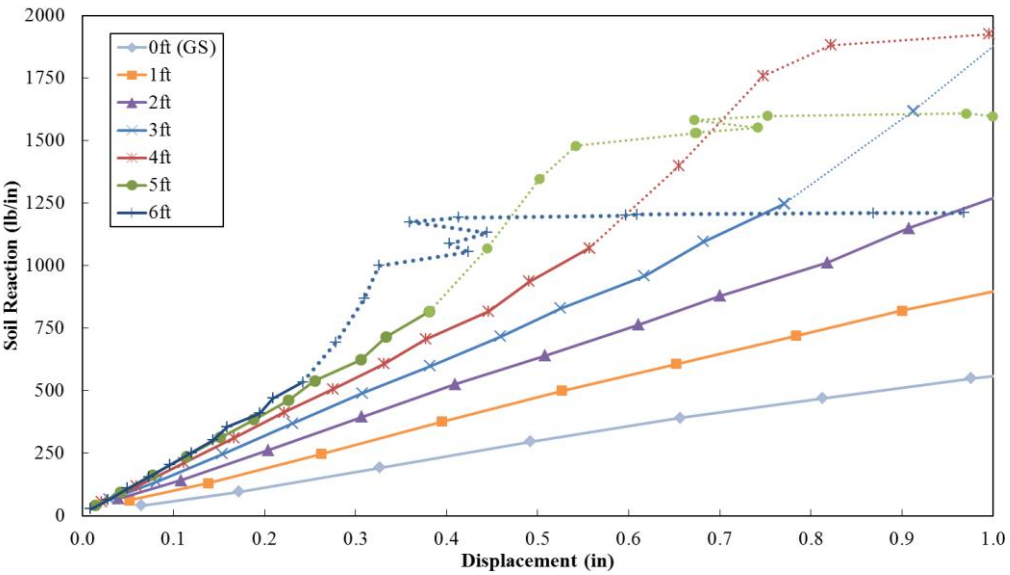

Figure 6-10. Back-calculated p-y curves for the 2D pile at lower displacements
note: dotted lines present data after initial pile yielding

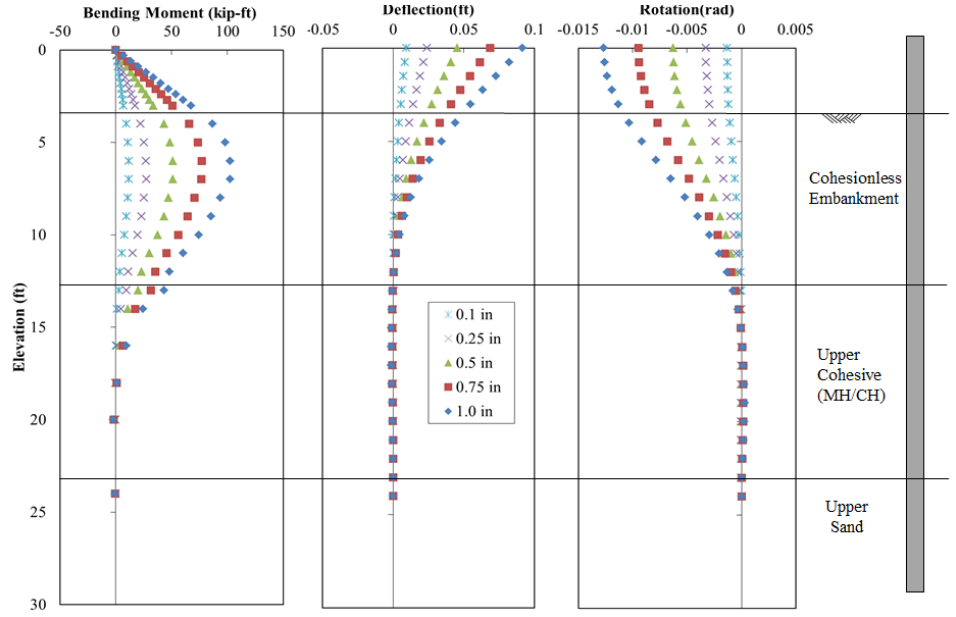

Figure 6-11. Comparison of tests for the 2D (P-6) for pile head displacement of 0.1, 0.25, 0.5 and 1.0 in.

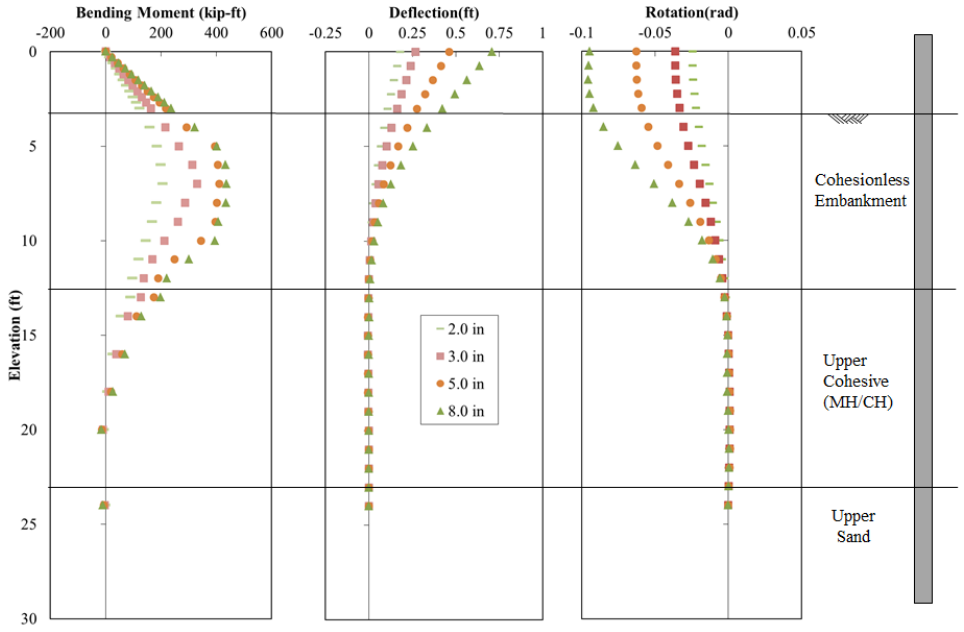

Figure 6-12. Comparison of test results the 2D Pile (P-6) for pile displacement of 2.0, 3.0, 5.0 and 8.0 in.

6.3.5 **Back-Calculated *p-y* Curves for the 0D Pile**

The back-calculated p-y curves for the 0D pile are shown in **Figure 6-13** and **Figure 6-13**. The p-y curves for the 0D pile have reliable data up to a displacement of 1.75 inches. The ultimate soil reaction was not obtained for this test, but a comparison up to 1.75 inches is possible. For the back-calculated p-y curves the apparent ultimate soil capacity is past the elastic range of the pile. When compared to the baseline, the soil reaction (p) is considerably less at similar displacements at all depths were slightly lower than the 2D results. This demonstrates that the proximity of the slope had a significant effect on the p-y curves for a pile located on the slope crest. **Figure 6-15** and **Figure 6-16** present the results from the analysis for the bending moment, deflection and rotation profiles for varying pile head displacements.

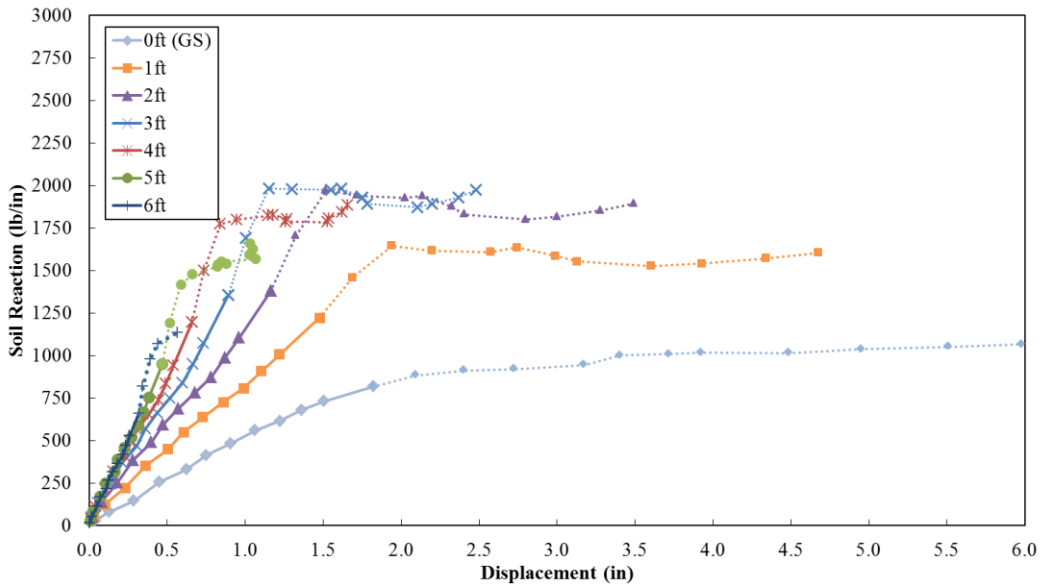

Figure 6-13. Back-calculated p-y curves for the 0D Pile (P-9)
note: dotted lines present data after initial pile yielding

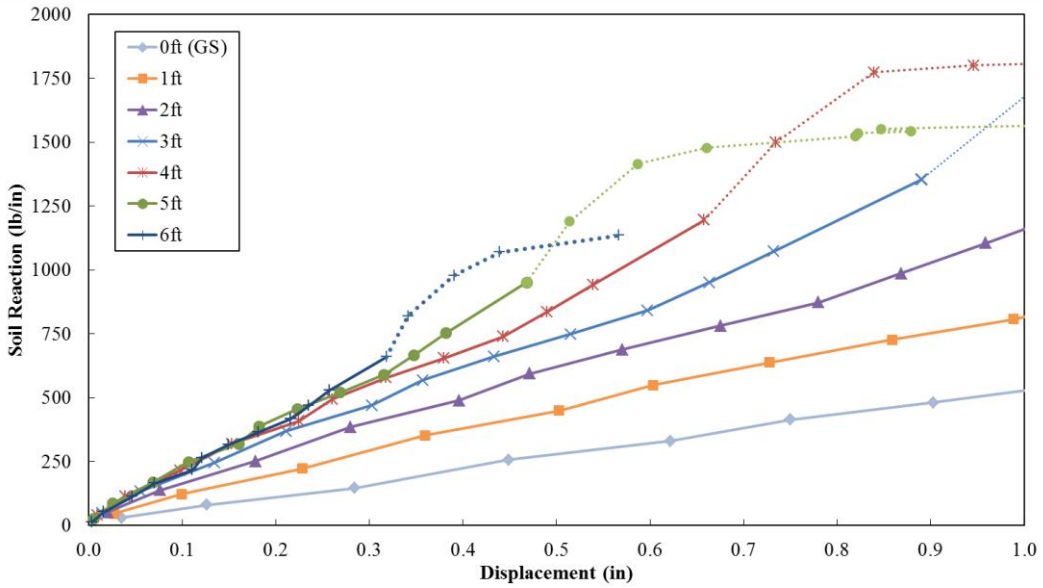

Figure 6-14. Back-calculated p-y curves for the 0D Pile at low displacements
note: dotted lines present data after initial pile yielding

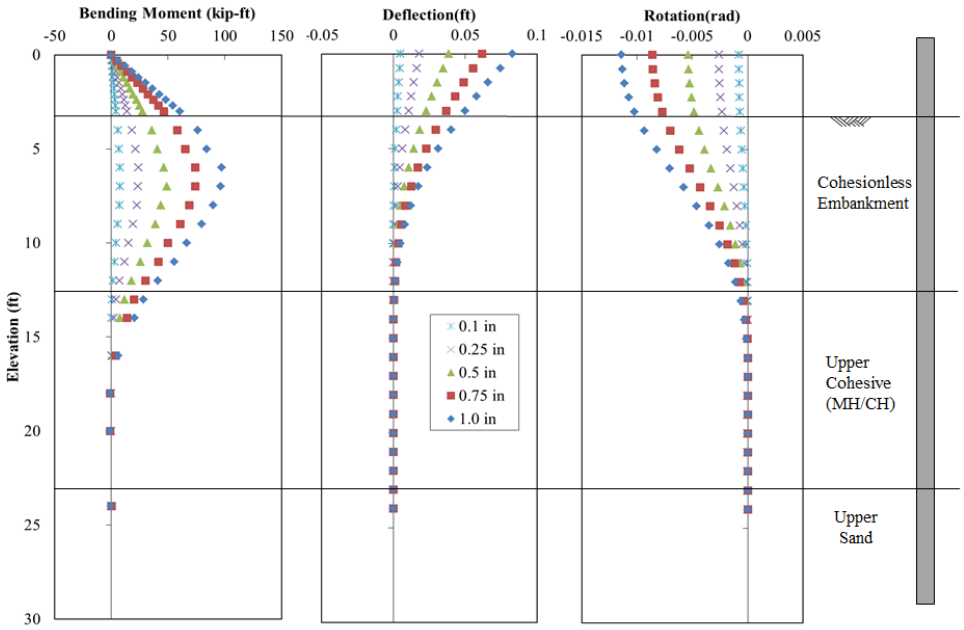

Figure 6-15. Comparison of test results for the 0D (P-9) for pile head displacement of 0.1, 0.25, 0.5 and 1.0 in.

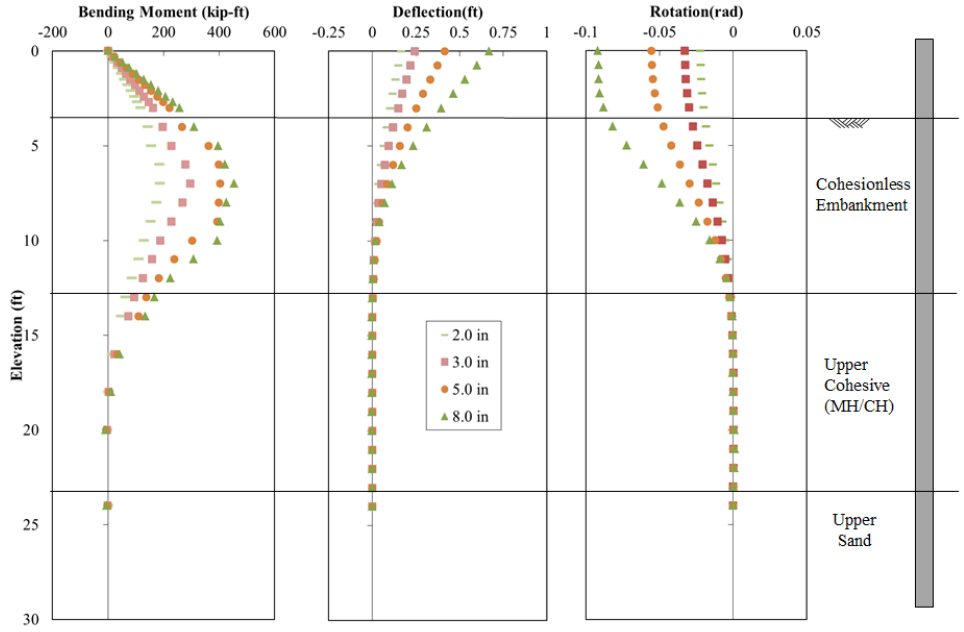

Figure 6-16. Comparison of test results for the 0D Pile (P-9) for pile displacement of 2.0, 3.0, 5.0 and 8.0 in.

6.4 **Back-Calculated *p-y* Curves for the -4D Pile**

The back-calculated p-y curves for the -4D pile are shown in **Figure 6-17** and **Figure 6-18** to depth of 6ft. The p-y curves for the -4D piles have reliable data up to a displacement of 2.25 inches. When compared to the baseline, the soil reaction (p) is significantly less at similar displacements at all depths. The resistance is also considerably less than the 0D results. This demonstrates that the slope has a significant effect on the p-y curves.

Figure 6-19 and **Figure 6-20** present the results from the analysis for the bending moment, deflection and rotation profiles for varying pile head displacements.

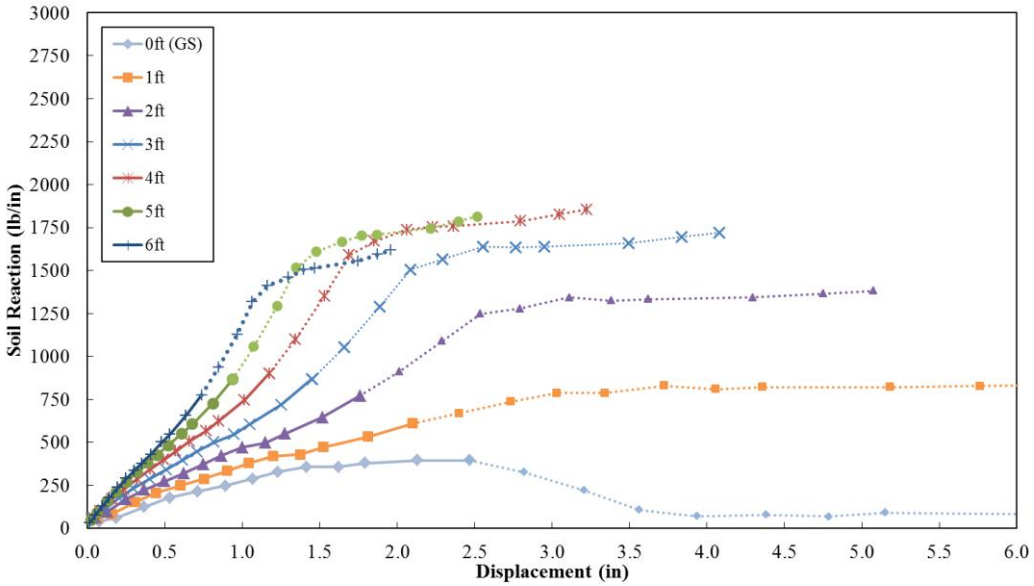

Figure 6-17. Back-calculated p-y curves for the -4D Pile (P-10)
note: dotted lines present data after initial pile yielding

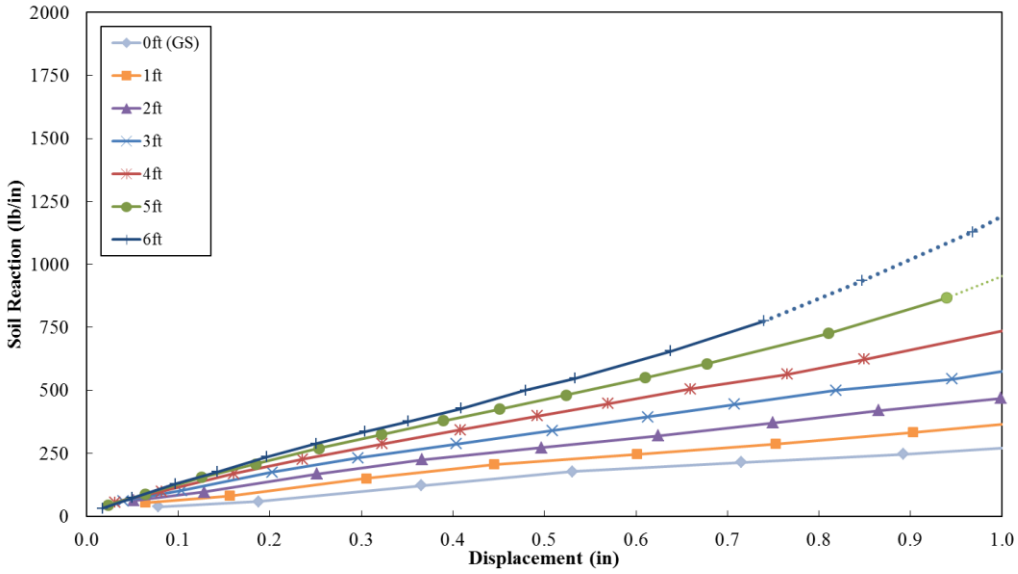

Figure 6-18. Back-calculated p-y curves for the -4D pile at lower displacements
note: dotted lines present data after initial pile yielding

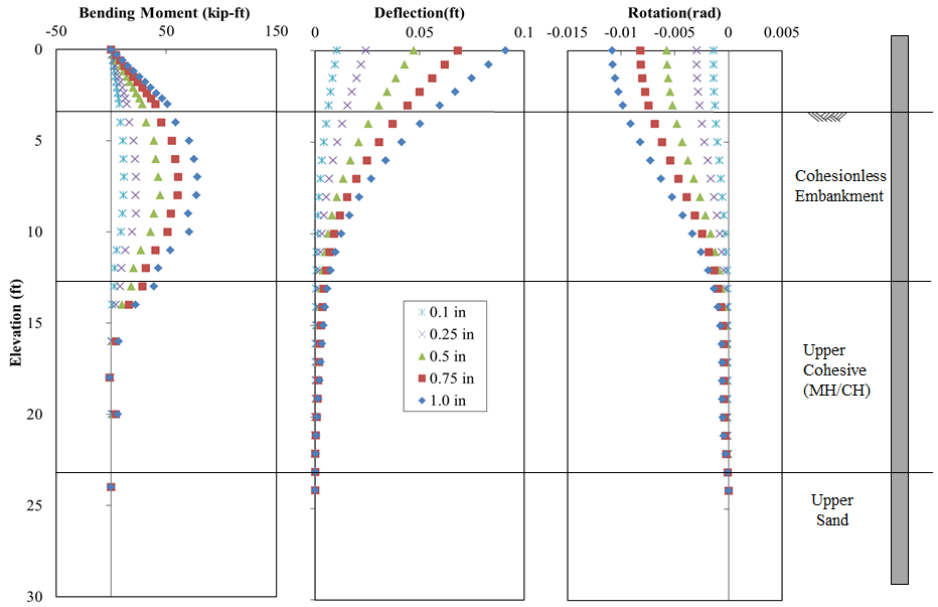

Figure 6-19. Comparison of test results for the -4D (P-10) for pile head displacement of 0.1, 0.25, 0.5 and 1.0 in.

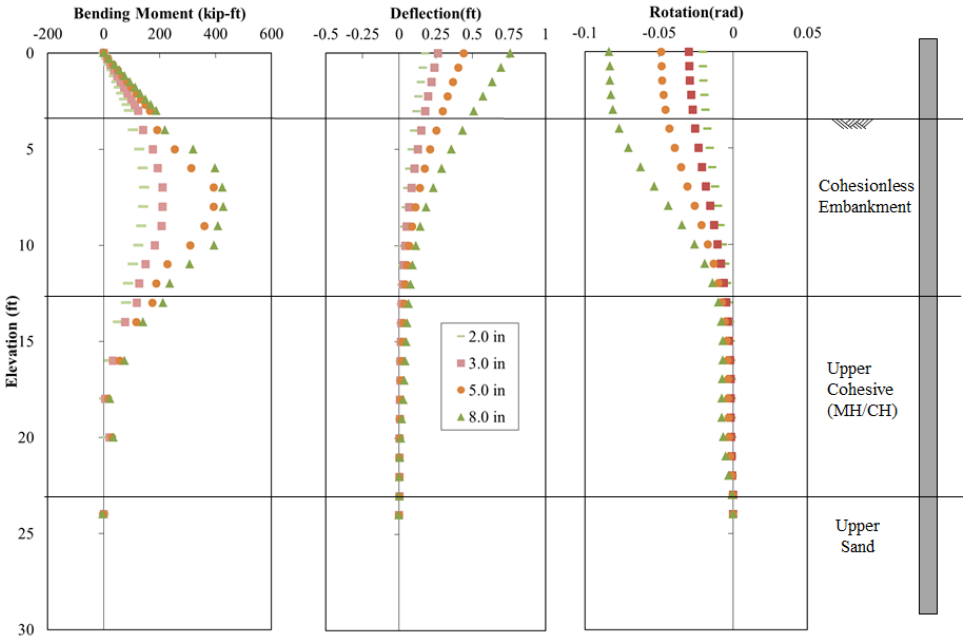

Figure 6-20. Comparison of test for the -4D Pile (P-10) for pile displacement of 2.0, 3.0, 5.0 and 8.0 in.

6.5 **Analysis of Back-Calculated *p-y* Curves and Profiles**

6.5.1 **Accuracy of Back-Calculations**

The accuracy of the back-calculated p-y curves, moment, deflection, and rotation profiles were examined (at pre-plastic yielding) with comparisons of deflection data and tiltmeter rotation data. The rotation profiles obtained from the tiltmeter data (found in Appendix B) matches reasonably well with the computed rotation profiles from the strain data at measured pile head displacements of less than 5 inches for the baseline pile and less than 8 inches for the 0D pile.

The accuracy of the back-calculated pile deflections were compared with the deflections measured with the linear string potentiometer measurements. The lower displacements (deflections less than 4.0 inches) were in good agreement, but the discrepancies increased with increased displacement. The 0D pile had good agreement up to displacements of 6.0 inches. For example, at a measured pile head displacement of 2.0 inches the back-calculated displacement was 1.98 inches and at a measured displacement of 6.0 inches a displacement of 5.85 inches was computed. The baseline pile is consistent up to 3.5 inches (back-calculated at 3.31in). The errors at higher displacements are seen in the deflection profiles in the previously presented figures. This represents the error in the back-

calculations at higher displacements from the high post yield strain gauge readings.

The back-calculated p-y curve sets for each test pile show an increase in subgrade modulus with increasing depth. For all curves, below the point of plastic yielding in this study, the soil resistance increases with increased displacement. These observations are consistent with the definition of p-y curves presented in Chapter 2.0 by other researchers.

For a cohesionless soil, typically the soil resistance, p, is considered zero at the ground surface. This was not found in this study and may be a result of error in the system during integration and differentiation of the polynomial function. The presence of some cohesive material (about 10% fines), the actual depth of top strain gauge after pile driving, and slight loading eccentricities may also account this back-calculated resistance at the ground surface. The resistance at the ground surface is slight and has the lowest magnitude for each test. A boundary condition of zero soil resistance at the ground surface was not imposed in the p-y curve back-calculation. Mezazigh and Levacher (1998) also obtained similar results (a slight soil resistance for the ground surface p-y curves) in centrifuge tests.

The back-calculated methods are considered to be reasonably accurate for data analyzed before the point of plastic yielding. This is based on comparisons of calculated displacement and rotation profiles with measured data. The shape

and location of the initial portion of p-y curves also follow predicted trends where there was an increase in soil modulus with depth and had a linear trend at low displacements (i.e. less than 0.5 inches).

6.5.2 **Comparison of Near Slope *p-y* Curves**

A comparison of the p-y curves on piles located at different distance (-4D, 0D, 2D, 4D) from the slope crest provides insight into the effect of a slope on the soil-pile system. The p-y curves for baseline piles are used to compare to all other experimental p-y curves.

Figure 6-21 and **Figure 6-22** present a comparison of the p-y curves of each test pile at varying depths within the cohesionless profile. Examination of these plots reveals almost identical p-y curves for the baseline and 4D piles from the ground surface to a depth of 5 ft. The baseline curves tended to be slightly higher for all depths except for the ground surface. The p-y data for the 2D and 0D piles were very similar in magnitude with the 2D pile just slightly stiffer. These piles were less stiff than the baseline and 4D results. The pile on the slope (-4D) was significantly less stiff than other four tests for all ranges of displacements. This data was used to develop methods to account for soil slope. The ratio of soil resistance, commonly known as p-multipliers, was calculated by

comparing the soil resistance at each soil displacement for each pile tests (-4D, 0D pile, 2D pile and 4D pile) and depths with baseline p-y curves.

It is important to note that the 2D and 4D load-displacement curves are almost identical at all displacements (Figure 5-24), but this is not seen in the p-y curves for the 2D and 4D results. The p-y curves for the 4D pile are similar to the baseline curves and the 2D results are similar to the 0D p-y curves. This was not expected after observing the similarities in the load-displacement curves. These trends suggest that the 2D p-y curve would be steeper than the 0D p-y curves, and more closely follow the 4D results. This may be a result of the 1.0 of rainfall that occurred over a five day period before the testing of the 2D pile. One day of dry weather separated the rainfall events and the testing of the 2D pile. This rainfall may have an effect on the resulting p-y curves by reducing the near surface stiffness. During pile installation of the 2D pile there was soil disturbance in front of the pile that extended out onto the slope. This disturbance consisted of a wedge of soil moving outward onto the slope during pile driving. The disturbance was about 3 ft in width and moved about 2 inches laterally onto the slope. This near slope disturbance and the rain event may have caused a decrease in near surface soil stiffness for the 2D p-y curves but may not have affected overall load-displacement of the entire 2D test pile. This may explain the discrepancies between the 2D and 4D load-displacement curves with the near surface 2D and 4D p-y curves.

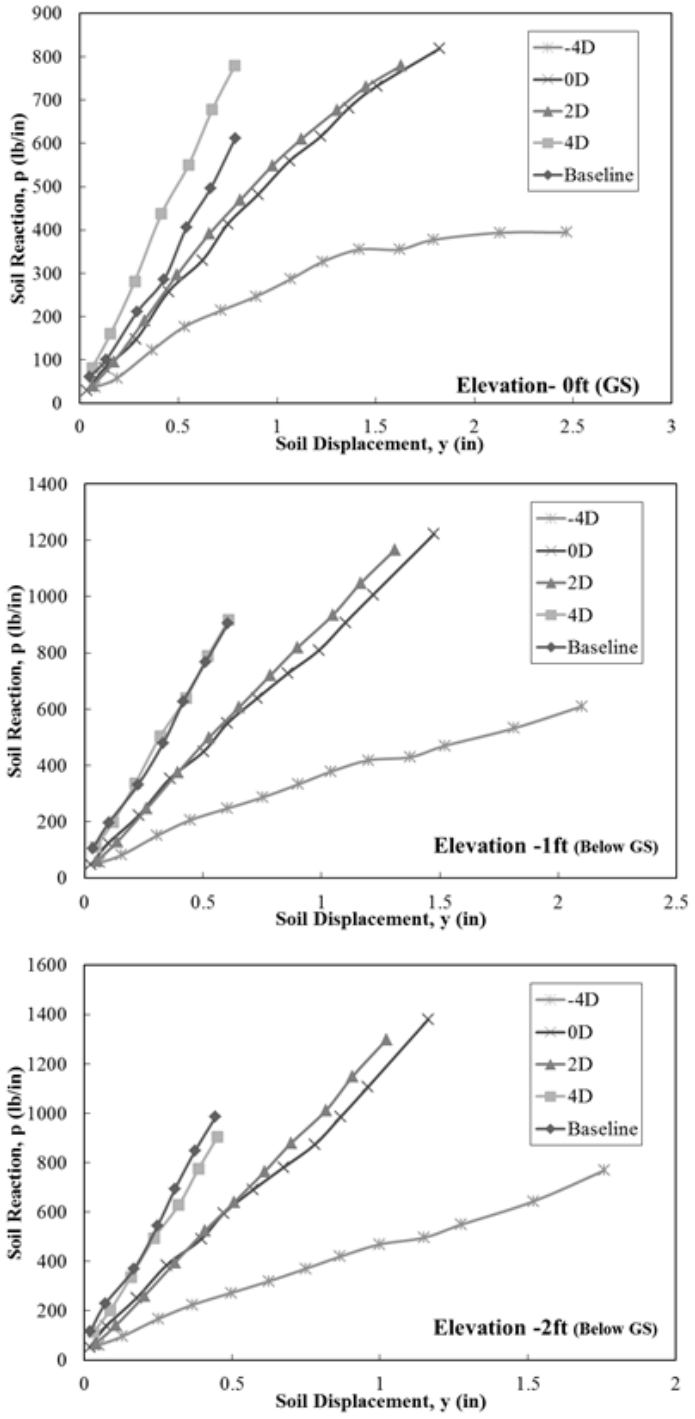

Figure 6-21. Comparison of p-y curves for each pile at the same depth (Depth: GS to -2ft)

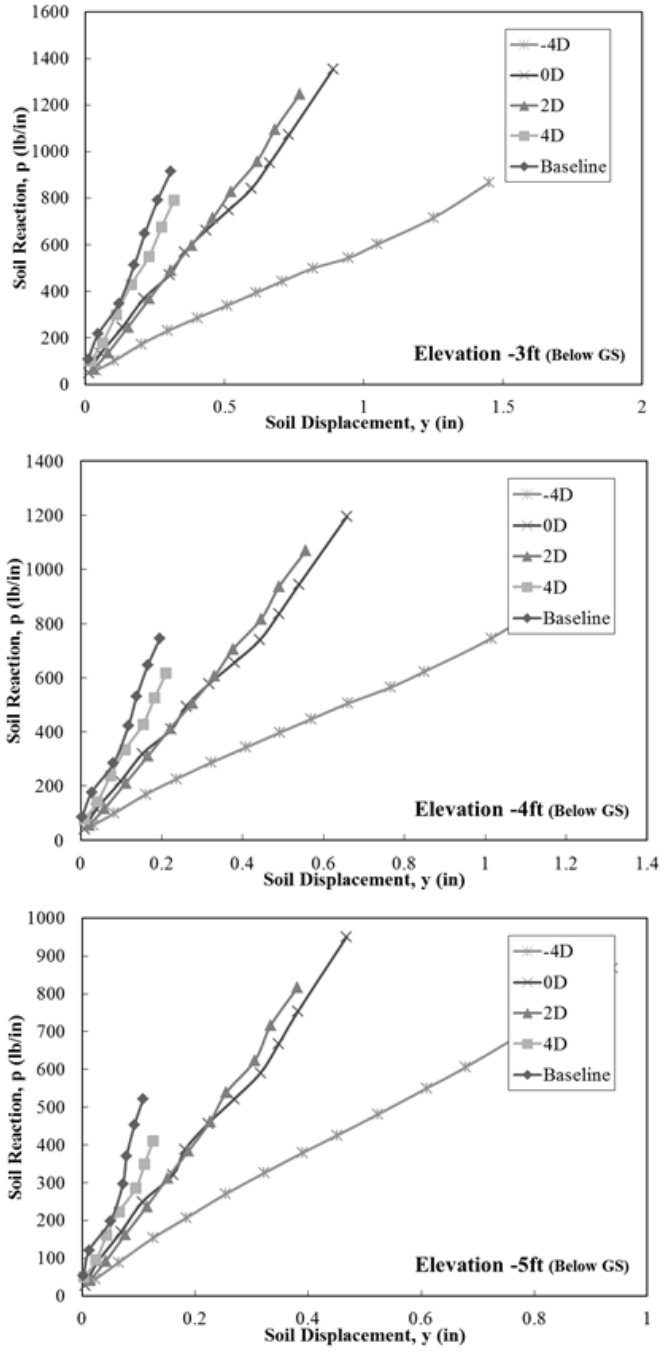

Figure 6-22. Comparison of p-y curves for each pile at the same depth (Depth: -2ft to -5ft)

6.6 **Summary**

A sixth order polynomial function was fit to the strain gauge data along the depth of each pile to compute the soil reaction and pile deflection profiles. The moment, shear, and rotation profiles were also calculated. Based on the comparison of p-y curves, for all displacements, the slope effect on lateral resistance is significant for piles located at 2D or closer from the slope crest. For a pile located at 4D or greater from the slope crest, the effect of slope is insignificant for the analyzed ranges of soil displacements.

The soil resistance (p) at a given displacement (y) of the p-y curves for the -4D, 0D, and 2D pile are significantly less than the baseline pile in the range of pre-plastic yielding p-y curve data. The curves for the baseline and 4D piles are similar in shape and ultimate capacities showing that the effect of the slope was relatively small at four pile diameters from the slope crest.

7. COMPARISON OF CURRENT METHODS & MODELS

7.1 Introduction

Several researchers have proposed methods to account for lateral pile capacities in level ground cohesionless soils and near slopes. With the results obtained from this study a comparison of existing methods was conducted. Comparisons were made between back-calculated and predicted p-y curves, load-displacement curves, reduction factors, and load resistance ratios. A simplified design procedure to account for the effects of soil slope is proposed from the results.

7.2 Comparison of Horizontal Ground Models

Two commonly used methods to predict lateral load capacity and p-y curves in level ground are the Reese et al. (1994) and API (1987) methods. The soil properties from the testing site were input in these models to compare the predictions with the back-calculated results.

7.2.1 Reese et al. 1794 (LPILE 6.0)

The pile properties obtained from the pile calibration test were input into the computer program LPILE Plus 6.0 (Reese et al., 2004). The average yield strength of the piles is 74.7 ksi and the effective yielding moment of the test piles was 416 kip-ft. A post yielding bending stiffness of 5% of the elastic stiffness was

chosen for the LPILE analysis. The recommended coefficient of subgrade reaction, K, of 225 pci was used with a soil unit weight of 127pcf.

Figure 7-1 shows the LPILE predicted load-displacement curve with the full-scale test results for the baseline pile. LPILE significantly underestimates the lateral capacity for all pile head displacements. The ultimate resistance was underestimated by almost 20% and the initial stiffness was less at lower pile head displacements.

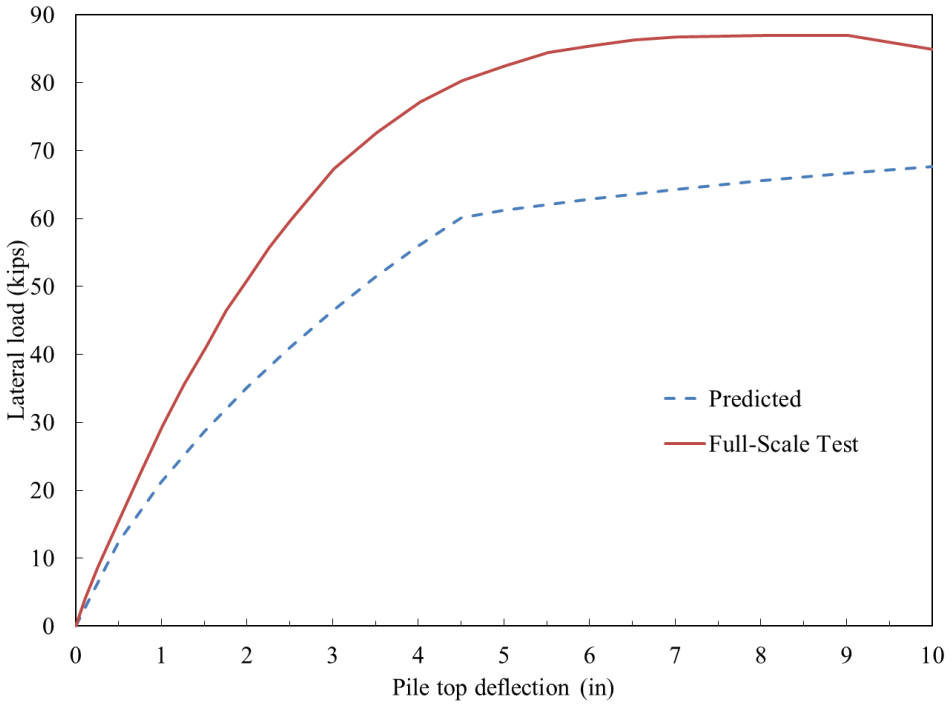

Figure 7-1. LPILE predicted baseline load-displacement curve with the full-scale test results

Figure 7-2 presents the predicted baseline p-y curves calculated using the same soil parameters with the Reese et al. (1974) cohesionless soil procedures. These curves are shown at 1ft intervals to a depth of 4 ft with displacements up to 0.6 inches. These values were chosen for comparison with the available back-calculated p-y curves. This model is based on an initial linear soil modulus and then a hyperbolic function before reaching the ultimate soil reaction. The ultimate soil reaction is reached in this model at just under 0.5 inches. A further comparison of these curves, API (1987) predictions, and the back-calculated results are presented in the following section.

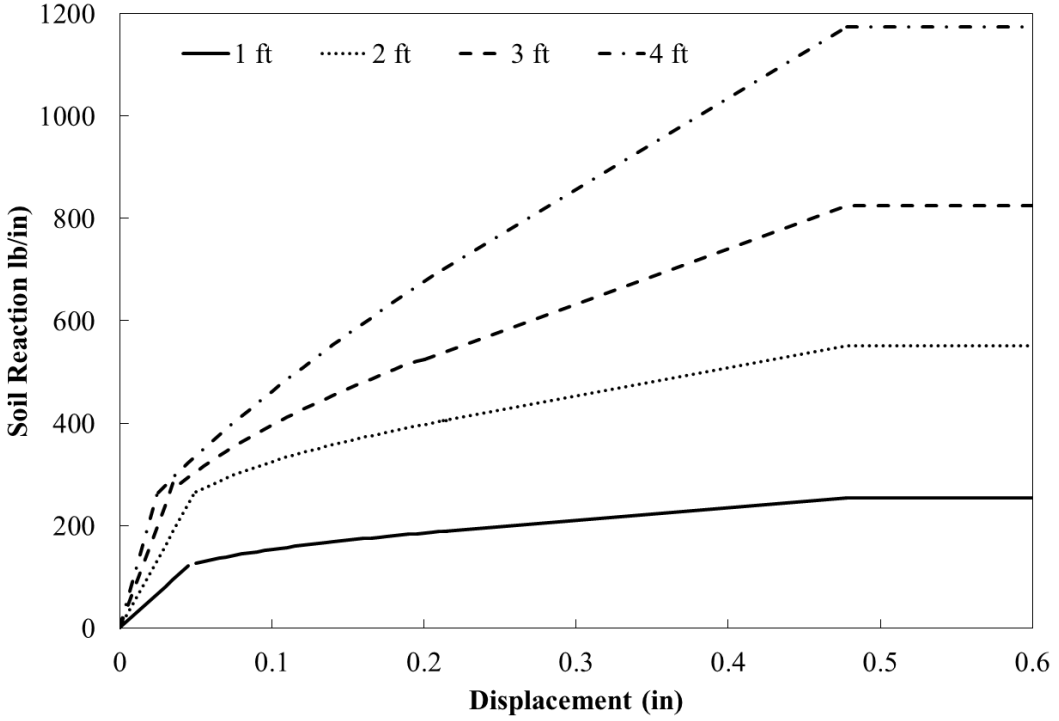

Figure 7-2. Reese et al. (1974) predicted baseline p-y curves with input soil properties matching the full-scale tests

7.2.2 **American Petroleum Institute (1987)**

The cohesionless embankment soil parameters were input into the API (1987) model to predict the baseline p-y curves. **Figure 7-3** presents the predicted baseline p-y curves with this procedure. A coefficient of subgrade reaction, K, of 225 pci was estimated in this model for sand above the water table using the API (1987) correlations with the friction angle as presented in Chapter 2.0. The p-y curves are shown at 1ft intervals to depth of 4 ft with displacements up to 0.6 inches. This model is based on hyperbolic functions before reaching the ultimate soil reaction. The ultimate soil reaction is reached in this model at a displacement of less than 0.2 inches.

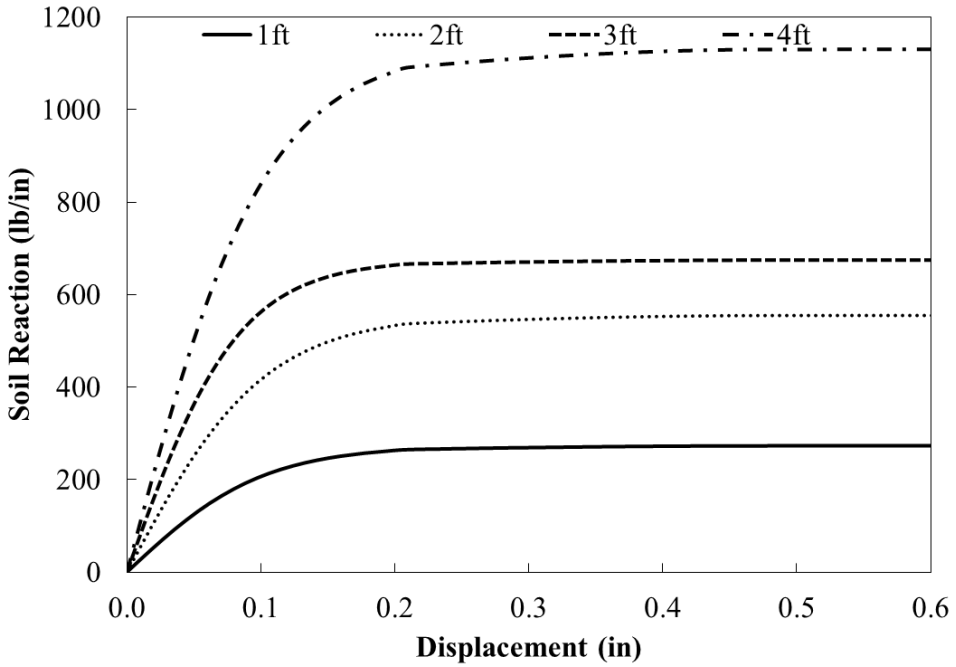

Figure 7-3. API (1987) predicted baseline p-y curves with input soil properties matching the full-scale tests

Figure 7-4 and **Figure 7-5** show the predicted baseline API (1987) and Reese et al. (1974) p-y curves with the back-calculated p-y curves from this study. Only p-y curves to depth of 4 ft are compared. Deeper comparisons are not made because the pile displacements back-calculated at these depths are less than 0.2 inches. Both models over predict the initial stiffness at displacements of less than 0.2 inches at depths below 1ft. The API model has the greatest subgrade modulus at these displacements and reaches ultimate resistance before the Reese et al. (1974) model. The soil stiffness of the full-scale results is more representative of Reese et al. (1974) prediction model. At higher displacements, more than 0.2 inches, the soil reaction is significantly under predicted by both models at depths

above 4ft. The available data from the back-calculated p-y curve at a depth of 4 ft is similar in stiffness to the Reese et al. (1974) p-y curve.

In **Figure 7-4** and **Figure 7-5** only the pre-plastic yielding p-y curves are presented for comparison. No apparent ultimate soil resistance is reached from the available back-calculated data. The ultimate soil resistance is about 200 lb/in for both models at a depth of 1ft, and the back-calculated resistance is close to 700 lb/in at a displacement of 0.45 inches without an obvious ultimate resistance reached. At depths of 2 ft and 3 ft the ultimate soil reaction is significantly under predicted by both models. The magnitudes of the Reese et al. (1974) model more closely predicted the resistances obtained in the full-scale test results.

Table 7-1 presents the mean bias and coefficient of variation (COV) values between the back-calculated and predictive model p-y curves at increasing pile displacements. A total of 110 data points were used in this statistical analysis. The mean bias was calculated by the observed divided by the predicted.

Table 7-1. Mean bias and COV between the back-calculated and predictive model p-y curves at various pile displacements

Displacement (in)	Mean Bias	COV (%)
0.1	0.7	29.8
0.2	0.8	35.0
0.3	1.3	30.3
0.4	1.9	29.5
0.5	2.6	33.3

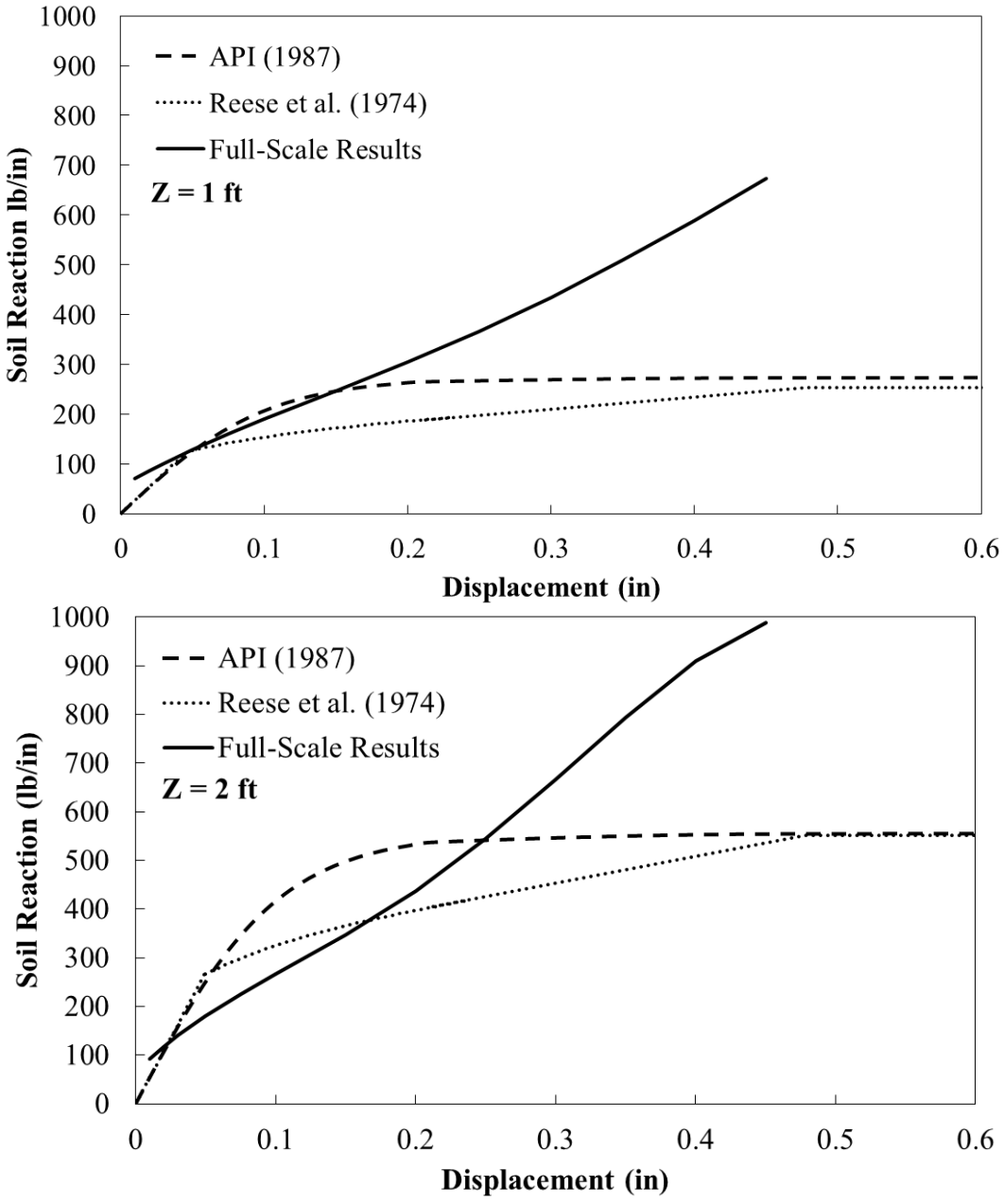

Figure 7-4. Comparison of the API (1987), Reese et al. (1974) predicted baseline p-y curves with full-scale results at depths of 1 ft (top) and 2 ft (bottom)

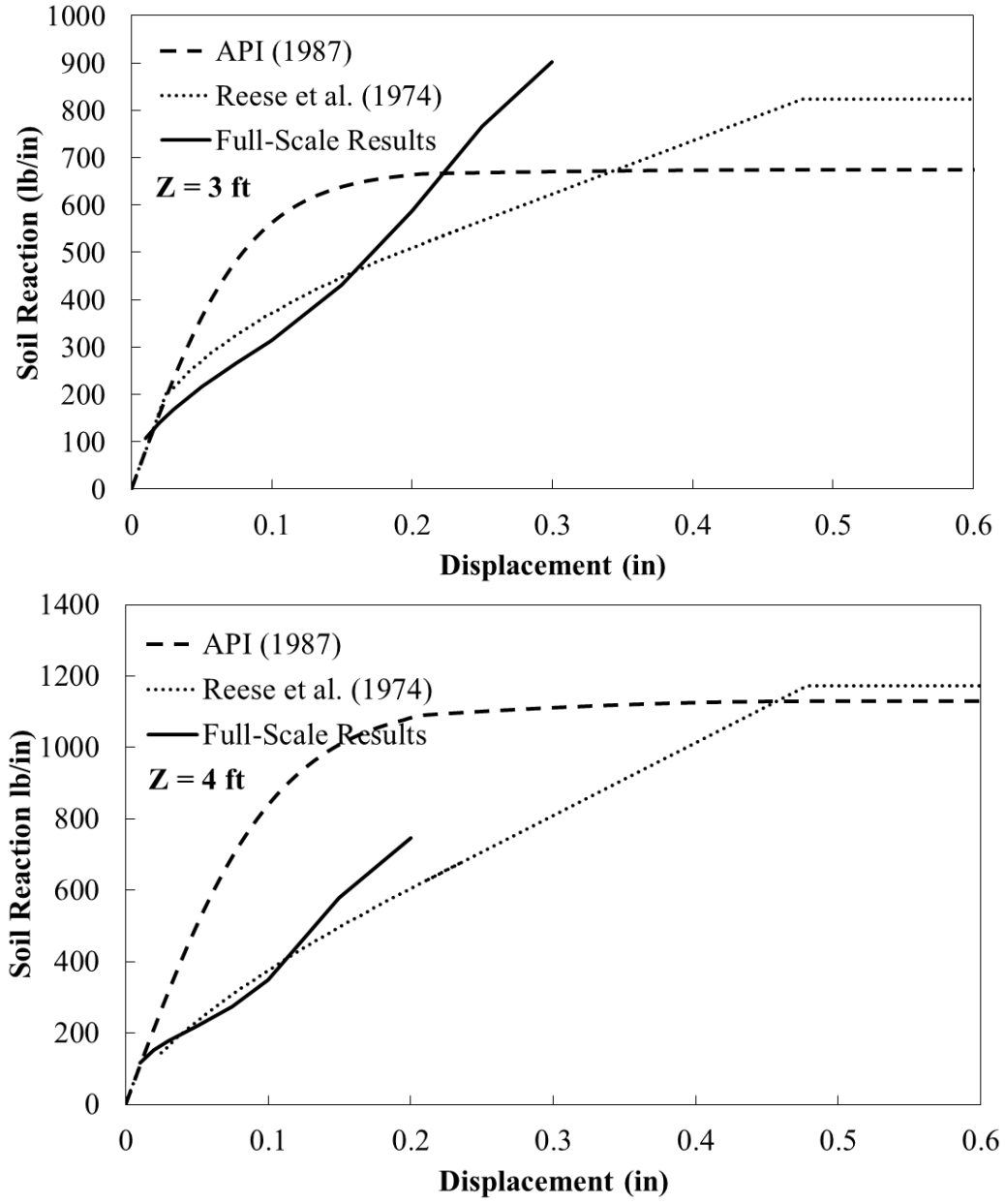

Figure 7-5. Comparison of the API (1987), Reese et al. (1974) predicted baseline p-y curves with full-scale results at depths of 3 ft (top) and 4 ft (bottom)

7.3 **Comparison of Sloping Ground Models**

7.3.1 **Reese et al. 2006 (LPILE 6.0)**

The embankment soil properties were input into LPILE 6.0 to predict to lateral response of a pile located on a crest slope. The Reese et al. (1974) soil model was used with a coefficient of subgrade modulus of 225pci. **Figure 7-6** shows the LPILE predicted load-displacement curve with the full-scale test results for the 0D test pile. LPILE slightly underestimates the lateral capacity for pile head displacements over 0.5 in. The ultimate resistance was underestimated by about 10% and the predicted initial stiffness was lower between pile head displacements of 0.5 in. and 3.0 in.

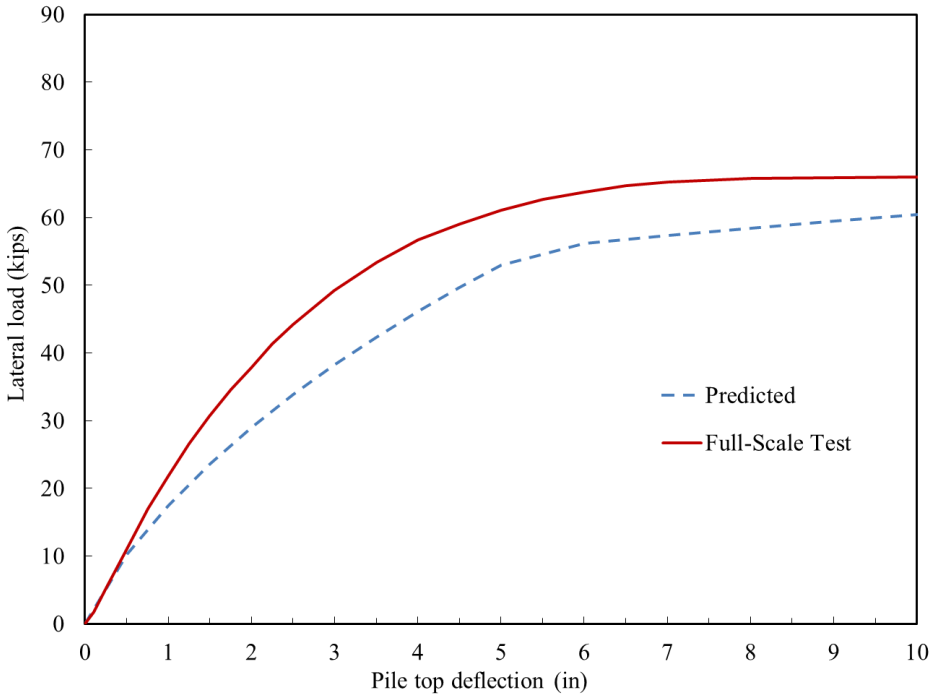

Figure 7-6. LPILE predicted 0D (slope crest) load-displacement curve with the full-scale test results

Table 7-2 shows the mean bias and COV between the full-scale load-displacement curves with LPILE predictions for the 0D and baseline pile tests. These results show that COV and mean bias are greater for both piles at low displacements (less than 3 inches).

Table 7-2. Mean bias and COV between the full-scale and LPILE load displacement curves

Pile	Pile Displacements < 3 inch		Pile Displacements > 3 inch	
	Mean Bias	COV (%)	Mean Bias	COV (%)
Baseline	1.41	5.5	1.34	3.2
0D	1.25	8.1	1.16	4.6

7.3.2 **Mezazigh and Levacher (1998)**

From the results obtained from centrifuge tests in sands, Mezazigh and Levacher (1998) presented reduction coefficients, $r_{(D)}$ that can be applied to p-y curves for piles in level ground. This reduction coefficient, also known as a p-multiplier, is then applied to the resistance pressure, p. The slope angle, pile diameter, and distance from slope crest all effect the value of this reduction factor. Using the parameters from this research project the proposed reductions factors from Mezazigh and Levacher (1998) are 0.25, 0.44, 0.62, and 1.0 for piles located at 0D, 2D, 4D, and 8D respectively. **Figure 7-7** through **Figure 7-9** show the results of applying the corresponding reduction factors to the back-calculated baseline p-y curves with the 0D, 2D, and 4D test results.

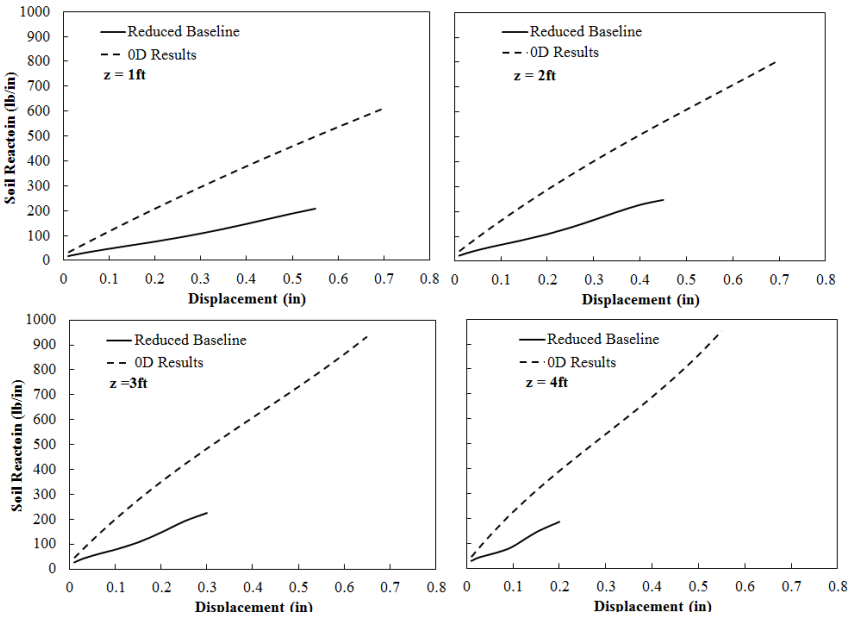

Figure 7-7. Reduced baseline (with Mezazigh and Levacher (1998) reduction coefficients**)** and 0D p-y curve comparison

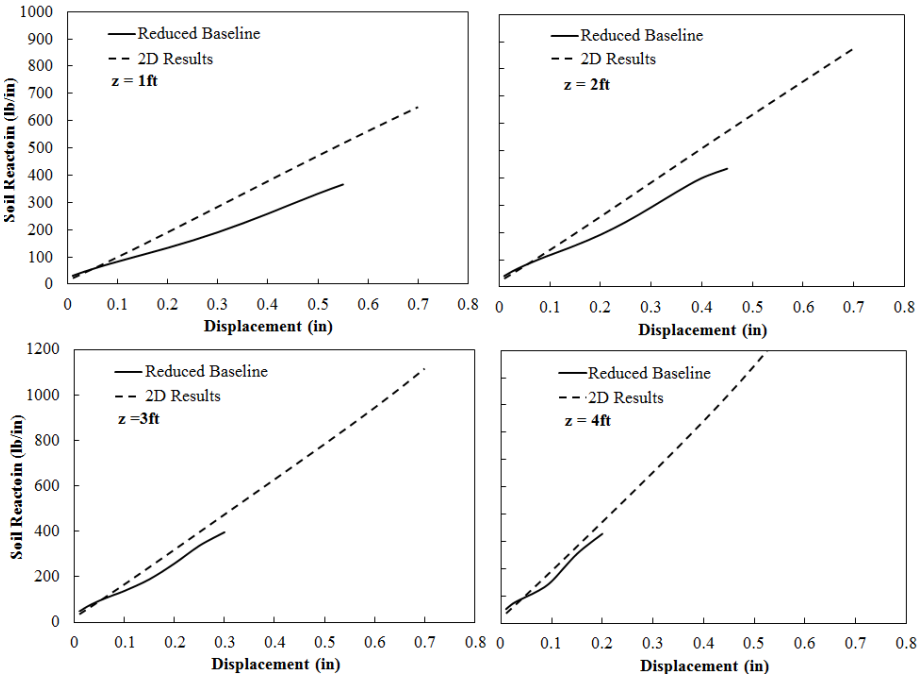

Figure 7-8. Reduced baseline (with Mezazigh and Levacher (1998) reduction coefficients**)** and 2D p-y curve comparison

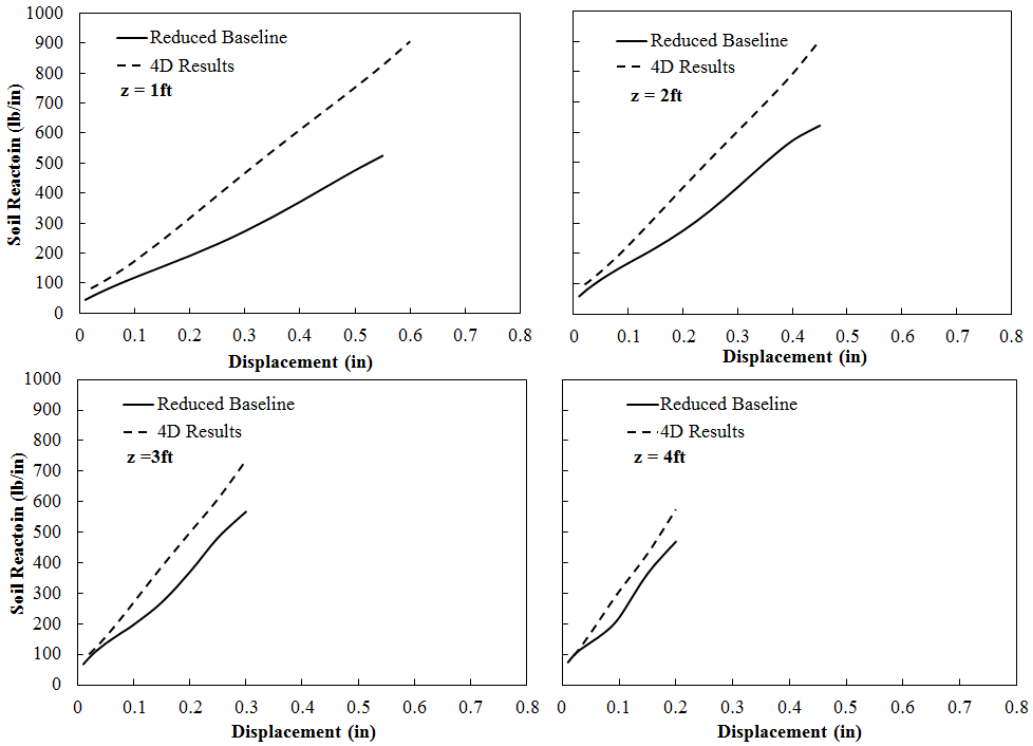

Figure 7-9. Reduced baseline (with Mezazigh and Levacher (1998) reduction coefficients**)** and 4D p-y curve comparison

The Mezazigh and Levacher (1998) reduction coefficients are considered conservative from this analysis. The baseline soil resistance was reduced to levels significantly below the 0D results for all depths investigated. At distances of 2D and 4D from the slope crest the reduced baseline curves better represent the p-y curves at these locations while still being conservative. The mean bias and coefficient of variance between the reduced baseline and the 0D, 2D, and 4D piles are shown in **Table 7-3** through **Table 7-5**. Each of these tables compare the baseline p-y curves reduced with Mezazigh and Levacher (1998) reduction coefficients with result from the 0D, 2D, and 4D pile. The mean bias and COV

was computed for targeted displacements along all p-y curves and between all p-y curves at target depths.

Table 7-3. Mean bias and COV between the reduced baseline and 0D p-y curves with the Mezazigh and Levacher (1998) reduction coefficients

Displacement (in)	Mean Bias	COV (%)
0.05	2.22	3.9
0.1	2.52	2.1
0.15	2.51	8.0
0.2	2.47	10.1
0.25	2.50	9.4
0.3	2.43	9.7
0.4	2.41	7.0
Mean	2.44	7.2

Depth (ft)	Mean Bias	COV (%)
1.0	2.42	11.5
2.0	2.27	11.8
3.0	2.18	13.6
4.0	2.14	16.7
Mean	2.25	13.4

Table 7-4. Mean Bias and COV between the reduced Baseline and 2D P-Y Curves with the Mezazigh and Levacher (1998) Reduction Coefficients

Displacement (in)	Mean Bias	COV (%)
0.05	1.00	4.1
0.1	1.20	2.7
0.15	1.25	7.0
0.2	1.29	8.6
0.25	1.33	9.1
0.3	1.33	9.0
0.4	1.37	6.9
Mean	1.25	6.8

Depth (ft)	Mean Bias	COV (%)
1.0	1.25	20.5
2.0	1.14	18.0
3.0	1.06	17.7
4.0	1.02	19.1
Mean	1.12	18.8

Table 7-5. Mean Bias and COV between the reduced Baseline and 4D P-Y Curves with the Mezazigh and Levacher (1998) Reduction Coefficients

Displacement (in)	Mean Bias	COV (%)
0.05	1.26	7.3
0.1	1.39	3.1
0.15	1.41	10.2
0.2	1.44	11.4
0.25	1.49	12.1
0.3	1.48	11.5
0.4	1.52	8.7
Mean	1.43	9.2

Depth (ft)	Mean Bias	COV (%)
1.0	1.58	6.1
2.0	1.39	6.5
3.0	1.26	7.8
4.0	1.18	12.3
Mean	1.35	8.2

The results from the calculated bias and COV for each pile locations demonstrates that the Mezazigh and Levacher (1998) reduction coefficients are more accurate for the 2D and 4D piles and for the deeper p-y curves. This model over predicts the reduction required from a slope crest and is conservative in all cases examined.

7.3.3 **Muthukkumaran et al. (2008)**

Muthukkumaran et al. (2008) conducted a centrifuge tests analyzing the effects of a pile located on a slope crest. A reduction factor, R, was developed to account for variable slope angles and depths (Z/D) for piles located at the slope crest (0D). The Muthukkumaran et al. (2008) reduction factor was constructed to be applied to the API (1987) method is applied to the level ground soil resistances.

The Muthukkumaran et al. (2008) reduction factor proposed for this study range from 0.45 to 0.60 for soils depths of 1 ft to 4 ft for the 0D pile. **Figure 7-10** shows the reduced baseline with the 0D p-y curves at this range of depths. The mean bias and coefficient of variation between the reduced baseline at target pile displacements and depths is presented in **Table 7-6**. The bias between curves is relatively close and slightly over predicts the reduction is soil resistance. The COV is less than 18% for all displacements and is less than 15% for the p-y curves at depths less than 4ft. These statistical results are based on 110 points.

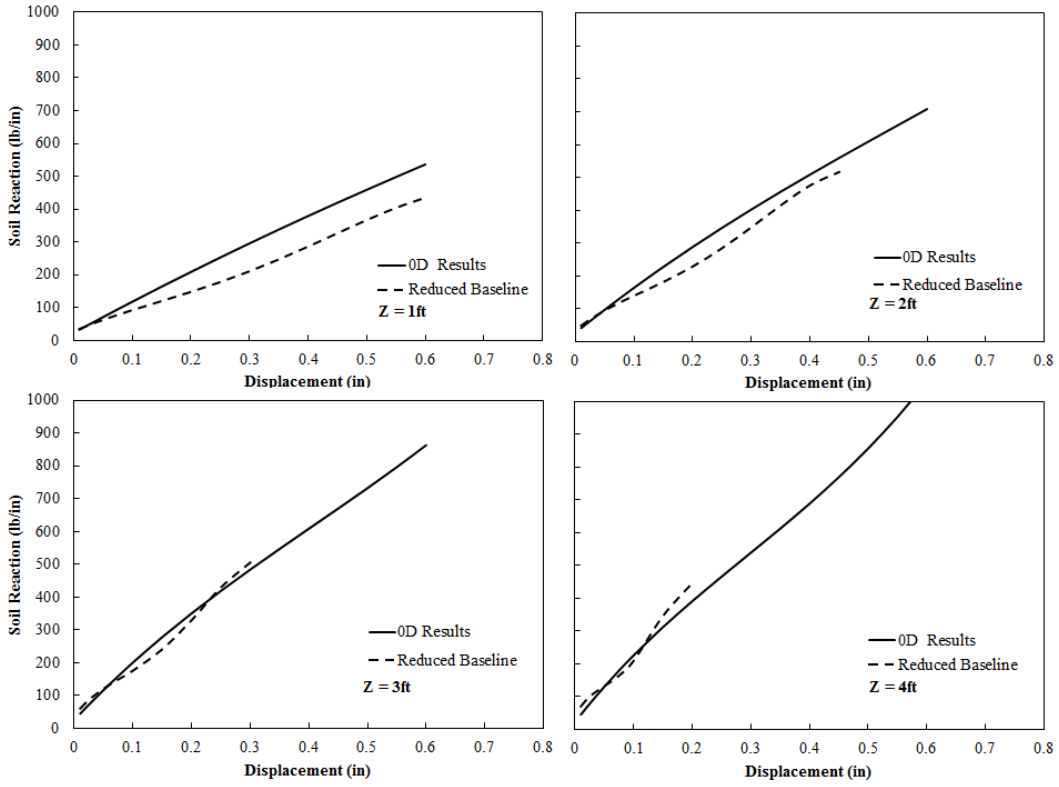

Figure 7-10. Reduced baseline and 0D p-y curve comparison with Muthukkumaran et al. (2008) reduction coefficients

Table 7-6. Mean bias and COV between the reduced baseline and 0D p-y curves with the Muthukkumaran et al. (2008) reduction coefficients

Displacement (in)	Mean Bias	COV (%)
0.05	1.03	6.5
0.1	1.17	6.2
0.15	1.17	14.7
0.2	1.15	17.5
0.25	1.21	15.1
0.3	1.17	15.5
0.4	1.20	10.69
Mean	1.16	12.32

Depth (ft)	Mean Bias	COV (%)
1.0	1.25	11.5
2.0	1.09	11.8
3.0	0.97	13.6
4.0	0.89	16.7
Mean	1.05	13.4

7.4 **Lateral Resistance Ratios**

In addition to reduction factors, many researchers use lateral load resistance ratios to compare baseline load-displacement curves with near slope curves. The data obtained at target pile head displacements for near slope tests were normalized with the baseline load-displacement data. **Figure 7-11** presents the lateral resistance ratios from this study.

The 8D pile, as previously discussed, has no reduction in lateral capacity and had a load ratio, Ψ, of 1.0. Single value averages of the load ratios (**Figure 7-11**) for the -4D, 0D, 2D and 4D piles are 0.55, 0.70, 0.90, and 0.95, respectively. The ratio of the 4D pile does not drop below 1.0 until 2.5 inches of pile head displacement. For the -4D, 0D, 2D piles, the load ratio increased from a minimum value during the first 0.75 inches of movement and stayed relatively

consistent for the remainder of the pile displacement. This may be caused by the reduced initial subgrade modulus observed in the p-y curves from the reduction of overburden pressure caused by the presence of the test slope.

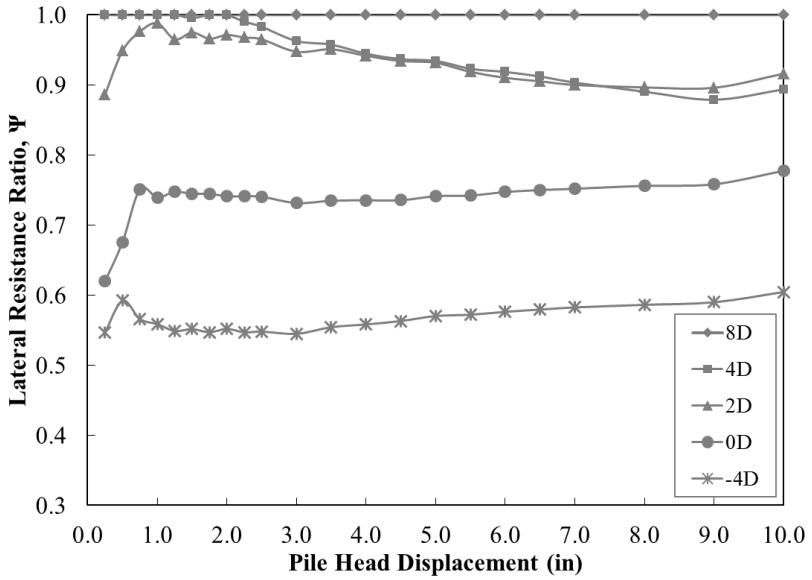

Figure 7-11. Lateral resistance ratios as a function of displacement

Figure 7-12 compares the load resistance ratios obtained from these full-scale tests with the finding from other researchers. The results from this project are near the upper bound of the recommendations and are very similar to the full-scale results of Mirzoyan (2007). The predictions from FEM, analytical equations, and scaled tests tend to overestimate the effects of soil slope.

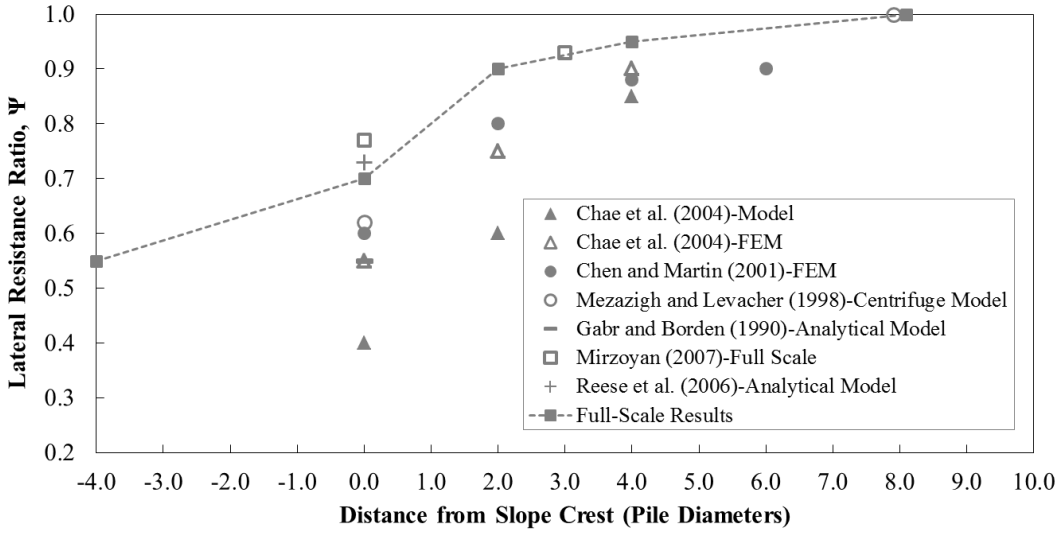

Figure 7-12. Comparison of resistance ratios presented by researchers as a function of distance from a slope crest with the findings from this study

7.5 **Simplified P-Multiplier Design Procedure**

p-multipliers, or reduction factors, were constructed for piles located near or in a cohesionless slope by analyzing the available back-calculated p-y curves. The near slope soil resistances, *p*, (-4D, 0D, 2D, and 4D) were normalized with the baseline soil resistance to obtain reduction factors.

A generalized cohesionless soil slope profile was constructed using the normalized p-multipliers for each near slope pile as shown in **Figure 7-13**. Linear interpolation was used to obtain the reduction in soil resistance at locations between each near slope pile. The recommended p-multipliers are based on the distance from the slope crest and depth below the ground surface measured in pile diameters, D.

These recommendations are created to account for a large range of pile displacements (i.e. more conservative, higher reduction in load) and do not need to be modified for increasing pile displacements during design. The conservatism built into the p-multipliers ranges from 5% to 25%. With increasing depth and increasing distance behind the crest the conservatism increases.

The recommended simplified design procedures to account for soil slope in cohesionless soils are:

- Determine the designed pile size (diameter) being installed within proximity of the slope
- Identify cohesionless soil properties and corresponding level ground *p-y* curves for the site
- Define the distance (in number of pile diameters) the pile will be located from the slope crest
- Using **Figure 7-13**, determine where the designed pile will be located on the generalized slope
- Apply the corresponding *p*-multipliers from the figure to the free-field p-y curves to account for the presence of the slope
    - For piles located on the slope: apply a reduction factor of 0.3 for the top four pile diameters and 0.4 for the next six pile diameters in depth.

- For piles located on the slope crest to four pile diameters back from the crest: apply a reduction factor of 0.5 for the top 4 pile diameters and 0.6 for the next 6 pile diameters in depth.
- No reduction factor (*p*-multiplier of 1.0) is required below 10D.
- For piles located outside of this range no reduction factors are required.

These recommendations are conservative due to the simplifications of this design procedure but present an efficient way to account for the reduction in lateral capacity for piles in proximity of a slope in cohesionless soils. The limitations of these recommendations should always be considered when extrapolating for other design conditions that differ from the testing conditions in this study including slope angle, pile diameter, and loading conditions.

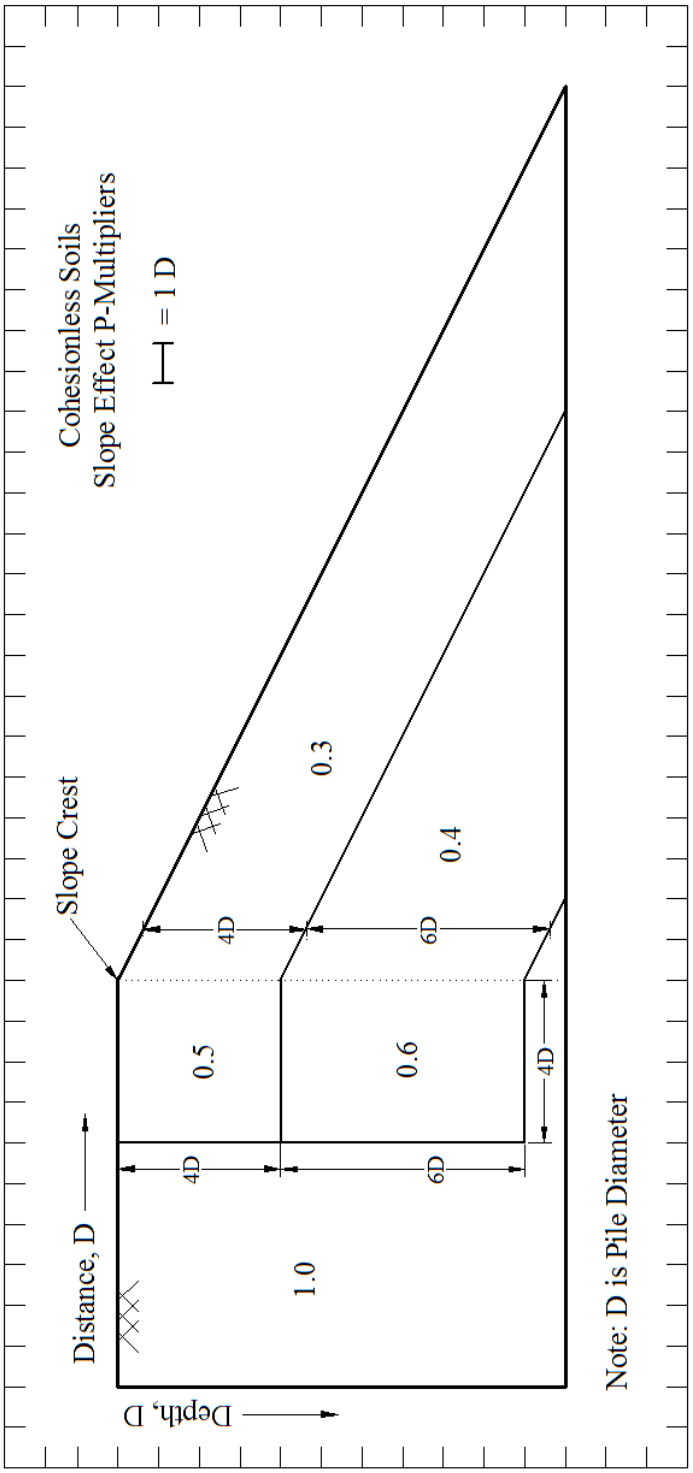

Figure 7-13. Recommended p-multipliers for a generalized cohesionless slope

7.6 **Summary**

Multiple observations and conclusions were made from comparisons between the back-calculated full-scale results and models proposed by other researchers. The significant points include:

1. The Computer program LPILE 6.0 significantly underestimates the initial stiffness and the lateral pile capacity in level ground conditions by as much as 20%. The predicted lateral capacity for the 0D pile was relatively accurate and only underestimated the lateral capacity by less than 10%.
2. The predicted baseline API (1987) and Reese et al. (1974) p-y curves over predict the initial stiffness at low displacements, less than 0.2 inches.
3. The API model has the greatest subgrade modulus at low displacements and reaches ultimate resistance at very low displacements.
4. API (1987) and Reese et al. (1974) models significantly under predicted the back-calculated soil reaction.
5. Reese et al. (1974) model more accurately predicted the back-calculated p-y curves but significantly underestimates soil resistance at displacements greater than 0.25 inches.
6. Mezazigh and Levacher (1998) reduction coefficients are conservative and significantly reduced the baseline p-y curve below the near slope back-calculated curves.

7. The Muthukkumaran et al. (2008) baseline reduction factors proposed for a pile located on a slope crest result in accurate representations between the back-calculated baseline and 0D p-y curves.

The load resistance ratio from this study were 0.55, 0.70, 0.90, and 0.95 for piles located at -4D, 0D, 2D, and 4D respectively. These results are on the upper bound of the ratios presented by other researchers, demonstrating that many models tend to overestimate the effects of a slope. A simplified design procedure was presented to account for the effects of soil slope on lateral pile capacities. P-multipliers or reductions factors were provided as a means to reduce the soil reaction, p, at given displacements in p-y curves. These p-multipliers are functions of depth and pile distance from the slope crest in pile diameters.

8. SUMMARY AND CONCLUSIONS

8.1 Project Summary

A full-scale deep foundation research project was conducted at the Geotechnical Engineering Field Research Site (GEFRS) located on the Oregon State University campus in Corvallis, Oregon. During this research program ten lateral load tests were conducted to analyze the effects of soil slope in cohesionless soils. Five piles were driven near or on a test slope. These piles were located 8D, 4D, 2D, 0D, and -4D from the slope crest where D is the pile diameter. Three battered piles were located in horizontal ground conditions with positive and negative batter angles. Two vertical baseline piles were also tested in level ground for comparison of results. Each test pile had a diameter of 12 inches.

A cohesionless embankment was constructed on the testing site to a height of 10 ft above the native surface with a 2 H: 1V or 26.6° test slope. The material was required to have less than 12% fines passing the number 200 sieve. The well-graded cohesionless backfill material used for this research project had less than 10% fines and a USCS classification of a well-graded sand (SW). The embankment was constructed in 8 inches lifts with a relative compaction of not less than 95% of Caltrans specifications. Nuclear density results showed the embankment material had an average unit weight of 127 pcf with a water content between six and ten percent. The friction angle of the embankment material was approximately 43° based on SPT correlations.

A monotonic or short term static loading condition was applied during all lateral load tests in which a 500 kip hydraulic actuator extending at rate of 0.1 inch/minute. Four types of instrumentation were utilized to collect data during lateral load testing. Strain gauges were installed at 16 levels along the length of each pile to record tension and compression data. Tiltmeters collected rotation data along the centerline of the pile during testing. Linear string potentiometers were connected to each pile at the loading elevation to measure lateral pile head displacement. Load cells were incorporated into the hydraulic actuator to measure the applied lateral load. The load-displacement curves and curvature profiles for the 8D pile and the baseline pile were very similar, therefore further results of the 8D pile were not included in this report.

During the design phase, the pile section was selected based on predicted soil properties of the cohesionless material and lateral resistance models. This pile section was also selected because it is a standard size presented in the Caltrans Bridge Design Specifications. Earlier than expect plastic yielding occurred in the test piles. A sixth order global polynomial curve fitting method was used to back-calculate the soil resistance, p, and displacement, y, along the length of each test pile along with shear, moment, and rotation profiles.

From the data obtained in the back-calculated results a comparison of the existing methods was carried out comparing p-y curves, load-displacement

curves, reduction factors, and load resistance ratios. A simplified design procedure to account for the effects of soil slope was proposed from these results.

8.2 Observations For Near Slope Piles in Cohesionless Soils

The following sections present observations made during full-scale lateral load testing.

8.2.1 Lateral Loading

- Piles located less than 8D from a slope crest have a reduced ultimate lateral capacity.
- For all soil displacements, the proximity of slope has a significant effect on the lateral response for piles located closer than 2D from the crest.
- Piles installed on a slope should not be considered to have similar lateral capacities as piles installed on the slope crest. In this study, the capacities and reduction factors were significantly different between these two cases.
- Lateral resistance ratios of 0.55, 0.70, 0.90, and 0.95 for piles located at -4D, 0D, 2D, and 4D respectively were obtained in this project.

8.2.2 Soil Resistance Mechanisms

- Extensive ground heaving was observed in front of the pile for the baseline pile tests, 8D test, and battered pile tests.

- The laterally loaded piles in proximity to the slope (4D, 2D, 0D, -4D piles) formed visible passive soil wedges with increasing pile head displacements.
- The closer the proximity to the slope the sooner (at lower displacements) a visible passive wedge formed on the slope.
- The shear failure angle, Ω, of the passive wedge ranged between 24° and 39°. This angle increased with greater distances from the slope crest. A recommendation of 70% of ϕ is proposed for the shear failure angle in dense cohesionless material.

8.2.3 Gap Formation and Active Pressure

- During all lateral load tests a gap formed behind the pile despite the fact that the embankment material consisted of less than 10% fines. This was most likely caused from the partially saturated state of the embankment.
- A conclusion can be made that the formation of a gap behind the test piles resulted in no application of active pressure on the back of the piles. The inclusion of active pressure in partially saturated cohesionless soils is considered to add conservatism to prediction models.

8.2.4 Model Comparisons

- LPILE 6.0 underestimates the initial stiffness and the lateral pile capacity in level ground conditions. The full-scale test results had an ultimate resistance of 20% more than predicted by LPILE 6.0. The lateral capacity

for the 0D pile was relatively close and only underestimated the lateral capacity by about 10%.

- The predicted baseline API (1987) and Reese et al. (1974) p-y curves over predict the initial soil stiffness at displacements of less than 0.2 inches
- API (1987) and Reese et al. (1974) models significantly under predicted the back-calculated ultimate soil reaction at displacements greater than 0.25 inches.
- Mezazigh and Levacher (1998) reduction coefficients are considered conservative when applied to the baseline p-y curve and then compared to the near slope results.
- The Muthukkumaran et al. (2008) baseline reduction factors proposed for a pile located on a slope crest result in accurate representations between the baseline and 0D p-y curves.

8.3 **Battered Pile Observations and Conclusions**

Pile P-4 with a -14° batter angle had the highest stiffness and capacity of all piles tested in this study. Pile P-3 (+14° positive batter) had the lowest capacity of the tested battered piles. The load displacement results from pile P-5 (+26°) do not fit the predicted trend. Predictions suggest that the lower the positive batter (closer to vertical) the higher the final capacity and the greater the initial stiffness. The LPILE predicted load-displacement curves from pile P-3

(+14°) and P-4 (-14°) follow the trend of the full-scale results, but LPILE is conservative in estimating the initial stiffness and ultimate lateral resistances. The full-scale results from Pile P-5 (+26°) had a significantly greater stiffness and capacity than the LPILE prediction, where it was predicted to have the lowest overall load.

An analysis of the load displacement data from the +26° battered pile showed that the testing equipment was likely near its limitations to laterally load a pile with this high batter angle. The unexpected stiffness and load from the full-scale test are likely due to unintended axial loading.

8.4 **Design Recommendations**

The following are lateral pile design recommendations to account for the presence of a cohesionless slope.

- To account for the effect of a cohesionless soil slope p-multipliers or reduction factors should be applied to level ground p-y curves.
- For piles located on the slope apply a reduction factor of 0.3 for the top four pile diameters and 0.4 for the next six deeper pile diameters.
- For piles located on the slope crest to four pile diameters back from the crest apply a reduction factor of 0.5 for the top 4 pile diameters and 0.6 for the following 6 deeper pile diameters.
- No reduction factor (p-multiplier of 1.0) is required below 10D or more than 4D behind the slope crest.

8.5 Conclusions from Full-Scale Testing Results

The major conclusions and findings from the full-scale lateral load testing program conducted on near or in slope piles in cohesionless soils are the following:

1. The effects of slope on lateral pile capacity are insignificant at displacements of less than 2.0 inches for piles located 2D and further from the crest.
2. For pile located at 4D or greater from the slope crest, the effect of slope is insignificant for the analyzed ranges of soil displacements on p-y curves.
3. Analytical, small scale, and computer models typically overestimate the effects of slope on lateral pile capacities and conservatively predict the ultimate resistance and initial soil stiffness.
4. Suggested p-multipliers, or reduction factors, are recommended based on depth and distance from the slope crest in pile diameters and range between 0.3 and 0.6.

The limitations of these conclusions and recommendations should always be considered when extrapolating for other design parameters that differ from the testing conditions in this study including slope angle, pile diameter, loading type, and pile type.

REFERENCES

American Petroleum Institute (API) (1987). "Recommended practice for planning, designing, and constructing fixed offshore platforms." *API Recommended Practice* 2A (RP-2A), 17th edn.

Ashford, S. and Juirnarongrit, T. (2003). "Evaluation of pile diameter effect on initial modulus of subgrade reaction." *Journal of Geotechnical and Geoenvironmental Engineering,* ASCE, Vol. 129, No. 3, pp.234-242.

Barber, E. S. (1953). "Discussion to paper by S. M. Gleser." *ASTM, STP* 154, 94-101.

Banerjee, P. K., and Davies, T. G. (1978). ''The behavior of axially and laterally loaded single pile embedded in non-homogeneous soils.'' *Geotechnique,* Vol. 21(3), pp. 309–326.

BDS Caltrans (2006). *Caltrans Bridge Design Specifications*

Bowman. E. R. (1958). "Investigation of the lateral resistance to movement of a plate in cohesionless soil," thesis presented to the University of Texas, at Austin, Tex., in partial fulfillment of the requirements of the degree of Master of Science.

Brinch J. H. (1961). "The ultimate resistance of rigid piles against transversal forces." *Bulletin No. 12,* Danish Geotechnical Institute, Copenhagen, Denmark, pp. 5–9.

Broms, B. B. (1964). "Lateral resistance of piles in cohesive soils." *Journal of Soil Mechanics and Foundation Division,* 90(2), pp. 27-64.

Brown, D. A., Reese, L. C., and O' Neill, M. W. (1987). "Cyclic lateral loading of a large scale pile group." *Journal of Geotechnical Engineering,* ASCE, Vol. 113(11), pp. 1326-1343.

Bogard, D., and Matlock, H. M. (1983). "Procedures for analysis of laterally loaded pile groups in soft clay." *Proc., Geotechnical Practice in Offshore Engineering,* ASCE, pp. 499-535.

Caduto, Donald P. *Foundation Design: Principles and Practices* second ed., Prentice-Hall Inc., 2001.

Chae K.S., Ugai K., and Wakai A. (2004). "Lateral resistance of short single piles and pile groups located near slopes." *International Journal of Geomechanics*, 4(2), 93-103.

Chen, C. Y. and Martin, G. R. 2001. "Effect of Embankment Slope on Lateral Response of Piles." *FLAC and Numerical Modeling in Geomechanics – 2001* (Proceedingsof the second International FLAC Conference, Lyon, France, October 2001). Billauxet al. (eds.). A.A. Belkema, Lisse, pp. 47-54.

Das, Braja M. Principles of Foundation Engineering 7th ed., Cengage Learning, 2007.

Davisson, M. T., and Gill, H. L. (1963). "Laterally loaded piles in a layered soil." *J. Soil Mech. and Found. Div.*, ASCE, 89(3), 63-94.

Dickenson, S. (2006). *Characterization of the geotechnical engineering field research site at Oregon State University*. 3rd Edition.

Dunnavant, T. W. (1986). "Experimental and analytical investigation of the behavior ofsingle piles in overconsolidated clay subjected to cyclic lateral loads." *Ph.D .Dissertation*, University of Houston; TX.

Frank R., Bangratz J.L., and Kutniak M. 1990. PILATE-LCPC: Programme de calcul d.un pieu isolé soumis à des efforts de flexion en tête et à des poussées latérales de sol. Laboratoire des Ponts et Chaussées, Paris, p 69.

Frank R., Shields D., and Domaschuk L. 1994. The effects of creep on laterally loaded piles. The Proceedings of 13th International Conference on Soil Mechanics and Foundation Engineering (ICSMFE), New Delhi, India, pp. 501.504.

Google Aerial Map Corvallis, OR, retrieved on January, 2012 from www.maps.google.com.

Gabr, M. A., Borden, R. H. (1990). Lateral Analysis of Piers Constructed on Slopes.
Journal of Geotechnical Engineering, vol. 116 (12), pp 1831-1850.

Hetenyi, M. (1946). *Beams on elastic foundations*. University of Michigan Press, Ann Arbor, Michigan.

Holtz, R. D. and Kovacs, W. D. (2011). *An Introduction to Geotechnical Engineering*, Prentice-Hall, Inc., Englewood Cliffs, N. J.,

Juirnarongrit, T. (2002). "Effect of diameter on the behavior of laterally loaded piles in weakly cemented sand." Ph.D. thesis, Dept. of Structural Engineering, University of California San Diego, CA.

Matlock, H. (1970). "Correlations for design of laterally loaded piles in soft clay." *Proceedings, second offshore Technology Conference,* Houston, Texas, 577-594.

McClelland, B., and Focht, J. A. Jr. (1958). "Soil modulus for laterally loaded piles." *Transactions,* ASCE, Vol. 123, pp. 1049-1086.

Mezazigh, S., and Levacher, D. (1998). "Laterally loaded piles in sand: slope effect on
p-y reaction curves", *Canadian Geotechnical Journal*, 35(3), 433-441.

Mirzoyan, A. D. (2007). "Lateral resistance of piles at the crest of slope in sand." M.S. thesis, Brigham Young University, Department of Civil and Environmental Engineering, Utah.

Muthukkumaran, K., Sundaravadivelu, R. and Gandhi, S. R. (2008). "Effect of slope on p-y curves due to surcharge load." *Soils and Foundations Journal,* Japanese Geotechnical Society, Vol. 48 No. 3, pp 353-361.

Nimityongskul, N. (2010). "Effects of Soil Slope on Lateral Capacity of Piles in Cohesive Soils." *Ph.D. Dissertation*, Dept. of Civil and Construction Engineering. Oregon State University.

Poulos, H. G., and Davis, E. H. (1980). *Pile foundation analysis and design*. John Wiley, New York.

Reese, L.C. (1962). "Ultimate resistance against a rigid cylinder moving laterally in a cohesionless soil." J. Soc. Pet. Engr., 355-359.

Reese, L. C., Cox, W. R., and Koop, F. D. (1974). "Analysis of laterally loaded piles in sand,"

Proc. *6th Offshore Technology Conference, Paper 2080,* Houston, Texas, pp. 473-483.

Reese, L. C., and Matlock, H. (1956). "Nondimensional solutions for laterally loaded piles with soil modulus assumed proportional to depth." *Proc. of the VIII Texas Conference on Soil Mechanics and Foundation Engineering,* University of Texas, Austin.

Reese, L. C. and Welch, R. C. (1975), "Lateral loading of deep foundations in stiff clay," *Journal of Geotechnical Engineering Division,* ASCE, Vol. 101(7), pp. 633-649.

Reese, L. C., Isenhower, W. M., Wang, S. T. (2006). *Analysis and design of shallow and*
deep foundations, Wiley, New Jersey, USA.

Reese, L. C., Wang, S. T., Isenhower, W. M., and Arrellaga, J. A., and Hendrix, J. (2004). *Computer Program LPILE Plus Version 5.0 Technical Manual*, Ensoft, Inc., Austin, Texas.

Reese, L. C., and Van Impe, W. F. (2001). *Single Piles and Pile Group under Lateral Loading*. A. A. Balkema, Rotterdam, pp. 463

Rollins, K. M., Johnson, S.R., Petersen, K.T., and Weaver, T.J. (2003). "Static and dynamic lateral load behavior of pile groups based on full-scale testing." *13th International Conference on Offshore and Polar Drilling,* International Society for Offshore and Polar Engineering, paper 2003-SAK-02, pp. 8.

Rollins, K. M., Land, J.K., and Gerber, T.M. (2005). "Measured and computed lateral response of a pile group in sand." *Journal of Geotechnical and Geoenvironmental Engineering,* ASCE, Vol. 131, No. 1, pp.103-114.

Spillers, W. R., and Stoll, R. D. (1964). ''Lateral response of piles.'' *Journal of Soil Mechanics and Foundation Division,* ASCE, Vol. 90(6), pp. 1–9.

Takeuchi, T., and Okada, A. (1986). "Prediction method for horizontal behavior of cast in- place pile foundation dug by manpower on slope using shear elastic constantsof ground." *Kisoko,* 14(6), 50-56

Terzaghi, K. (1955). "Evaluation of coefficients of subgrade reaction." *Geotechnique,* Vol. 5(4), pp. 297-326.

Vesic, A. S. (1961). "Beam on elastic subgrade and the Winkler hypothesis." *Proc. 5th Int. Conf. Soil Mechanics and Foundation Engineering,* Paris, Vol. 1, pp. 845-850

Wilson, D., 1998, "Soil-Pile-Superstructure Interaction in Liquefying Sand and Soft Clay," Ph.D. Dissertation, University of California at Davis.

Winkler, E. (1867). "Die lehre von elasticzitat and festigkeit (elasticity and fixity)." *Prague, Czech Republic;* pp. 182.

Walsh, J. M. (2005). "Full scale lateral load test of a 3x5 pile group in sand." M.S.thesis, Brigham Young University, Department of Civil and Environmental Engineering.

Yang, K., and Liang, R. (2007). "Methods for deriving *p-y* curves from instrumented lateral load tests." *ASTM Geotechnical Testing Journal,* Vol. 30, pp 31-38.

APPENDIX A

Table A-1. Summary of All Borings Conducted at GEFRS Site (Dickenson, 2006)

Date	Boring Name	Boring Description	Note
7/16/72	B-1	Exploratory Boring	Prior to 2008
7/16/72	B-2	"	
7/16/72	B-3	"	
1/18/96	B-4	"	
8/23/96	B-5	"	
10/6/97	B-6	"	
10/6/97	B-7	"	
10/11/97	CPT-1	CPT Boring	
10/11/97	CPT-2	CPT Boring	
Fall '97	DMT-1	DMT Boring	
Fall '97	DMT-2	DMT Boring	
4/7/00	CPT-3	CPT Boring	
4/7/00	CPT-4	CPT Boring	
10/2/01	B-8	Exploratory Boring	
10/2/01	B-9	Exploratory Boring	
10/12/01	CPT-5	CPT Boring	
10/18/01	DMT-3	DMT Boring	
10/2/08	B-10	Exploratory Boring	2008-Present
10/2/08	B-11	Exploratory Boring	
10/3/08	CPT-6	CPT Boring	
10/3/08	DMT-4	DMT Boring	
10/14/09	B-12	Exploratory Boring	
10/14/09	B-13	Exploratory Boring	
10/14/09	CPT-7	CPT Boring	
10/14/09	CPT-8	CPT Boring	
10/14/09	DMT-5	DMT Boring	

Table A-2. Summary of Water Contents, Atterberg Limits and Percent Fines from GEFRS Report (Dickenson, 2006)

Sample Depth (ft)	Natural Water Content (%)	PL	LL	PI	USCS Classification	Percent Fines (%)
3.5	28	21	64	43	CH	
4						92
5	33	25	75	50	CH	
6.5	33	28	48	20	ML	93
6.5	36					72
8	36	28	37	9	ML	
8.5	38					
9	40	27	51	24	CH	62
10	46	37	55	18	MH	62
10	38					
15.5	30	22	39	17	CL	
25.5	58	52	90	38	MH	
26.5	68	57	81	24	MH	93
35	41					
36.5	37					
40	52	46	85	39	MH	
46.5	85					
48	48					
49	55					
49.5	53					

Note: Two additional samples from 13-18 ft were classified as MH

Table A-3. Summary of Water Contents, Atterberg Limits from Caltrans Site Samples (Dickenson, 2006)

Sample Depth (ft)	Natural Water Content (%)	PL	LL	PI	USCS Classification	Percent Fines (%)
1	19.3	29	46	17	ML/MH	
2.5	25.0	29	69	40	CH	
3	25.8	29	70	41	CH	
3.5	28.7	34	61	28	MH	
4	32.6	30	70	40	CH	
6	34.9	33	68	35	MH/CH	
7	34.9	32	59	27	MH	
9	39.8	33	49	16	ML	

Table A-4. Corrected Blow Count Versus Depth from GEFRS Report (Dickenson, 2006)

Sample Depth (ft)	Corrected Blow Counts, N_1 (blows/ft)
3	24
3.5	16
6	7
6	9
6	12
7	6
7.5	22
8.5	4
10.5	75
17.5	21
17.5	25
18	56
20	40
20.5	41
21	42
25.5	26
26	16
31	15
31.5	19
35	15
35	22
42	17
42	18

Table A-5. Corrected Blow Count versus Depth from Caltrans Boring B-10 and B-11(Dickenson, 2006)

Sample Depth (ft)	Corrected Blow Counts, N_1 (blows/ft)
2	38
5.5	14
5.5	12
9	19
10.5	47
10	23
12	28
15	5
18	10
18	35
20	71
25	27
28	29

Table A-6. Summary of TXCU Tests from GEFRS Report (Dickenson, 2006)

Sample No.	Shipton #1	Shipton #2	Shipton #3	#101	#102
Type of Test	CU	CU	CU	CU	CU
Date of Testing	09/96	11/96	11/96	10/01	10/01
Sample Depth (ft)	10	15	16	8	48
Sample Length (in)	7.44	7.25	7.75	-	-
Sample Width (in)	2.75	2.75	2.75	-	-
Consolidation Pressure (psi)	50	56	65	27.77	40
Sample Pressure (psi)	43	45	54	7.5	20
Induced OCR	1.2	1.2	1.2	3.7	2.0
Strain Rate (mm/min)	0.096	0.096	0.096	0.048	0.021
Wet unit weight (pcf)	126	130	123.4	113.9	103.7
Water Content (%)	38.5	44.3	42.6	42	55.4
B-Parameter	0.987	0.987	0.971	-	-
Initial Void Ratio, e_0	-	-	-	1.14	-
$\Delta_{dev,max}$ (psi) @ Fail. Criteria 1	23	22	28	16	29.5
Δ_{Axial} (%) @ Fail. Criteria 1	2.5	2	4	9.7	11.3
$\Delta_{dev,max}$ (psi) @ Fail. Criteria 2	-	-	-	12.25	26.8
Δ_{Axial} (%) @ Fail. Criteria 2	-	-	-	5.2	10.2

Note: Failure criteria 1 - condition at which maximum deviator stress occurs
Failure criteria 2 - condition at which maximum principle stress ratio (σ'_1/σ'_3) occurs

Table A-7. Summary of TXCU Tests from Reser Stadium Expansion Project (Dickenson, 2006)

Sample No.	SH-2-3 (No. 1)	SH-2-3 (No. 2)	SH-2-3 (No. 3)	SH-5-6 (No. 1)	SH-5-5 (No. 2)	SH-5-5 (No. 3)	B-4-3 (No. 1)
Type of Test	CU	CU	CU	CU	CU	CU	CU
Date of Testing	10/03	10/03	10/03	11/03	11/03	11/03	04/02
Sample Depth (ft)	7.5-9	7.5-9	7.5-9	12.5-14.5	12.5-14.5	12.5-14.5	8.5
Sample Length (in)	5.56	5.72	5.56	5.69	5.7	5.65	6
Sample Width (in)	2.84	2.86	2.84	2.86	2.86	2.86	2.87
Cell Pressure (psi)	36	30	42	42	36	48	-
Sample Pressure (psi)	30	25	35	35	30	40	-
Induced OCR	1.2	1.2	1.2	1.2	1.2	1.2	
Strain Rate (mm/min)	0.02	0.02	0.02	0.01	0.01	0.01	0.03
Dry Unit Weight (pcf)	82.2	81.3	82.2	83.8	84.8	83.8	79.6
Water Content (%)	38.9	38.9	38.9	35.9	35.9	35.9	40.6
Initial Void Ratio, e_0	1.05	1.04	1.05	0.97	0.97	0.97	1.12
% Saturation	99.9	99.5	99.9	97.8	99	97.8	97.9
$\Delta_{dev,max}$ (psi) @ Fail.	14.7	11.5	21.8	17.9	15.5	26.8	12.5
Δ_{Axial} (%) @ Fail.	5	6.2	2	4.6	5.25	3.75	1.8
c (total stress) , psi	1.97	1.97	1.97	2.84	2.84	2.84	-
□ □(total stress) , psi	20	20	20	21.7	21.7	21.7	-

Table A-8. Summary of UUTX Tests from Caltrans Borings (B-12 and B-13)

Sample No. (Boring No.)	SH 1-15 (B-12)	SH-2-6 (B-13)	SH-2-5 (B-13)	SH-1-3* (B-12)	SH-1-5* (B-12)	SH-1-1 (B-12)	SH-1-1a (B-12)	SH-1-5a (B-12)
Type of Test	UU	UU	UU	UU	UU	UU	UU	UU
Date of Testing	1/21/10	1/26/10	1/28/10	2/2/10	2/4/10	2/9/10	2/9/10	2/11/10
Sample Depth (ft)	26-26.5	8.5-9	6.5-7	3.5-4	7.5-8	0-0.5	1-1.5	8-8.5
Sample Length (in)	6.02	6.11	6.07	5.69	6.01	6.67	5.93	6.05
Sample Width (in)	2.85	2.88	2.70	2.85	2.86	2.86	2.82	2.88
Cell Pressure (psi)	14.6	7.1	6.2	3.0	6.8	-	-	7.2
Strain Rate (%/min)	1	1	1	1	1	1	1	1
Unit Weight (pcf)	94	114	123	108	117	103	99	117
Water Content (%)	68	37	34	25	43	13	19	34
$q_{,max}$ (psi)	34.5	8.2	17	(4.91)	(1.8)	15.3	6.3	7.9
$\square_{Axial}$ @ q_{max}	5.5	5.6	5.9	(9.2)	(8.6)	1.6	2.0	1.5
$\square_{50}$	2.3	1.4	1.9	(0.55)	(0.11)	0.7	1	0.5

Table A-9. Summary of nuclear density gauge results

Date of Test	Test No.	Field Moist.	In-Place Density (g/cm^3)		In-Place Density (lb/ft^3)		Compaction
		%	Wet	Dry	Wet	Dry	%
5/20/2011	1	9.6	2.07	-	128.9	-	97.4
5/20/2011	2	-	2.04	-	127.0	-	96.0
5/20/2011	3	6.3	2.04	1.92	127.2	119.7	96.1
5/20/2011	4	4.5	2.01	1.92	125.3	119.7	95
5/20/2011	5	8.6	2.07	1.91	129.4	119.1	97.7
5/20/2011	6	6.9	2.01	1.86	125.4	116.2	95
5/20/2011	7	9.0	2.01	1.85	125.7	115.4	95.0
5/20/2011	8	9.1	2.04	1.87	127.5	116.8	96.3
5/20/2011	9	9.2	2.05	1.88	127.9	117.1	96.6
5/20/2011	10	8.4	2.04	1.88	127.1	117.2	96.0
5/23/2011	11	6.0	2.02	1.89	125.9	117.8	95.1
5/23/2011	12	6.9	2.02	1.89	126.0	117.9	95.2
5/23/2011	13	8.4	2.05	1.89	127.8	117.9	96.6
5/23/2011	14	6.8	2.02	1.88	125.8	117.2	95.0
5/23/2011	15	8.5	2.11	1.94	131.6	121.3	99.4
5/23/2011	16	8.3	2.04	1.88	127.2	117.5	96.1
5/23/2011	17	6.5	2.02	1.89	125.9	118.2	95.1
5/23/2011	18	8.6	2.09	1.93	130.5	120.2	98.6
5/23/2011	19	6.6	2.02	1.89	126.0	118.2	95.2
5/23/2011	20	6.9	2.04	1.91	127.5	119.4	96.4
5/23/2011	21	9.2	2.05	1.88	127.8	117.1	96.6
5/23/2011	22	6.8	2.02	1.89	125.9	117.9	95.1
5/23/2011	23	7.0	2.04	1.90	127.1	118.8	96.0
5/23/2011	24	6.8	2.02	1.89	126.1	118.1	95.3
5/23/2011	25	7.6	2.01	1.87	125.4	116.6	95.0
5/23/2011	26	8.5	2.09	1.93	130.7	120.4	98.7
5/24/2011	27	7.4	2.01	1.87	125.5	116.9	95.0
5/24/2011	28	8.6	2.14	1.97	133.6	123.0	100.9
5/24/2011	29	6.0	2.02	1.90	125.9	118.7	95.1
5/24/2011	30	9.5	2.07	1.89	129.3	118.1	97.7
5/24/2011	31	8.5	2.07	1.90	128.9	118.7	97.4
5/24/2011	32	7.5	2.01	1.87	125.7	117.0	95.0
5/24/2011	33	8.4	2.02	1.86	125.8	116.1	95.0
5/24/2011	34	9.5	2.06	1.88	128.3	117.1	96.9

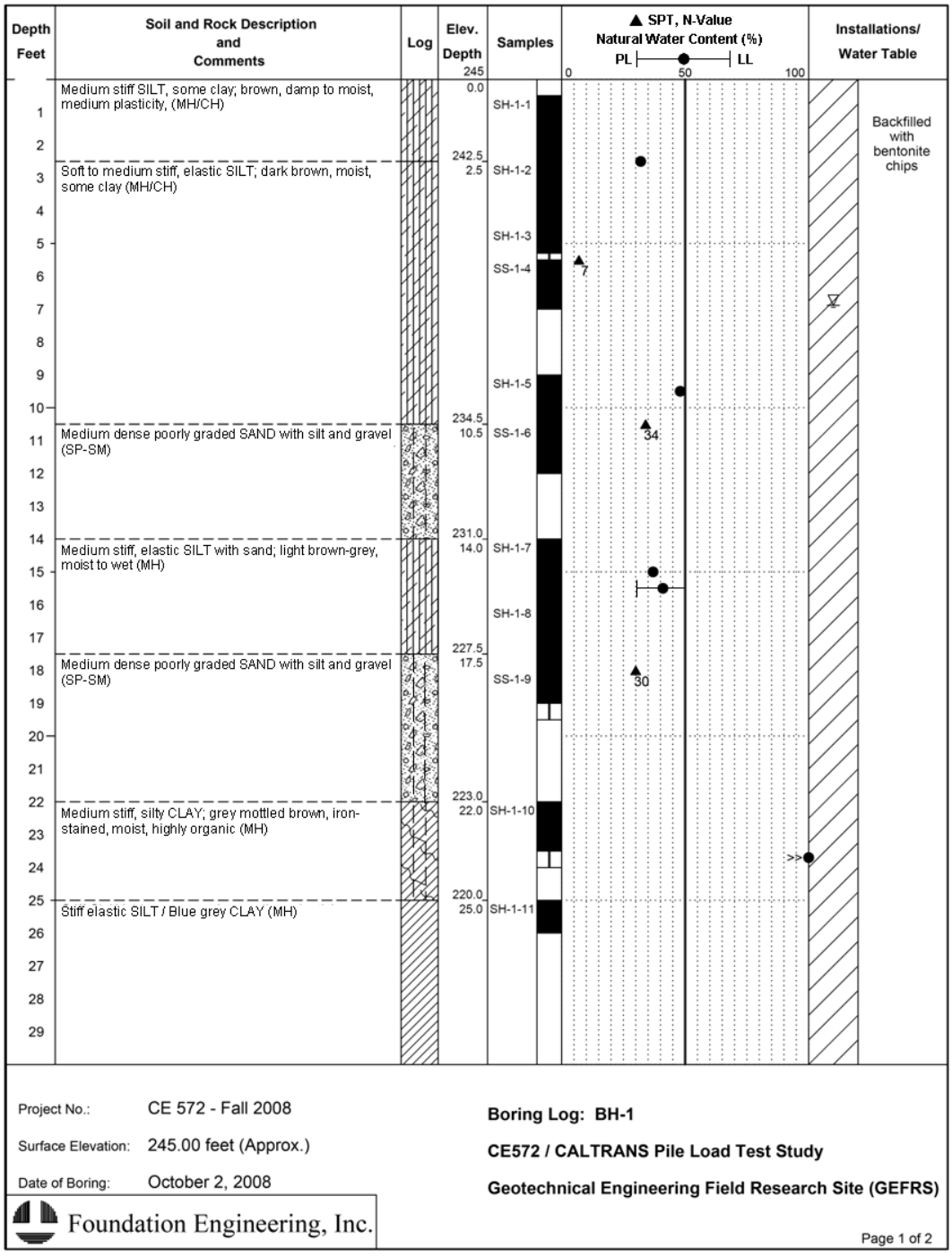

Figure A-1. Soil Boring Log, B-10

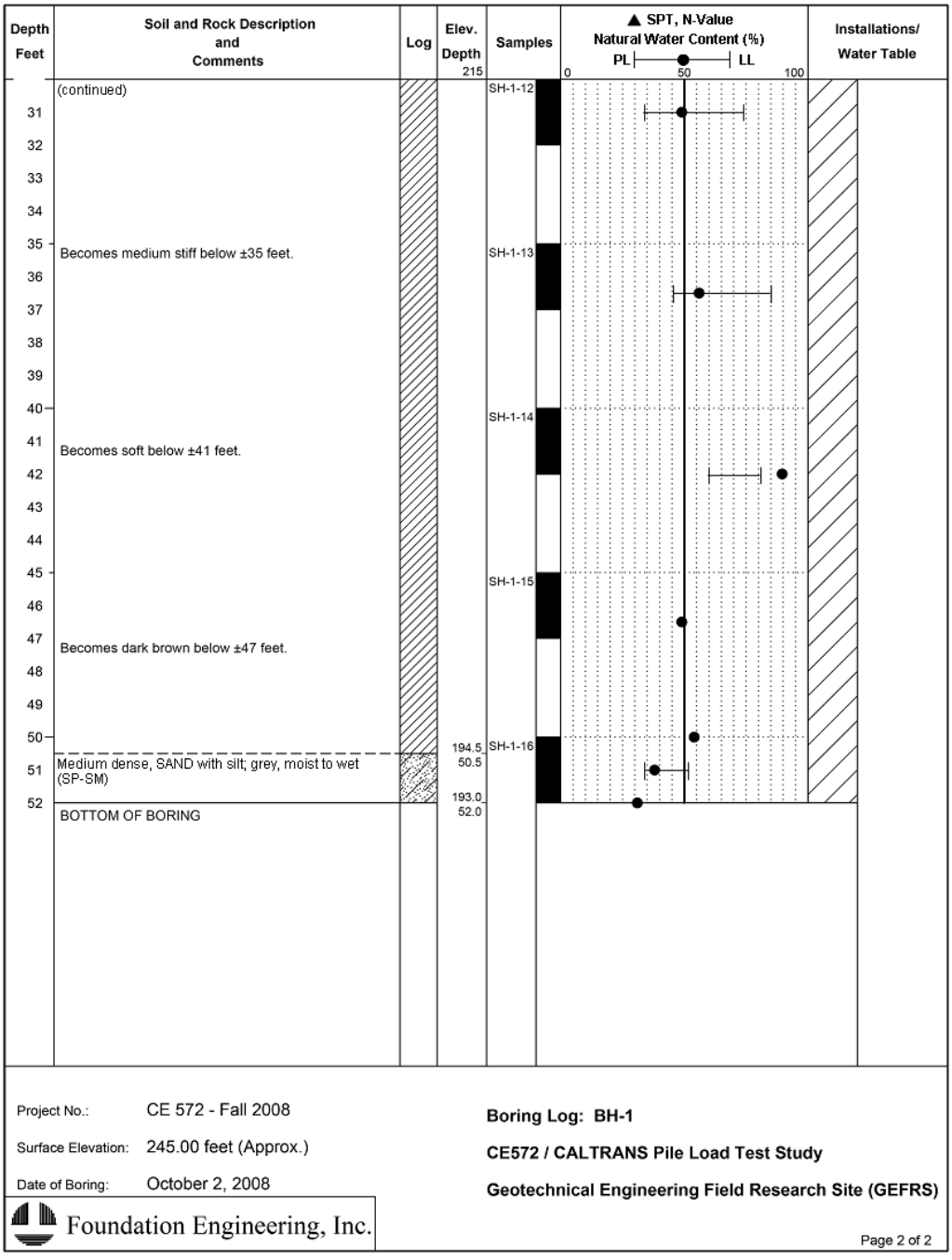

Figure A-2. Soil Boring Log, B-10 (continued)

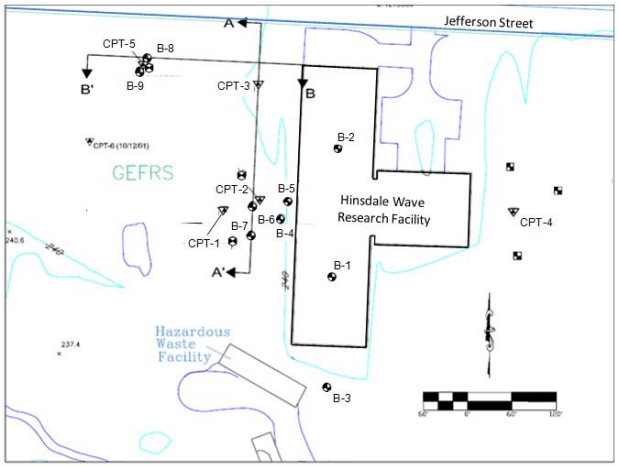

Figure A-3. Existing Boring Locations at the GEFRS (Dickenson, 2006)

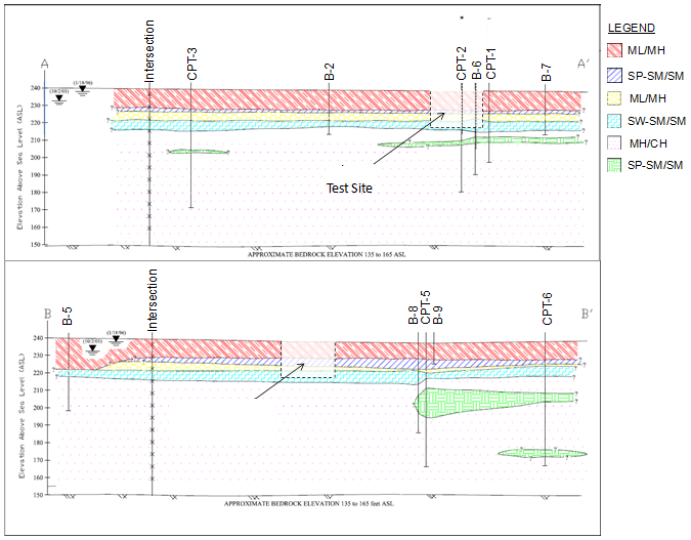

Figure A-4. A-A and B-B sections from Figure 3-3 (Dickenson, 2006)

APPENDIX B

Table B-1. Reported Yield Strength for Steel Pipe Piles

Pile No.	Heat Number	f_y (psi)
P-2	US5151A	70.6
P-3	US0152A	71.4
P-4	US151	75.4
P-5	US0152A	71.4
P-6	US0125	71.6
P-7	US0115	75.4
P-8	M87657A	81.3

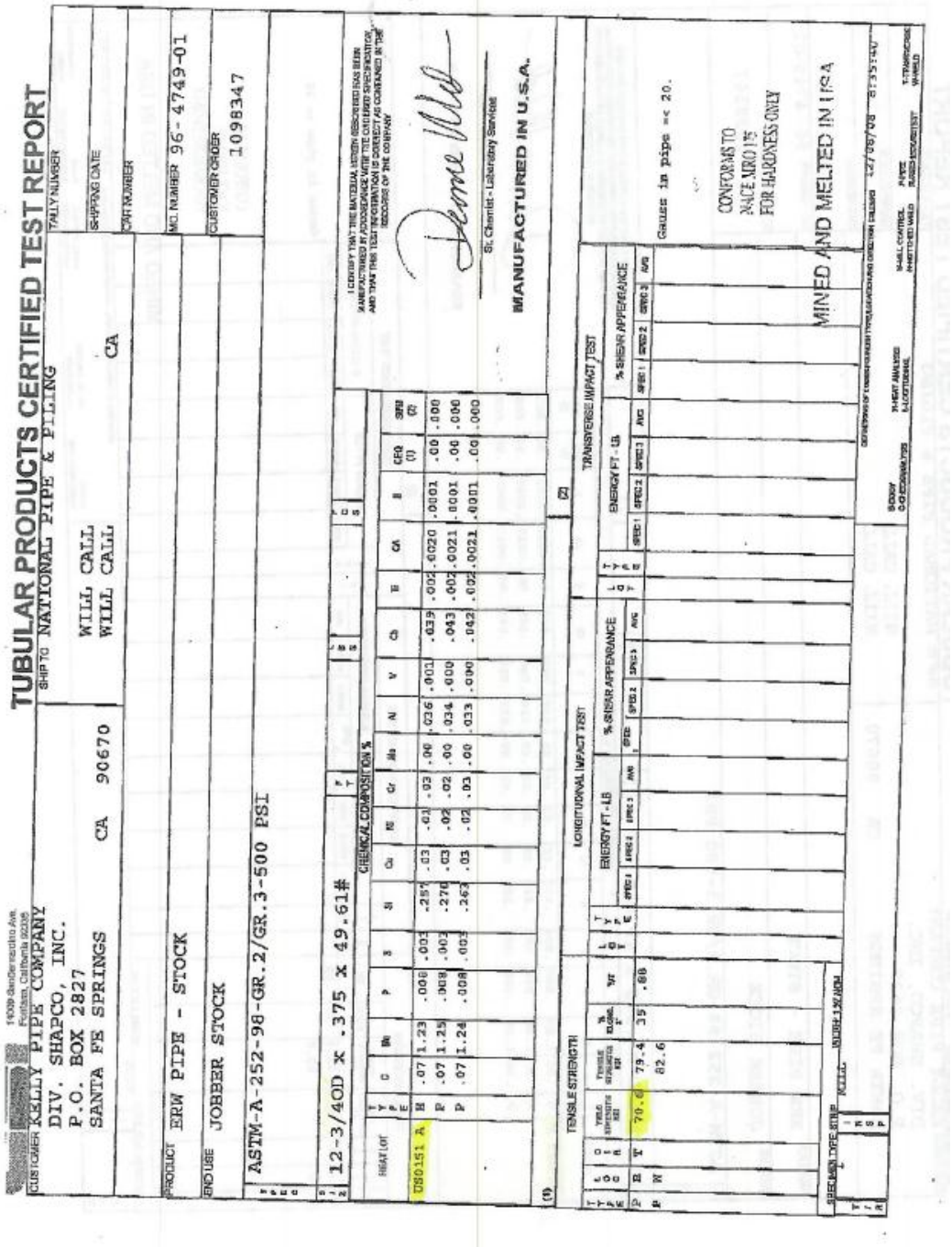

Figure B-2. Material Properties for Steel Test Pile

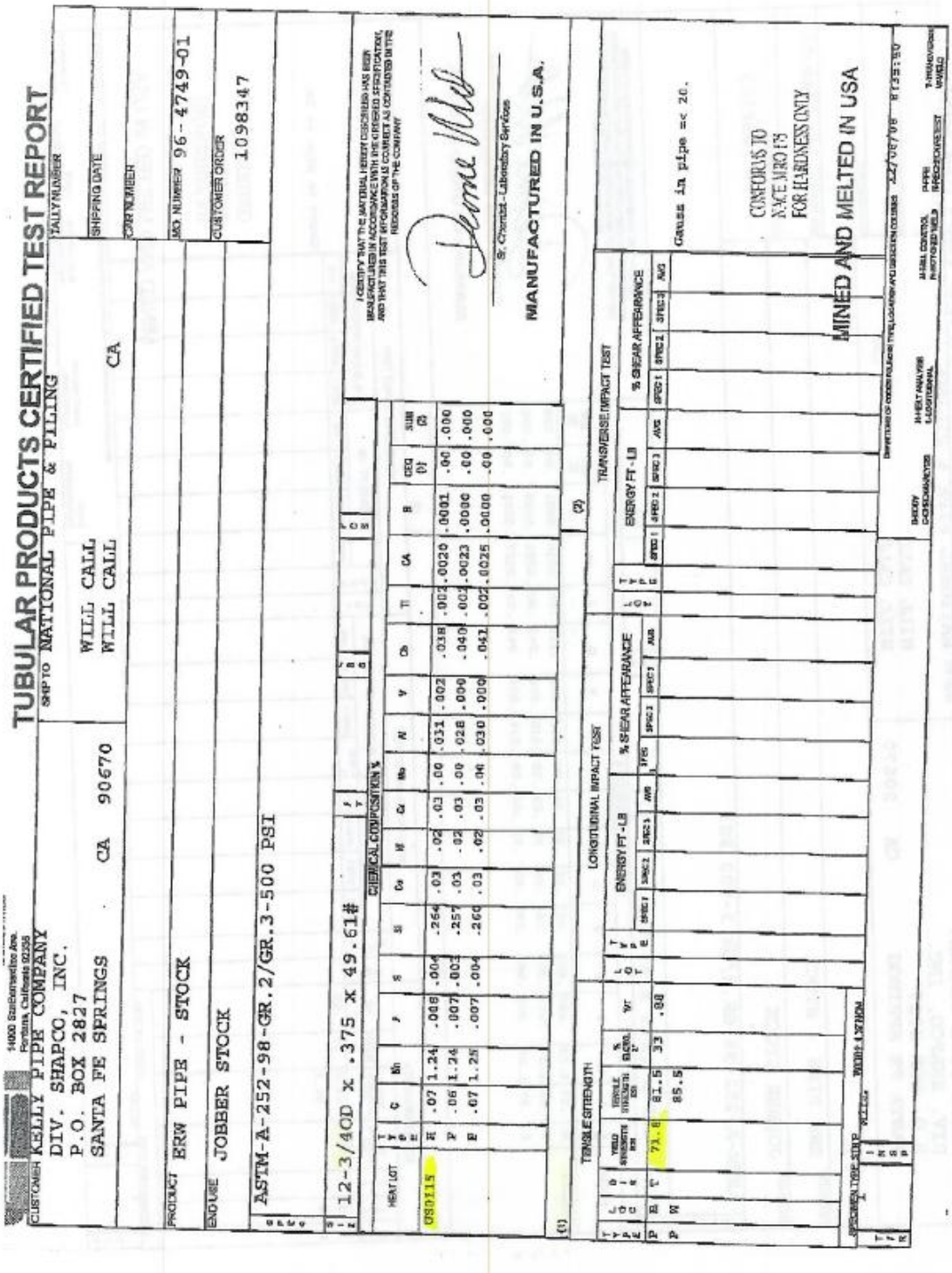

Figure B-3. Material Properties for Steel Test Pile

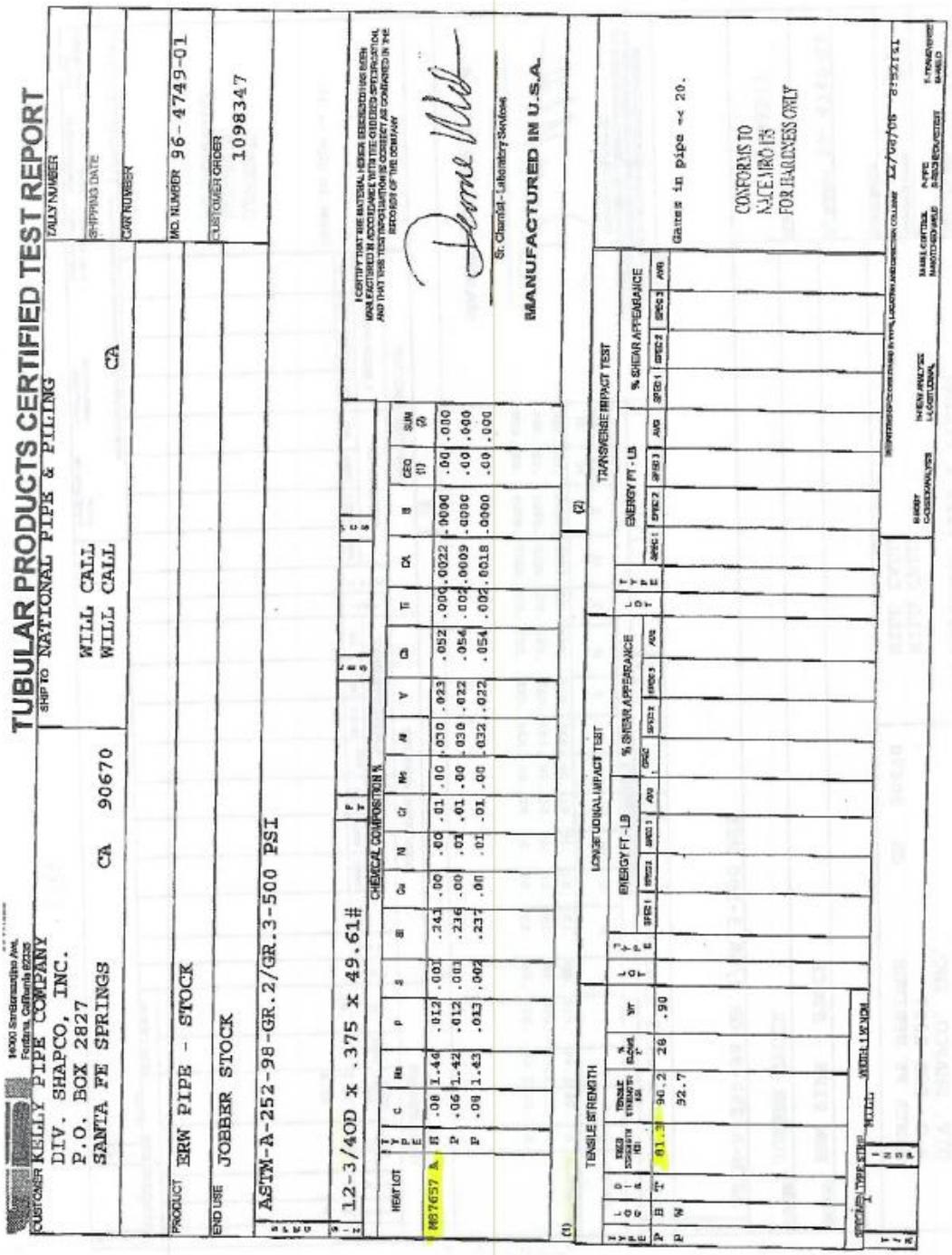

Figure B-4. Material Properties for Steel Test Pile

14000 San Bernardino Ave.
Fontana, California 92335

TUBULAR PRODUCTS CERTIFIED TEST REPORT

CUSTOMER KELLY PIPE COMPANY DIV. SHAPCO, INC. P.O. BOX 2827 SANTA FE SPRINGS CA 90670	SHIP TO NATIONAL PIPE & PILING WILL CALL WILL CALL CA	TALLY NUMBER SHIPPING DATE CAR NUMBER
PRODUCT ERW PIPE - STOCK		MO. NUMBER 96-4749-01
END USE JOBBER STOCK		CUSTOMER ORDER 1098347
SPEC ASTM-A-252-98-GR.2/GR.3-500 PSI		
SIZE 12-3/4OD x .375 x 49.61#		

CHEMICAL COMPOSITION %

HEAT LOT	TYPE	C	Mn	P	S	Si	Cu	Ni	Cr	Mo	Al	V	Cb	Ti	CA	B	CEQ (1)	SUM (2)
M87660 A	H	.06	1.41	.010	.002	.192	.00	.00	.01	.00	.031	.023	.048	.000	.0022	.0000	.00	.000
	P	.07	1.41	.010	.002	.198	.01	.01	.01	.00	.048	.022	.052	.002	.0015	.0000	.00	.000
	P	.06	1.40	.010	.002	.193	.00	.01	.01	.00	.032	.022	.051	.002	.0017	.0000	.00	.000

(1) (2)

I CERTIFY THAT THE MATERIAL HEREIN DESCRIBED HAS BEEN MANUFACTURED IN ACCORDANCE WITH THE ORDERED SPECIFICATION, AND THAT THIS TEST INFORMATION IS CORRECT AS CONTAINED IN THE RECORDS OF THE COMPANY

Sr. Chemist - Laboratory Services

MANUFACTURED IN U.S.A.

TENSILE STRENGTH

TYPE	LOC	DIR	YIELD STRENGTH KSI	TENSILE STRENGTH KSI	% ELONG. 2"	Y/T
P	B	T	80.7	89.9	27	.89
P	W			83.8		

LONGITUDINAL IMPACT TEST: LOT, TYPE, ENERGY FT-LB (SPEC 1, SPEC 2, SPEC 3, AVG), % SHEAR APPEARANCE (SPEC 1, SPEC 2, SPEC 3, AVG)

TRANSVERSE IMPACT TEST: LOT, TYPE, ENERGY FT-LB (SPEC 1, SPEC 2, SPEC 3, AVG), % SHEAR APPEARANCE (SPEC 1, SPEC 2, SPEC 3, AVG)

Gauss in pipe << 20.

CONFORMS TO
NACE MR0 175
FOR HARDNESS ONLY

SPECIMEN TYPE STRIP WIDTH 1-1/2" NOM.

12/06/08

Figure B-5. Material Properties for Steel Test Pile

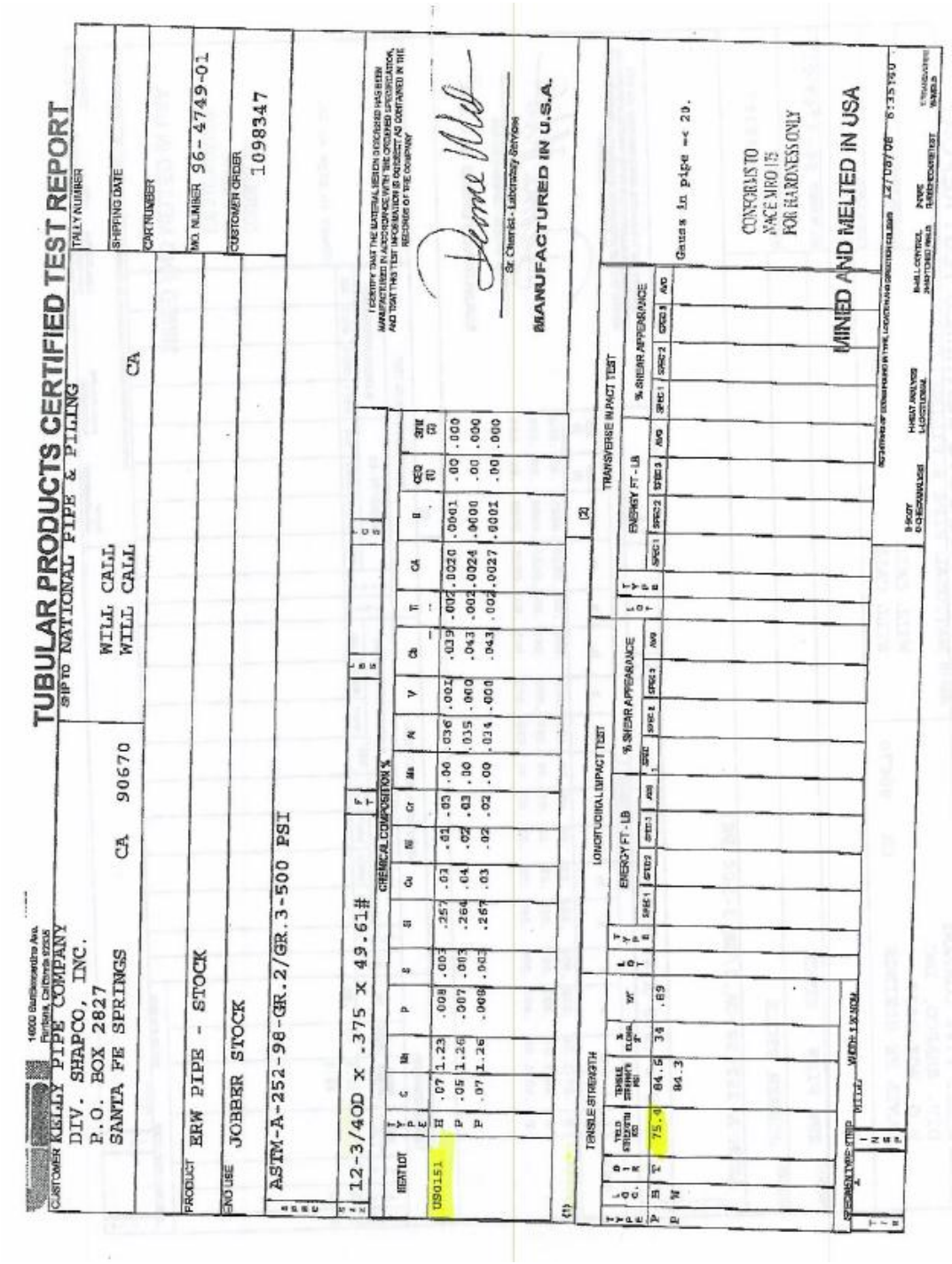

Figure B-6. Material Properties for Steel Test Pile

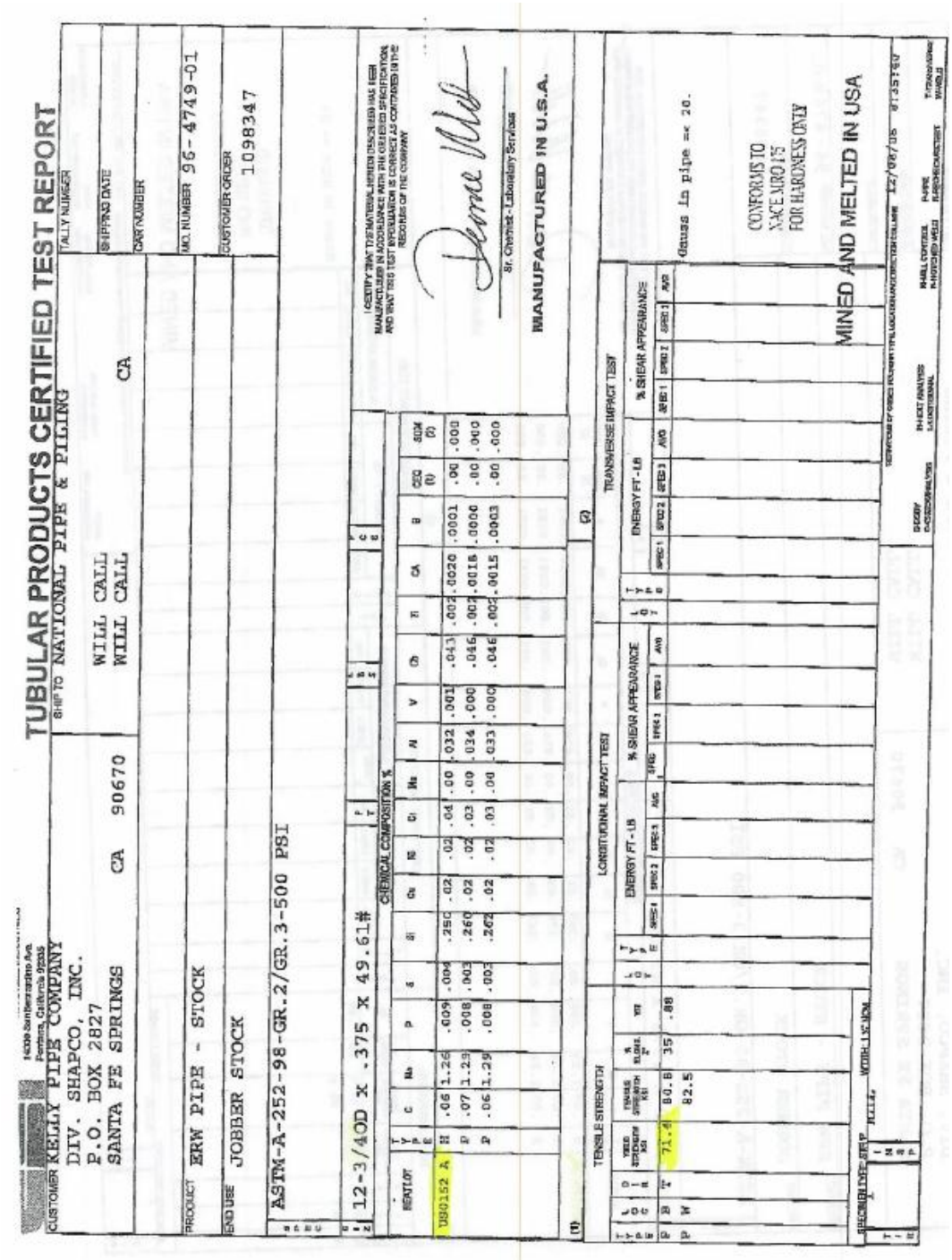

Figure B-7. Material Properties for Steel Test Pile

STATE OF CALIFORNIA DEPARTMENT OF TRANSPORTATION
RELATIVE COMPACTION TEST
TL-297 (REV 10/2005)

Job Stamp	Location STOCKPILE		Test No. 1
	Material SAND		From -
	Impact by BOB NIKA		Sand Vol. By
	Date TESTED 5-18-11		Date SAMPLED 5-12-11

Remarks: TESTED BY
AC&S MATERIALS TESTING SERVICES
2495 PROGRESS DRIVE, SUITE A
REDDING, CA 96001

SAND VOLUME DATA

A	Initial Wt. of Sand (g)	
B	Wt. of Residue (g)	
C	Wt. of Sand Used (A-B)	
D	Cone Correction (g)	
E	Wt. of Sand in Hole (C-D)	
F	Sand Density (g/cc)	
G	Volume of Hole (E/F)	
H	Wet Density (g/cc) (L/G)	

IMPACT TEST DATA

		1	2	3	4
I	Initial Wet Weight of Test Specimen (g)				
	Increment				
	Water Adjustment (g)	+100	+150	+200	
J	Tamper Reading	11.6	11.2	11.4	
K	Adjusted Wet Density (g/cc)	2.04	2.12	2.08	

ROCK CORRECTION

L	Total Sample Weight	(g)	22,756.3
M	+ 3/4-inch Weight in Air	(g)	-0-
N	+3/4-inch Weight in Water	(g)	
O	+3/4-inch Volume	(M - N)	
P	% +3/4-inch	100 * (M / L)	-0-
Q	% -3/4-inch	100 - P	
R	Density of +3/4-inch	(M / O)	
S	(%+3/4-inch) / Density of +3/4-inch	(P / RY)	
T	(%-3/4-inch) / Density of -3/4-inch	(Q / K)	
U	Sum of S and T	(S + T)	
V	Average Adjusted Wet Density	(100 / U)	2.12

Percent Relative Compaction*	Spec	Failed	or less
		Passed	

*(H / K) for 10% or less +3/4-inch; (H / V) for > 10% +3/4-inch

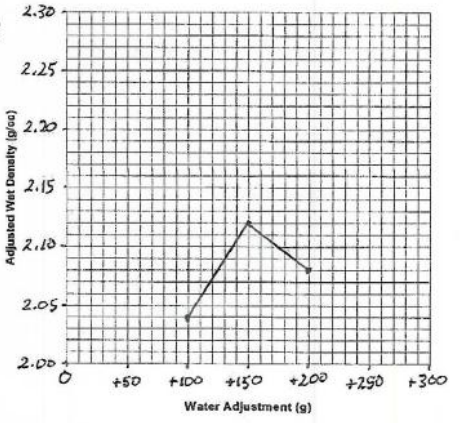

MOISTURE ADJUSTMENT FOR AGGREGATE BASE PAY QUANTITY

a	In-place Wet wt.		e	Test Spec. Wet Wt. (opt.)	
b	In-place Dry wt.		f	Test Spec. Dry Wt.	
c	In-place Water (a - b)		g	Test Spec. Water (e - f)	
d	In-place % Water (c / b)		h	Test Spec. % Water (g / f)	

Moisture Corr. (h + 1%) - d =

Moisture Corr. in excess of Opt. + 1% | % Moisture by CTM 226

+ 3/4-Inch Aggregate Adjustment (Y)

% + 3/4-inch (P)	Adjustment
20 or less	1.00
21-25	0.99
26-30	0.98
31-35	0.97
36-40	0.96
41-45	0.95
46-50	0.94

ATTACHMENT 2

Figure B-8. Relative Compaction Test Data Sheet (Caltrans Test 216)

Carlson Testing, Inc.

Bend Office (541) 330-9155
Geotechnical Office (503) 601-8250
Eugene Office (541) 345-0289
Salem Office (503) 589-1252
Tigard Office (503) 684-3460

Report Of In-Place Density Tests

Client: Knife River (Corporate Operations) Date: May 20th, 23rd and 24th, 2011

Project: OSU Hinsdale Wave Research Lab CTI Job No. S1106470

Job Address: 3550 SW Jefferson Way – Corvallis, Oregon Permit No.: n/a

Material Description: Cohesionless Soil from Knife River

Method of Test: Cal Trans 216

Maximum Wet Density 2.12 g./cc. Optimum Moisture: n/a % Required Compaction: 95 %

Source of Value Lab log # 11-3309 Source of Value Dated 5-18-11 ☑ Project Specific ☐ Current Fill Source Proctor

☐ Supplied By: AC & S Material Tests

Gauge Serial #: 39525 Standard Counts – Density: 2660 Moisture: 741 Calibration Date: 2/2011

Date of Test	Test No.	Test Location	Density Count	Moist. Count	Mode	Depth	Elev. Ft.	% Field Moist.	In-Place Density (lbs/cu.ft.) Wet	In-Place Density (lbs/cu.ft.) Dry	% Comp.
5-20-11	1	CENTERLINE; 25' FROM WEST	2345		DT	6"	-9 ½'	9.6	2.065		97.4
5-20-11	2	50' FROM SOUTH, 36' FROM EAST	2699		DT	6"	-9 ½'		2.035		96.0
5-20-11	3	EAST – CENTERLINE, 9' FROM TOE	1579	122	DT	8"	-9'	6.3	2.038	1.918	96.1
5-20-11	4	NORTH – CENTERLINE, 12' FROM TOE	1686	92	DT	8"	-9'	4.5	2.007	1.917	95
5-20-11	5	SOUTH – CENTERLINE, 6' FROM TOE	1495	160	DT	8"	-9'	8.6	2.072	1.908	97.7
5-20-11	6	WEST – CENTERLINE, 15' FROM TOE	1671	138	DT	8"	-9'	6.9	2.009	1.862	95
5-20-11	7	SW CORNER	1634	162	DT	8"	-8 ½'	9.0	2.014	1.848	95.0
5-20-11	8	SE CORNER	1563	167	8"	-8 ½'	9.1	2.042	1.871	96.3	96.3
5-20-11	9	NE CORNER	1548	169	8"	-8 ½'	9.2	2.048	187.5	96.6	96.6

Asterisked (*) percent compaction test results did not meet listed acceptance criteria.

Remarks:
Bold / Circled – Failing Shots

Inspector: Gordon Cooper Reviewed by: Date: 5/25/11

Figure B-9. In-Place Density Test (Nuclear Density Gauge) for Cohesionless Embankment

Carlson Testing, Inc.

Bend Office (541) 330-9155
Geotechnical Office (503) 601-8250
Eugene Office (541) 345-0289
Salem Office (503) 589-1252
Tigard Office (503) 684-3460

Report Of In-Place Density Tests

Client: Knife River (Corporate Operations) Date: May 20th, 23rd and 24th, 2011

Project: OSU Hinsdale Wave Research Lab CTI Job No. S1106470

Job Address: 3550 SW Jefferson Way – Corvallis, Oregon Permit No.: n/a

Material Description: Cohesionless Soil from Knife River

Method of Test: Cal Trans 216

Maximum Wet Density 2.12 g./cc. Optimum Moisture: n/a % Required Compaction: 95 %

Source of Value Lab log # 11-3309 Source of Value Dated 5-18-11 ☑ Project Specific ☐ Current Fill Source Proctor

☐ Supplied By: AC & S Material Tests

Gauge Serial #: 39525 Standard Counts – Density: 2660 Moisture: 741 Calibration Date: 2/2011

Date of Test	Test No.	Test Location	Density Count	Moist. Count	Mode	Depth	Elev. Ft.	% Field Moist.	In-Place Density (lbs/cu.ft.) Wet	In-Place Density (lbs/cu.ft.) Dry	% Comp.
5-20-11	10	NW CORNER	1574	157	DT	8"	-8 ½'	8.4	2.036	1.878	96.0
5-23-11	11	EAST, CENTERLINE	1659	116	DT	8"	-6'	6.0	2.016	1.887	95.1
5-23-11	12	SOUTH, CENTERLINE	1615	130	DT	8"	-6'	6.9	2.018	1.888	95.2
5-23-11	13	WEST, CENTERLINE	1542	155	DT	8"	-6'	8.4	2.047	1.888	96.6
5-23-11	14	NORTH, CENTERLINE	1647	128	DT	8"	-6'	6.8	2.015	1.878	95.0
5-23-11	15	SE CORNER	1402	161	DT	8"	-5'	8.5	2.108	1.943	99.4
5-23-11	16	SW CORNER	1562	153	DT	8"	-5'	8.3	2.038	1.882	96.1
5-23-11	17	NE CORNER	1661	108	DT	8"	-5'	6.5	2.016	1.893	95.1
5-23-11	18	NW CORNER	1521	162	DT	8"	-5'	8.6	2.091	1.925	98.6

Asterisked (*) percent compaction test results did not meet listed acceptance criteria.

Remarks:
Bold / Circled – Failing Shots

Inspector: Gordon Cooper Reviewed by: Date: 5/25/11

Figure B-10. In-Place Density Test (Nuclear Density Gauge) for Cohesionless Embankment

Carlson Testing, Inc.

Bend Office (541) 330-9155
Geotechnical Office (503) 601-8250
Eugene Office (541) 345-0289
Salem Office (503) 589-1252
Tigard Office (503) 684-3460

Report Of In-Place Density Tests

Client: Knife River (Corporate Operations) Date: May 20th, 23rd and 24th, 2011

Project: OSU Hinsdale Wave Research Lab CTI Job No. S1106470

Job Address: 3550 SW Jefferson Way – Corvallis, Oregon Permit No.: n/a

Material Description: Cohesionless Soil from Knife River

Method of Test: Cal Trans 216

Maximum Wet Density 2.12 g./cc. Optimum Moisture: n/a % Required Compaction: 95 %

Source of Value Lab log # 11-3309 Source of Value Dated 5-18-11 ☑ Project Specific ☐ Current Fill Source Proctor

☐ Supplied By: AC & S Material Tests

Gauge Serial #: 39525 Standard Counts – Density: 2660 Moisture: 741 Calibration Date: 2/2011

Date of Test	Test No.	Test Location	Density Count	Moist. Count	Mode	Depth	Elev. Ft.	% Field Moist.	In-Place Density (lbs/cu.ft.) Wet	In-Place Density (lbs/cu.ft.) Dry	% Comp.
5-23-11	19	WEST, CENTERLINE	1670	123	DT	8"	-4'	6.6	2.019	1.894	95.2
5-23-11	20	SOUTH, CENTERLINE	1554	131	DT	8"	-4'	6.9	2.043	1.912	96.4
5-23-11	21	EAST, CENTERLINE	1540	167	DT	8"	-4'	9.2	2.047	1.875	96.6
5-23-11	22	NORTH, CENTERLINE	1664	127	DT	8"	-4'	6.8	2.017	1.889	95.1
5-23-11	23	WEST, CENTERLINE	1595	132	DT	8"	-3'	7.0	2.036	1.903	96.0
5-23-11	24	NORTH CENTERLINE	1634	127	DT	8"	-3'	6.8	2.020	1.891	95.3
5-23-11	25	SOUTH, CENTERLINE	1638	140	DT	8"	-3'	7.6	2.008	1.867	95
5-23-11	26	EAST, CENTERLINE	1436	160	DT	8"	-3'	8.5	2.093	1.929	98.7
5-24-11	27	SE CORNER	1620	137	DT	8"	-1'	7.4	2.010	1.872	95.0

Asterisked (*) percent compaction test results did not meet listed acceptance criteria.

Remarks:
Bold / Circled – Failing Shots

Inspector: Gordon Cooper Reviewed by: Date: 5/25/11

Figure B-11. In-Place Density Test (Nuclear Density Gauge) for Cohesionless Embankment

Carlson Testing, Inc.

Bend Office (541) 330-9155
Geotechnical Office (503) 601-8250
Eugene Office (541) 345-0289
Salem Office (503) 589-1252
Tigard Office (503) 684-3460

Report Of In-Place Density Tests

Client: Knife River (Corporate Operations) Date: May 20th, 23rd and 24th, 2011

Project: OSU Hinsdale Wave Research Lab CTI Job No. S1106470

Job Address: 3550 SW Jefferson Way – Corvallis, Oregon Permit No.: n/a

Material Description: Cohesionless Soil from Knife River

Method of Test: Cal Trans 216

Maximum Wet Density 2.12 g./cc. Optimum Moisture: n/a % Required Compaction: 95 %

Source of Value Lab log # 11-3309 Source of Value Dated 5-18-11 ☑ Project Specific ☐ Current Fill Source Proctor

☐ Supplied By: AC & S Material Tests

Gauge Serial #: 39525 Standard Counts – Density: 2660 Moisture: 741 Calibration Date: 2/2011

Date of Test	Test No.	Test Location	Density Count	Moist. Count	Mode	Depth	Elev. Ft.	% Field Moist.	In-Place Density (lbs/cu.ft.) Wet	In-Place Density (lbs/cu.ft.) Dry	% Comp.
5-24-11	28	NE CORNER	1336	1663	DT	8"	-1'	8.6	2.140	1.971	100.9
5-24-11	29	NW CORNER	1610	110	DT	8"	-1'	6.0	2.016	1.902	95.1
5-24-11	30	SW CORNER	1485	172	DT	8"	-1'	9.5	2.071	1.891	97.7
5-24-11	31	EAST, CENTERLINE	1502	157	DT	8"	0'	8.5	2.065	1.902	97.4
5-24-11	32	WEST, CENTERLINE	1625	138	DT	8"	0'	7.5	2.014	1.874	95.0
5-24-11	33	SOUTH, CENTERLINE	1623	151	DT	8"	0'	8.4	2.015	1.859	95.0
5-24-11	34	NORTH, CENTERLINE	1523	171	DT	8"	0'	9.5	2.055	1.876	96.9

Asterisked (*) percent compaction test results did not meet listed acceptance criteria.

Remarks:
Bold / Circled – Failing Shots

Inspector: Gordon Cooper Reviewed by: Date:

Figure B-12. In-Place Density Test (Nuclear Density Gauge) for Cohesionless Embankment

Initial Dry Mass (g):	1313.7				
		Sieve Test 5/09/2011			
Seive #	**Mass (g)**	**% Retained**	**% Finer**	**Size (mm)**	**FM**
1/2"	0	0.0%	100%	12.5	0.0%
3/8"	6.3	0.4%	100%	9.5	
1/4"		7.3%	92%	6.3	
4	182.6	12.8%	80%	4.75	12.8%
6	219.8	15.5%	64%	3.35	28.3%
8	190.6	13.4%	51%	2.36	41.7%
16	273.1	19.2%	31.4%	1.18	60.9%
30	150.9	10.6%	21%	0.6	71.5%
50	92.8	6.5%	14%	0.3	78.0%
100	54.1	3.8%	11%	0.15	81.8%
200	35.9	2.5%	8%	0.075	
Pan	4.9				
Total Mass:	1211			Fineness Modulus:	3.75

Initial Dry Mass (g):	1444.5				
		Seive Test 5/13/2011			
Seive #	**Mass (g)**	**% Retained**	**% Finer**	**Size (mm)**	**FM**
1/2"	0	0.0%	100%	12.5	0.0%
3/8"	1.2	0.1%	100%	9.5	
1/4"	169.7	10.5%	89%	6.3	
4	222.6	13.7%	76%	4.75	13.7%
6	237.7	14.7%	61%	3.35	18.4%
8	202.5	12.5%	49%	2.36	40.9%
16	281.4	17.4%	31%	1.18	58.3%
30	148	9.1%	22%	0.6	67.4%
50	87.2	5.5%	16%	0.3	72.8%
100	55.6	3.4%	13%	0.15	76.2%
200	34.9	2.2%	11%	0.075	
Pan	4				
Total Mass:	1444.8			Fineness Modulus:	3.58

Figure B-13. Sieve data on embankment material

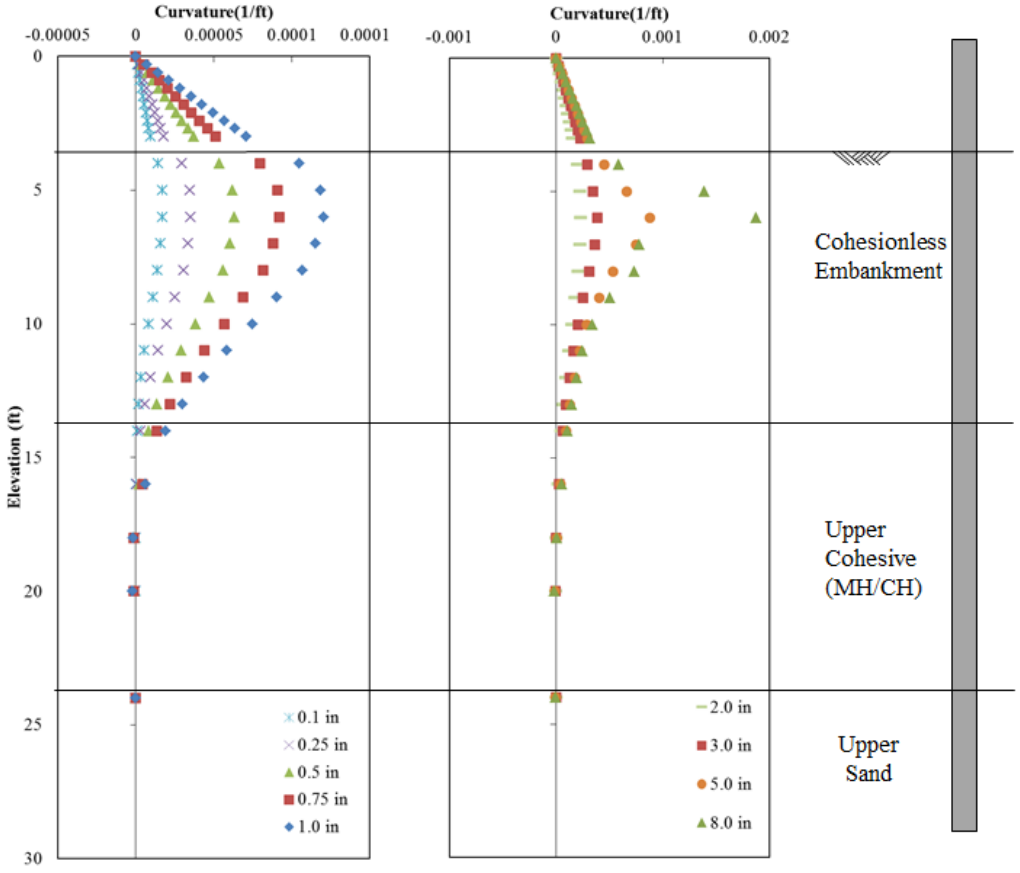

Figure B-14. Curvature Results for Baseline Pile (P-2) at varying Displacements

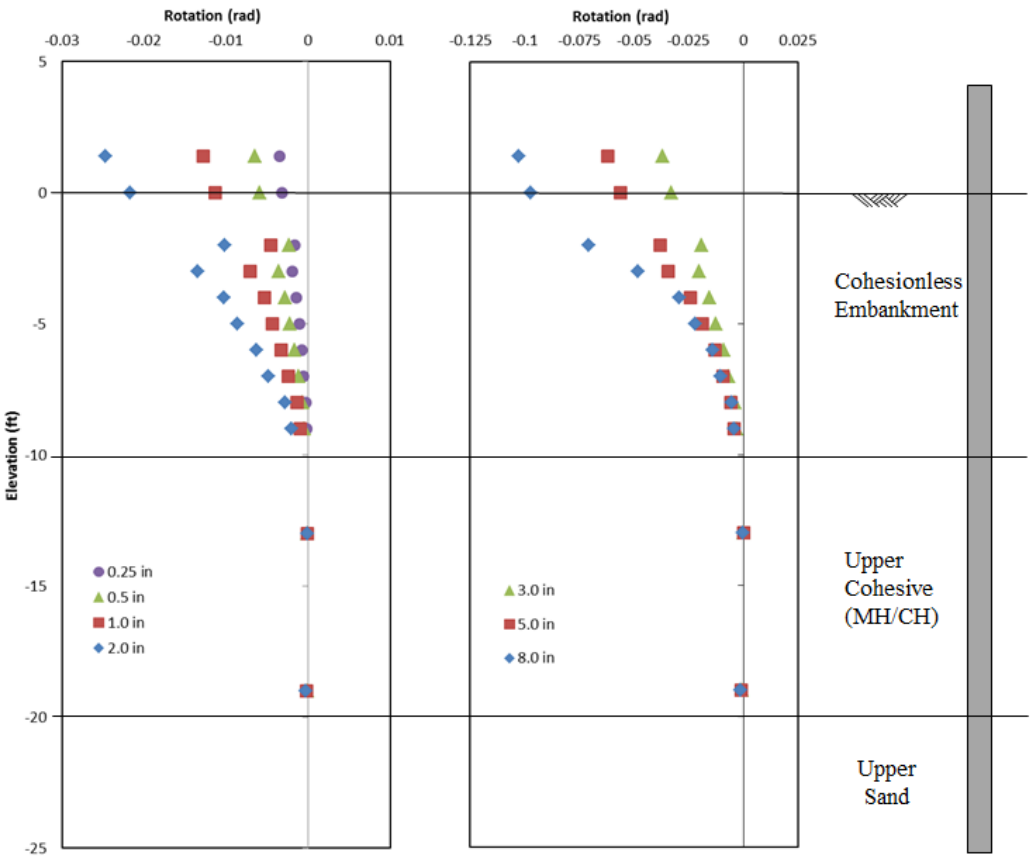

Figure B-15. Rotation Results for Baseline Pile (P-2) at varying Displacements

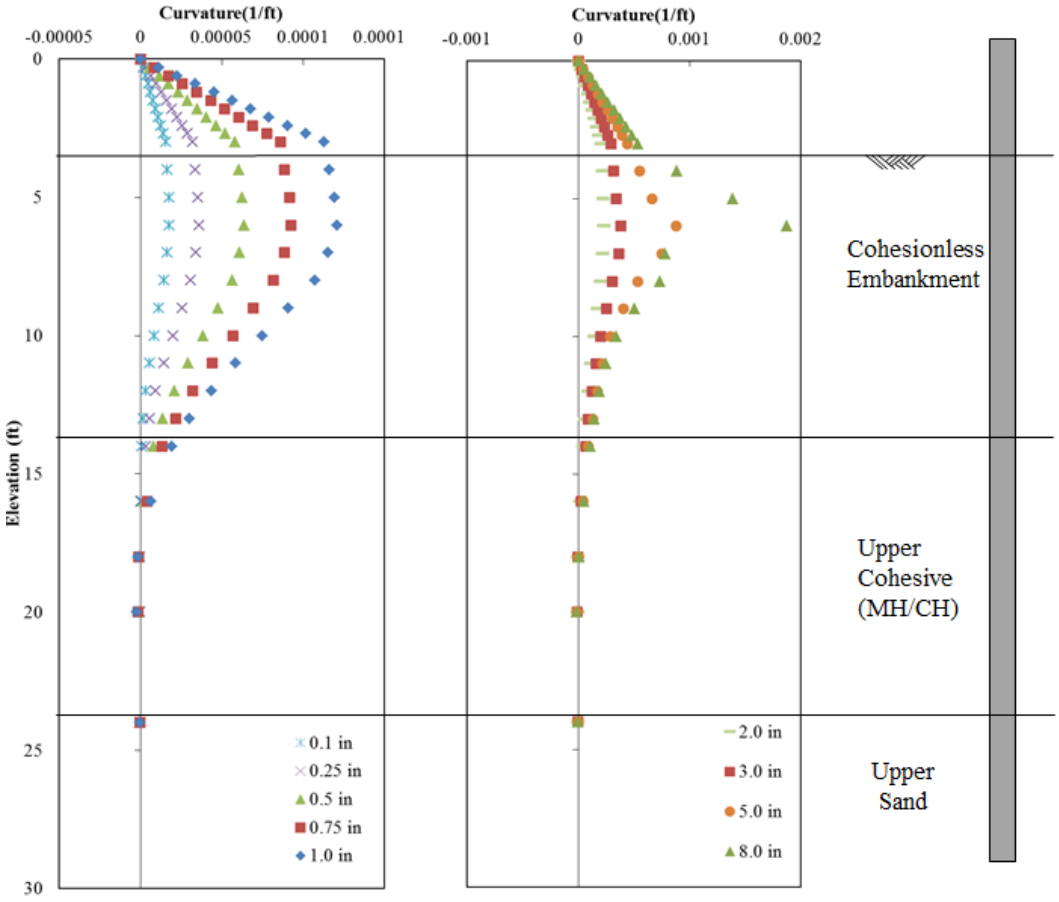

Figure B-16. Curvature Results for the 4D Pile (P-7) at varying Displacements

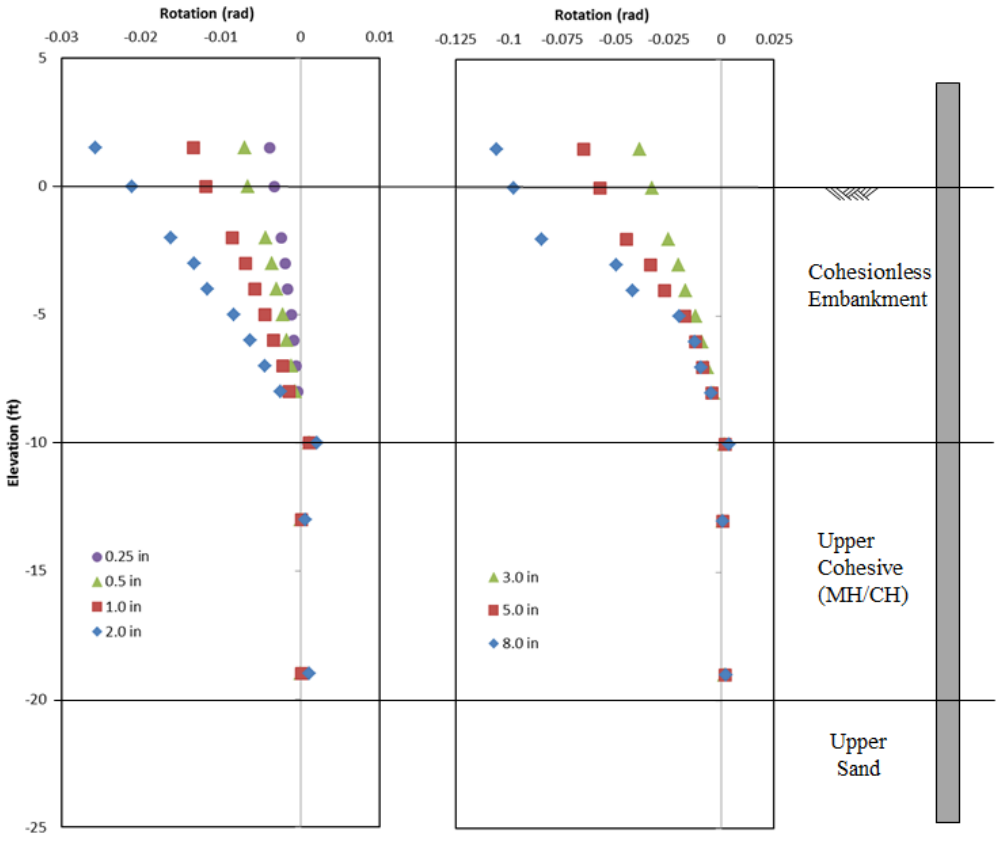

Figure B-17. Rotation Results for the 4D Pile (P-7) at varying Displacements

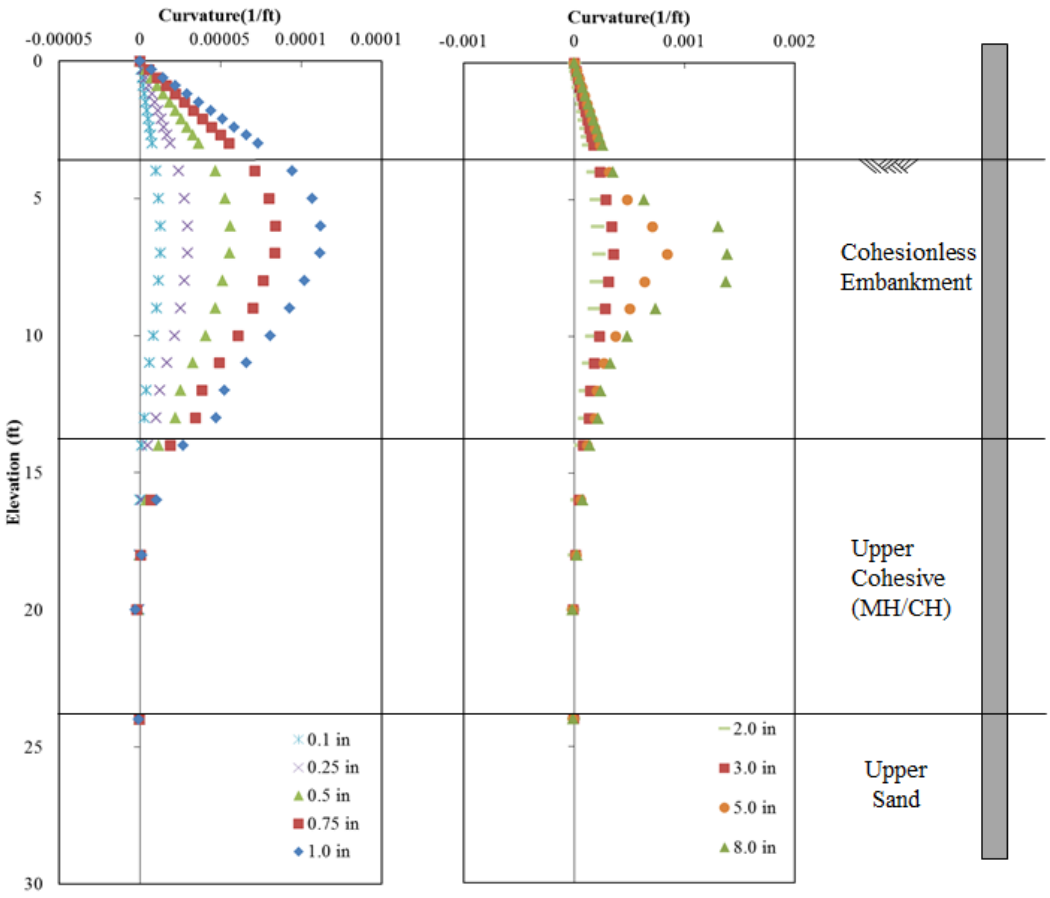

Figure B-18. Curvature Results for the 2D Pile (P-6) at varying Displacements

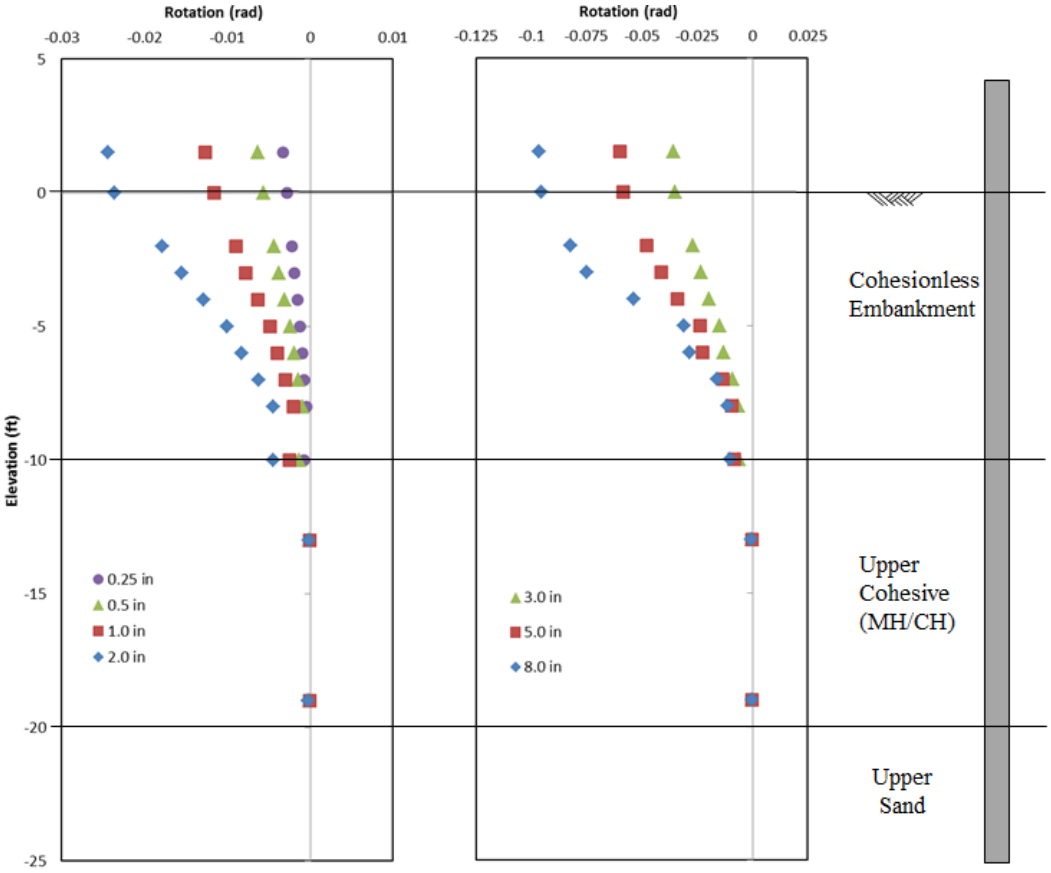

Figure B-19. Rotation Results for the 2D Pile (P-6) at varying Displacements

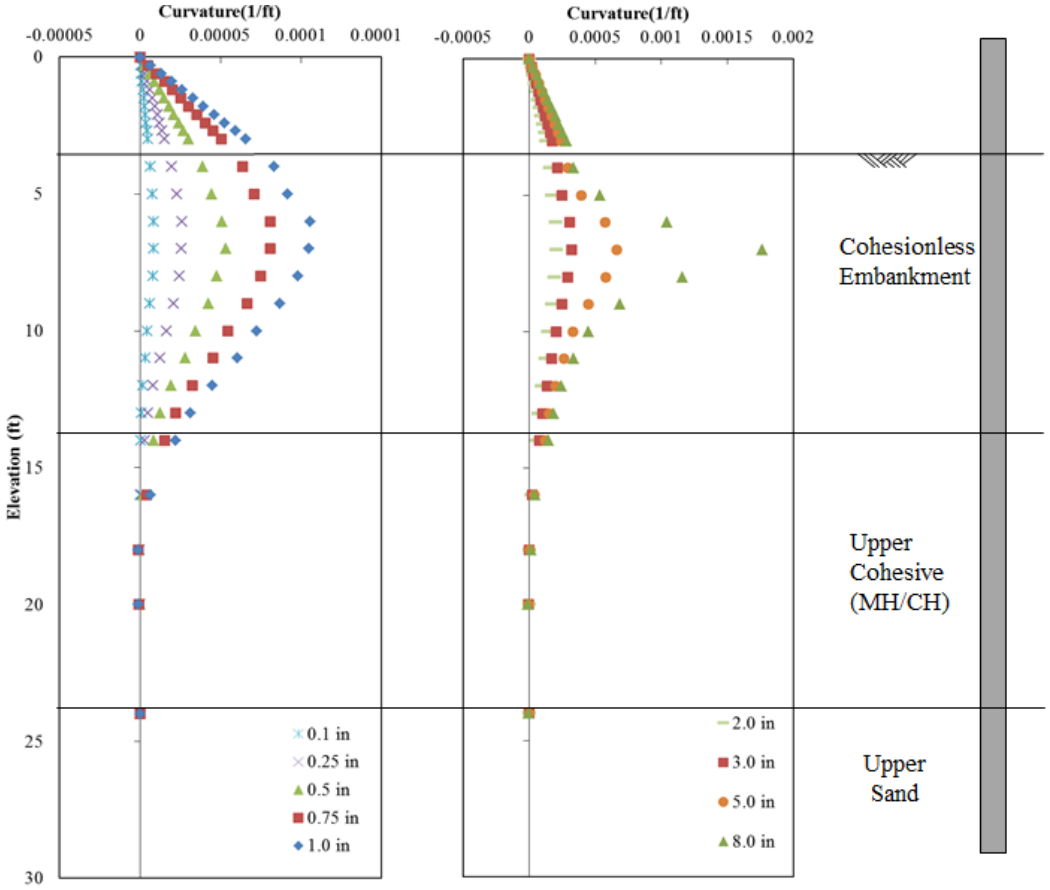

Figure B-20. Curvature Results for the 0D Pile (P-9) at varying Displacements

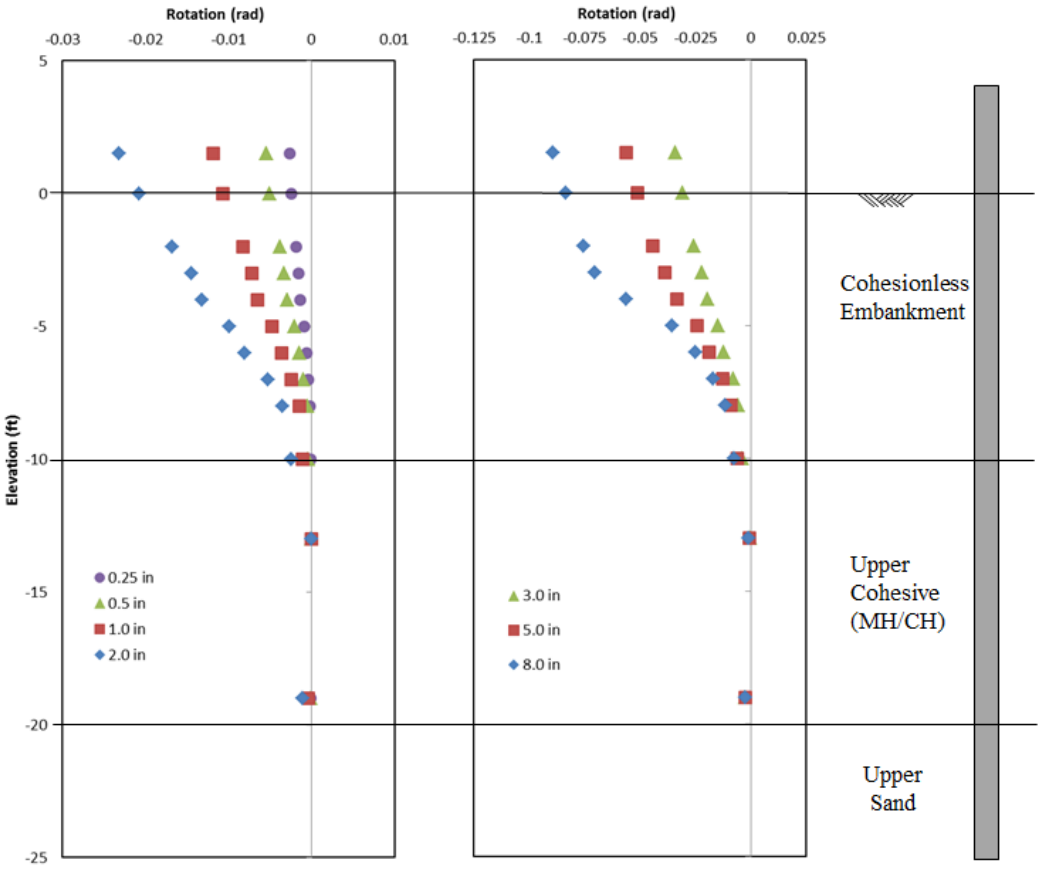

Figure B-21. Rotation Results for the 0D Pile (P-9) at varying Displacements

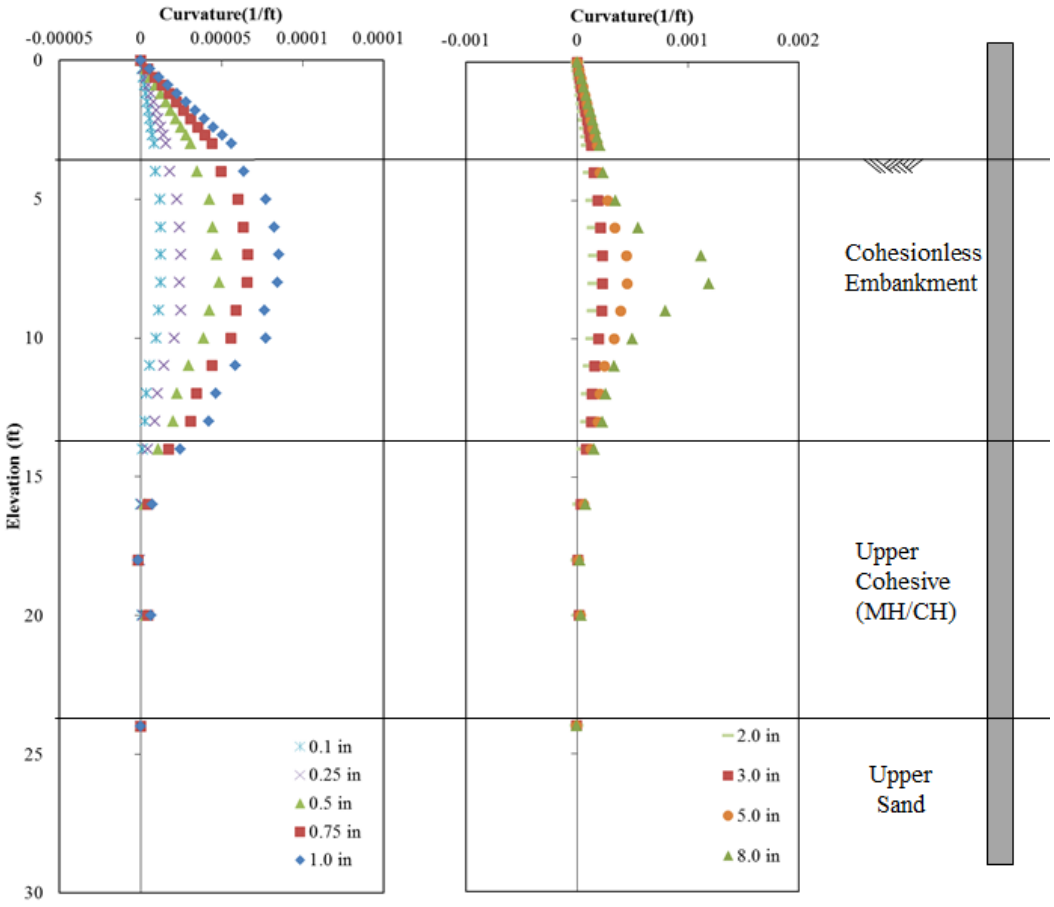

Figure B-22. Curvature Results for the -4D Pile (P-10) at varying Displacements

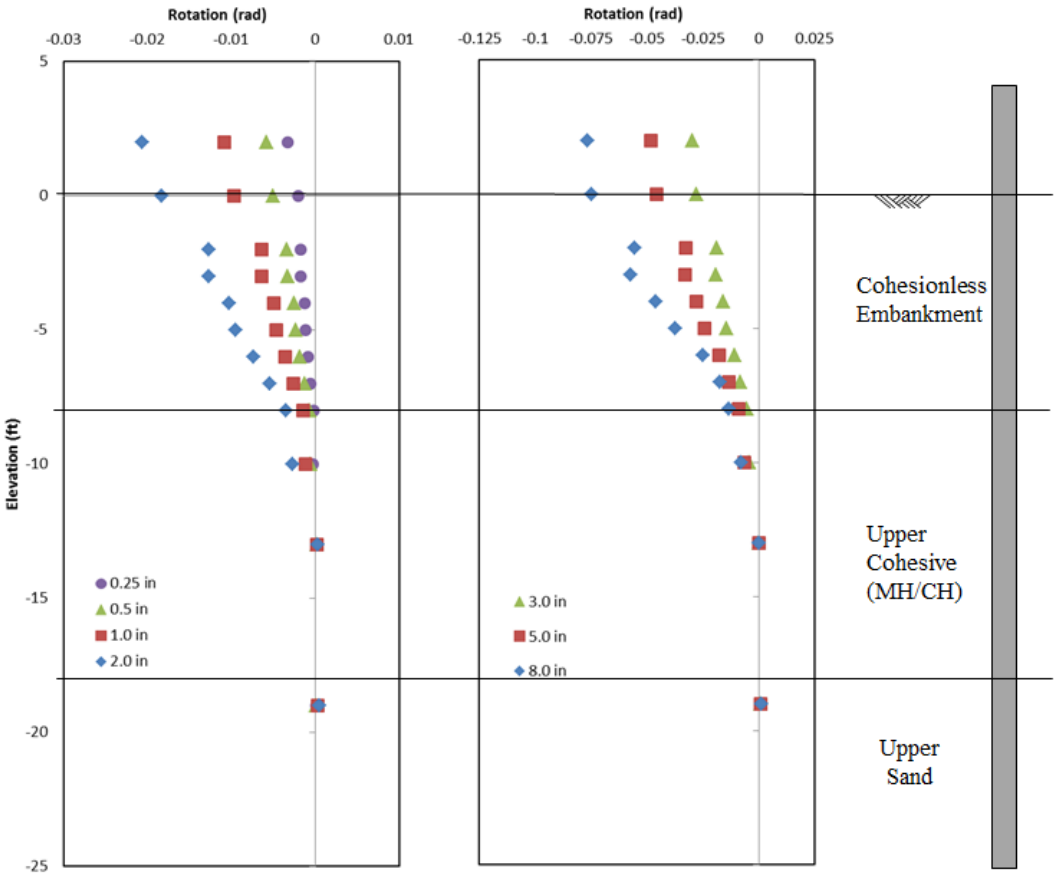

Figure B-23. Rotation Results for the -4D Pile (P-10) at varying Displacements